UNIVERSITY OF MISKOLC

FACULTY OF MECHANICAL ENGINEERING AND INFORMATICS

OPTIMIZATION APPROACH TO PREDICT DAMAGE MODEL PARAMETERS FOR DUCTILE FRACTURE OF PIPELINE USED IN NUCLEAR REACTOR

PHD THESES

Prepared by

CHAHBOUB YASSINE

Engineering of Nuclear Techniques and Radiation Protection (BSc),

Mechanical Engineering (MSc)

ISTVÁN SÁLYI DOCTORAL SCHOOL OF MECHANICAL ENGINEERING SCIENCES
TOPIC FIELD OF MECHANICAL ENGINEERING SCIENCES
TOPIC GROUP OF DESIGN OF MACHINES AND ELEMENTS

Head of Doctoral School

Dr. Gabriella Vadászné Bognár

DSc, Full Professor

Head of Topic Group

Dr. Gabriella Vadászné Bognár

Scientific Supervisor

Dr. SZAVAI SZABOLCS

Miskolc

2022

ACKNOWLEDGMENTS

First and foremost, I want to thank and praise God, the Almighty, who has provided me with innumerable blessings, opportunities, and knowledge that have allowed me to complete the thesis, *Alhamdulillah*.

The success of this thesis is largely dependent on the support and direction of many others, in addition to my efforts to reap the benefits of this work.

Therefore, I want to take the chance to thank everyone who contributed to the successful completion of this substantial project.

To my supervisor, friend, and second family in Hungary, *Dr. Szavai Szabolcs*. I appreciate your assisting me and being there for me in good and bad times, especially during the pandemic. It was a pleasure to get to know and work with you. I learned a lot from you. Thank you for all the opinions and opportunities; working with you was one of the best decisions I have ever made. I am truly grateful for the opportunity.

Dr. Tóth László I appreciate your support and presence during good and bad times. I appreciate the opportunity to work with you and gain knowledge from your strategies and recommendations, which have consistently encouraged me to do well in my research and publish quality work.

 I want to thank *Zoltan, Bezi, Spisák Bernadett, and Réka Erdei* for their support and help while working on my thesis; they were always here to help me.

A Big thanks to Bay Zoltán Alkalmazott Kutatási Közhasznú Nonprofit Kft for providing me the opportunity to work with them, during different European projects, for supporting me with the technical tools to work on my thesis, and for providing me with the opportunities to travel abroad and participate in summer schools and workshops worldwide.

I want to thank all the staff and students at the Faculty of Mechanical Engineering and Informatics and the Institute of Information Science for their support, cooperation, and encouragement.

A special thanks to *Prof. Dr. Gabriella Vadaszné Bognár* for moral guidance and encouragement to accomplish my thesis; thank you for your availability and for allowing us to participate in conferences abroad; your presence and support were a great help during this adventure.

To my parents, my guardian angels with my best interests at heart. They have my utmost respect and gratitude for their love, prayers, concern, and sacrifices made for my upbringing and future preparation. I appreciate you both for giving me the courage and trustees to aim high and pursue my ambitions. I want to continue to make you proud. I appreciate my two brothers (*Bader*, and *Soufiane*) and my lovely sister (*Azhare*).

A special thanks to *Bader and Anas*, *who supported and motivated me and made my life easier in Hungary*

Acknowledgments

To *Soukaina Bensaid*, my best friend. Thank you for always believing in me, and for being here beside me all the time.

Hajar, Salma, Issam Adnan, and Oumaima, my best friends who always believed in me, who had always supported me morally and encouraged me for four years, who supported me when I got depressed and when I lost motivation, your presence was great support for me during this long way.

A special thank you to H. E. Ms. Karima KABBAJ, Ambassador Extraordinary and Plenipotentiary of Morocco in Hungary, for her support and motivation during my stay in Hungary

All my thanks to my home country Morocco and the Stipendium Hungaricum Scholarship Program for this opportunity to pursue my Ph.D. and master's studies in Hungary.

Contents

III

Figures

Tables

Supervisor's recommendations

Mr Chahboub graduated at the University of Dunaújváros as MSc mechanical engineer.

He started his PhD studies in 05.09.2018 at the University of Miskolc in Hungary in Mechanical Engineering under my leadership.

His research is mainly focused on the damage mechanism of materials and local fracture mechanical analysis of the components by Gurson Tveegard Needleman approach. So he started to learn the structural integrity analysis method for pressure vessels and connecting pipes of nuclear power plants.

He has intensively studied the physical meaning of its material parameters as well related to the degradation processes to ensure a long safe operation of the Reactor Pressure Vessel.

Comparing the GTN model to other damage models like Rice and Tracey Model, Johnson–Cook, Damage Model, the GTN model is a powerful tool, however the determination of GTN parameters it's still not an easy task, and it required much time to find the right combination, but the problem is that with different sets of parameters we could see the same results, so we need to study more this phenomena by defining the most sensitive parameters. F

or determination the GTN parameters he applied experiment, polynomial regression, and kriging methods, artificial neural network, genetic algorithm. He has got significant knowledge in the determination of Gurson parameters by applying a neural network. He was able to determine the most sensitive parameter for certain cases. He took an active part in the research tasks in several projects including the ADVIVE+ H2020 EURATOM international project.

In my opinion, its publication activity is adequate, according to the MTMT database, it currently has 15 publications are closely related to the PhD topic.

In 2020, he successfully passed the complex examination. He obtained the pre-degree certificate with an outstanding 320 credits. He successfully passed the departmental discussion on 27 January 2023.

The candidate worked independently and very often took the initiative, always following instructions. During his doctoral studies he further developed his knowledge, research affinity and presentation skills. He has acquired new knowledge and competences which he will be able to use in his future academic life.

Date 11 April 2023

Supervisor: Dr. Szávai Szabolcs

List of symbols and abbreviations

> ➢ ABBREVIATIONS
- ANN: Artificial Neural Network
- GTN: Gurson Tveegard Needleman
- SENT: Single Edge Notch Tension
- CT: Compact tension
- NT:Notched
- R and D : Research and Development
- EDF : Electricite De France
- LEFM : Linear Elastic Fracture Mechanics
- NLFM : Nonlinear Fracture Mechanics
- RNN : Recurrent Neural Network
- FNN : Feed-Forward Neural Networks
- COD : Crack Opening Displacement (mm)
- COMD : Crack Opening Displacement (mm)
- CV : The Coefficient Of Variation
- FEM: Finite Element Modelling
- ASTM: American Society for Testing and Materials
- MSC : Marc Mentat Software
- RPV : Reactor Pressure Vessel

> ➢ SYMBOLS
- D : constant parameter (has no units)
- σ_k: constant parameter MPa
- q : von Mises equivalent stress MPa
- f: void volume fraction (has no units)
- f_c : critical void volume fraction (has no units)
- $f_{f;}$: final void volume fraction (has no units)
- R(p) : material's true stress–true plastic strain curve MPa
- σ_m: hydrostatic stress MPa
- f : fraction of cavities in the matter (has no units)
- σ_0: equivalent flow stress, MPa
- σ_e: effective stress MPa
- φ_j: hydrostatic stress, MPa
- f : void volume fraction (has no units)
- σ_e: von Mises equivalent stress MPa
- V_0 : volume of the matrix without counting the voids (m^3)
- V_t : global material volume (m^3)
- q_1 : material constant (has no units)
- J-R curve : Crack growth resistance curve
- q_2 : material constant (has no units)
- $tr\sigma$: sum of principal stresses MPa

- σ_M : equivalent flow stress MPa
- f*: ratio of voids effective volume to the material volume ratio (has no units)
- f : voids volume ratio (has no units**)**
- f_0 : void volume ratio at the beginning of nucleation (has no units**)**
- f_c : critical void volume ratio (has no units**)**
- f_f : void volume ratio when a fracture occurs. (has no units**)**
- σ_M : equivalent flow stress MPa
- n : strain-hardening exponent, (has no units**)**
- ε_M : equivalent plastic strain. (has no units**)**
- fg: existing void growth **(has no units)**
- fn: new void nucleation (has no units)
- $tr\varepsilon^{pl}$: volume plastic strain rate (s^{-1})
- SN : voids nucleation mean quantity (m^{-3})
- fn : volume ratio of the second phase particles (has no units**)**
- ε_N : mean strain at the time of voids nucleation (has no units**)**
- w_0 (σ): function of the third normalized invariant's stress state ξ.
- k_w : component parameter of the material used in this procedure. (has no units)
- ξ: third normalized invariant's stress state (has no units)
- vj: local induced field (has no units)
- φj: activation or squashing function   (has no units)
- yj: output of the neuron j (has no units)
- bj:the bias (has no units)
- F_{ij}: sigmoid function (has no units)
- E: mean squared error (has no units)
- Rij : target value (has no units)
- n: number of the predictions (has no units)

1. INTRODUCTION

The Titanic was thought to be unsinkable, the dream ship, until it hit a large iceberg on April 14, 1912, and sunk in less than three hours. The Titanic carried about 2200 passengers and staff on her first journey to America. Only 705 people made it out alive.

The main question following the Titanic disaster was, "What caused this accident ?" Many analyses were conducted to provide rational solutions to the world's curiosity about why the massive Titanic sank.

Many speculations and theories circulated among people regarding the exact cause of the catastrophe; some said that the ship's captain was to blame; others claimed that it was a political matter and that Germany was to blame, but the material scientists found the logical answer.

The main reason behind the titanic sink was the material failure at low temperatures, the material had to behave in ductile mode, but unfortunately, brittle failure took place !!!!

After this accident, the researchers decided to study the fracture of the materials deeply and give more importance to the mechanical phenomenon near the crack tip, which gave birth to the new science field of Fracture mechanics [1]

Fracture mechanics is mainly based on studying the crack initiation and propagation in the steels.

The material has two modes of failure ductile or brittle mode.

Steel is failed in the ductile mode; this material is used in the industry in most fields because of its mechanical properties, so it is important to study how the steel fails and how the crack behave in the material; in other words, it is needed to be able to predict its failure, especially in the nuclear field, and for example, the pipeline used in the nuclear power plants.

The pipeline leakage problem is one of the main critical issues that might affect the performance of Nuclear Power Plants [2-4]. Austenitic steel is the primary material from which pipelines are usually constructed. The majority of austenitic steels deformed plastically before failure [5].

Over the last five decades, deep research has been undertaken to explore the ductile failure of pipelines using mechanical damage models such as the Gurson Tveegard Needelman model. [6–12].

Even so, there has been no detailed investigation into predicting GTN parameters for failure of pipelines in the nuclear field using optimization models such as artificial neural networks. Most studies have only focused on direct methods to find the GTN parameters to predict the failure of

pipelines. However, little attention has been given to combining the GTN model with other optimization features, such as artificial neural networks or hybrid swarm optimization [13–19].

As a result, there is a clear gap in the literature for an optimization model based on an artificial neural network that accurately predicts the GTN parameters. In this dissertation, I present an approach to predicting GTN parameters using an artificial neural network, where the dissertation starts with a general overview of the GTN model and goes deeply into the following topics: The backpropagation approach to studying the sensitivity of GTN parameters, the use of an optimization approach for SENT (single edge notch tension) and PIPELINE; the study of the failure of SENT specimens based on subsidized specimens;

1.1. Motivation

My research interest is focused on the damage to engineering materials and analyzing industrial degradation to develop a recommendation for mitigating actions to avoid future degradation.

When researching the damage to engineering materials, one of the most important questions is extending the component's lifetime while avoiding damage to those components.

It is possible to prevent catastrophes by deeply understanding material properties, degradation processes, and external effects like temperature and radiation.

Ensuring the nuclear safety of nuclear power plants means keeping all the parts working correctly and with high performance. The pipeline is one of these parts. The leakage problem in the pipes is a critical issue that might affect the performance of the nuclear power plant if it is not detected from the beginning. The Prediction of the failure of pipelines is an important topic because it helps design the nuclear power plant parts and prevents problems that might occur due to the leakage of the pipelines.

 The European Union is financing many R and D projects dealing with nuclear safety— furthermore, issues related to pipelines leaking. Furthermore, failure prediction is based on local approaches such as the GTN model [20].

From my point of view, the Prediction of a pipeline's failure can be made smart and optimized using a combination between the GTN model and ANN tool. The concept is based on training a neural network with data found from simulations done with MARC MENTAT software [21]. After training the network, I can quickly get GTN parameters for the material of the pipelines. The model can do the same task with other specimens with different geometries.

The experiments mentioned in this study were done by the project partners, EDF France and Framatome Germany. A general overview of the experiment will be explained in the next sections.

1.2. Aims and Scope.

The main objectives of this study are to validate the applicability of the GTN model and determine the GTN parameters by using ANN for predicting the ductile failure of ferritic steel material based on different geometries.

Various sub-objectives or activities can be identified and conducted to achieve these objectives.

- The first sub-objective is to validate the usability of the GTN model: to reach the first goal, an experiment and simulations were conducted using the Marc mentat model to determine the GTN parameters required to predict the failure of the SENT specimen based on the CT specimen, In addition, the research delved into the mysterious phenomena of the convergence of GTN parameters and evaluated their sensitivity based on hundreds of simulations. The most sensitive GTN parameters were identified through this study, which can help other researchers working with the GTN model to determine the correct set of GTN parameters with greater precision.

- The second sub-objective is to apply the direct method using GTN parameters to predict the failure of a large component, which in this case is the pipeline, and analyze the time consumed during the process.

- As a third sub-objective, the study aims to optimize the time consumed when determining GTN parameters and include the backpropagation approach to reduce it; this study will be based on an NT specimen.

- Lastly, the fourth sub-objective investigates subsidized specimens as an alternative to normal-sized specimens and determines the J-R Curves.

- These sub-objectives will be conducted in a way that supports the main objective of validating the applicability of the GTN model and the GTN parameters determination through ANN for predicting the ductile failure of material for different geometries.

2. LITERATURE REVIEW

Ensuring the safety of nuclear power plants is the main goal of each country's authorities and the public; employees must follow strict guidelines and approaches to avoid reactor shutdowns and accidents.

The development in fracture mechanics during the last few years has been impressive, especially with powerful computers with high data processing speeds and simulation.

This part of the dissertation describes the literature review and is divided into four main subchapters. It starts with an overview of the local approach and its definition and presents the main models based on this approach. The following parts describe the GTN model, its parameters, and their sensitivity. The next section deals with artificial neural networks and optimization methods. Finally, the last part presents a developed optimization approach based on backpropagation analysis, which will be employed in this work.

Conclusions and remarks in the literature have mostly focused on predicting a pipeline's failure using different micromechanical models. Therefore, this work aims to fill this gap and provide an accurate way to understand how the ANN can determine accurate GTN parameters, which will lead to the main goal of predicting the failure of pipelines based on the GTN model.

2.1. Local approach for ductile failure

To answer the question, why did the Titanic sink? Thirty-three different hypotheses and assumptions were given, but the mechanical engineers could find the main reason behind this big accident: the brittle failure of the steel used in the ship's body, as the temperature was very low. The failure happened on the lower rather than the upper shelf without warming. After the Liberty ship accident, a new field of mechanics came on board: fracture mechanics.

The assumptions and investigation of fracture mechanics [22-23] began with a macroscopic approach directly applying basic continuum mechanics. No material is perfect; voids and cracks are always present and crack initiation and propagation can lead to failure.Current structural integrity studies concentrate on pre-existing cracks in structural and mechanical models that estimate crack initiation and propagation path.

The theory and analysis of fracture mechanics started with a global approach as a direct application of classical continuum mechanics. Then they switched to the concept of cracks and voids. The global approach to fracture is widely used to evaluate the structural integrity of

mechanical components. This approach is based on linear elastic fracture mechanics (LEFM) and nonlinear fracture mechanics (NLFM).

This approach is practical because, based on it, it is possible to get the main mechanical properties of the material, such as fracture resistance. Unfortunately, the global approach has many limitations, mainly the large-scale yielding and the transferability issue of the small-scale specimen to large-scale equipment. To deal with some limitations so the global approach can be overcome, The local approach was initially developed by McClintock [24-25]

The main concept of the local approach is to estimate the stress and strain near the crack tip, which could be done using the finite element method analysis.

Compared to the global approach, the local approach could deal with complex geometries and situations found in welds; for example, with the local approach, it is possible to describe and analyze the brittle fracture and the three main steps of the ductile fracture mechanism: micro void nucleation, growth, and coalescence, in this thesis I will focus on the application of the local approach for a ductile material.

During the last century, two researchers built the basics of the local approach (Rice and Tracey) [26], during which the single void was analyzed. After a few years, a well-known scientist in applied mechanics (Gurson) [27] developed the first micro-mechanical model based on microvoid nucleation. However, the Gurson model did not consider the three stages of ductile failure.

This limitation was overcome by Tvergaard and Needleman [28], which led to the development of the most used model in the industry and scientific research (GTN model).

The GTN model was applied to metals, including microvoids. Based on a local approach, another scientist, Rousselier [29], developed a model which also led to describing the crack initiation and propagation. Next, in section 2.2, the GTN model will be described in detail, as it will be the main model used in this work.

As a summary of the above paragraph in the Rice-Tracey model, void formation is highly dependent on stress-field multiaxiality. Rice and Tracey investigated the formation of an isolated vacuum in a distant uniform stress field. The model neither considers interactions between voids nor predicts ultimate failure.

The Gurson model describes progressive material degradation by introducing the void volume fraction, f, which was then modified to GTN and the Complete GTN model (Zhiliang Zhang) [30]

2.2. Rousselier model

This part is dedicated to giving a general overview of the Rousselier model because it is one of the main models based on a local approach.

Rousselier model is a micromechanical model. Describing the three stages of ductile mechanism void nucleation, growth, and coalescence [29].

The last step of ductile mechanics is the most critical part in which the voids are large enough to coalesce. They form microcracks which lead to crack initiation and propagation and, in the end, to macroscopic failure; for this reason, it is really important to be able to predict the crack initiation and propagation to avoid the failure of the material, and this is why Rousselier's model is useful.

In other words, the Rousselier model describes the damage induced by the plastic expansion of cavities in a metal. It makes it possible to model cracking and ductile fracture. The behavior model is elastoplastic or viscoplastic with isotropic hardening. It allows plastic volume changes and takes into consideration the small deformations

The yield function presents Rousselier's model as follows [29].

$$\phi = \frac{q}{1-f} + D\sigma_k f exp\left(\frac{-p}{(1-p)\sigma_k}\right) - R\left(\varepsilon_{eq}\right) = 0 \qquad \textit{Equation 1}$$

The parameters of the equation are defined below:

D and σ_k are constant parameters, and p is defined as the von Mises equivalent stress. In addition to this, q is the von Mises equivalent.

f is the void volume fraction, depending on the loading status; the void volume fraction starts with the initial void volume fraction f_0. By increasing the load, the void volume parameters reach its critical value f_c, where the voids coalesce with each other until reaching the final void volume fraction f_f; when the value of f = 0, it presents the defect-free material or f = 1 refers to material that has been damaged, for the last parameter $R(\varepsilon_{eq})$ is presented as material's true stress–true plastic strain curve/

Unfortunately, Rousselier model is more rarely implemented in industrial computer codes than the GTN model, which slows down its development.

Many authors made their studies based on an enhanced, modified Rousselier model; for example, (M. K. Samal. 2013) [31] used the Rousselier model to find the mechanical properties of

Zircaloy Fuel Pin Specimens; also (S. D. Zhao et al. 2014) [32] could analyze the failure behavior of clinched joint based on Rousselier model.

The next section will describe in detail the GTN model

2.3. GTN model

2.3.1. Introduction

The Gurson–Tvergaard–Needleman (GTN) model was frequently used to assess ductile damage and fracture processes. One of the most extensively utilized ductile damage models is GTN.

In 1975, Gurson developed a fundamental model that permits the Prediction of crack initiation and propagation using finite element calculations.

As the majority of materials fail in the ductile regime, the development of a model was needed to study the mechanical behavior of the material locally.

The GTN model was chosen in this research for its simplicity and recognition in the industry field. Many studies prove that the model successfully describes the ductile deformation behavior of materials with accurate results.

The GTN model is already implemented in MSC MARC Mentat software and allows determining GTN parameters without considering the void nucleation parameters.

However, no literature was found on the issue related to the time consumed to implement the GTN model and predict the failure of materials. The GTN model predicts the frictional effects, stress states, and displacements.

Implementing the GTN model requires determining different material parameters, and simulation procedures are required.

The successful implementation of the GTN model during the design phase would be beneficial to the nuclear industry in getting more specific and accurate data about material behavior during its service life and the conditions that might lead to material failure, which for instance, helps to boost the final product quality and ensure long-term service operation without failure.

In 1970, Gurson was one of the earliest researchers to study and develop a micromechanical model for ductile metal deformation, including micro voids.

2.3.2. Presentation of GTN model

As already mentioned, the idea of Gurson is based on the model of Rice and Tracy. Gurson [27] suggested a micromechanical model based on a fracture mechanics perspective, such as the critical evolution of voids.

Gurson developed an approximate yield criterion for ductile materials by proposing a continuum theory for ductile failure based on void nucleation and void growth and by showing the important role of hydrostatic stress in plastic yield and void growth. The yield criterion developed by Gurson took the idealization of the material matrix as being perfectly rigid and obeying the Von Mises yield criterion.

Gurson examined the approximate limit of a hollow sphere (elementary representative volume characteristic of a medium porous) plastic (Fig.1)[20], obeying the von Mises criterion and exposed to any loading inspired by the Rice and Tracey model.
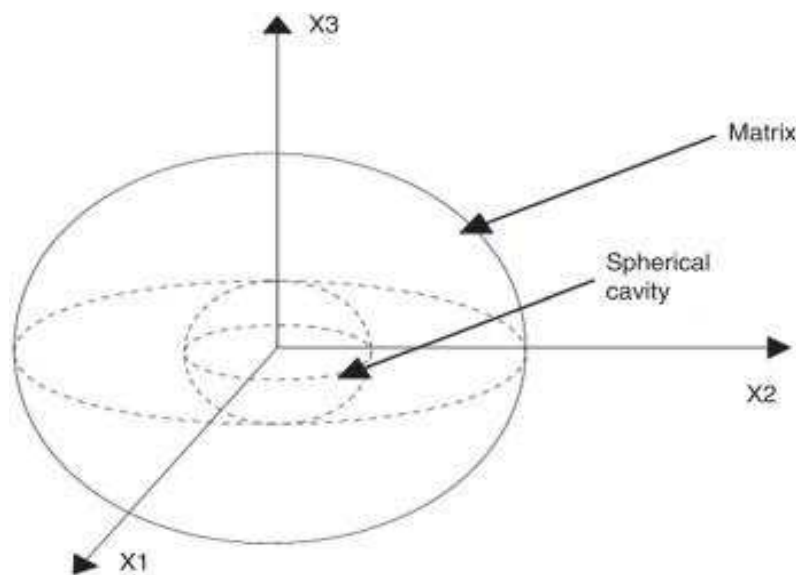
Figure 1. Hollow sphere with a spherical void

The Gurson model allows the fraction of cavities to range from 0 to 1, unlike the Rice and Tracey model's zero porosity.

Gurson presented a threshold function that links plastic hardening with the new variable, porosity f, which represents the fraction of cavities in the matter.

For hard, completely plastic materials, the estimated yield requirement was first proposed as follows:

$$\phi = \left(\frac{\sigma_e}{\sigma_0}\right)^2 + 2f\cosh(\frac{3\sigma_h}{2\sigma_0}) - (1+f^2) \hspace{2cm} \textit{Equation 2}$$

In which the parameters of the function are defined below

σ_0 is the equivalent flow stress, σ_e the effective stress σ_h is the hydrostatic stress, and f is the void volume fraction

The von Mises equivalent stress σ_e is defined according to the stress tensor below :

$$\sigma_e = \sqrt{(\sigma_1 - \sigma_2)^2 + (\sigma_2 - \sigma_3)^2 + (\sigma_3 - \sigma_1)^2} \hspace{2cm} \textit{Equation 3}$$

Alternatively, the main parameters in the Gurson model, which is the void fraction volume, are defined as :

$$f = (\frac{1}{V_t})(V_t - V_0) \hspace{2cm} \textit{Equation 4}$$

The parameter V_0 is the volume of the matrix without counting the voids and V_t is the global material volume.

By pretending in equation 2, $\phi = 2f - (1+f^2) = 0 \ \sigma_e = 0 \ \ \sigma_h = 0$ we will find the following equation :

$$\phi = 2f - (1+f^2) = 0 \hspace{2cm} \textit{Equation 5}$$

After a quick analysis of the above equation, it is obvious that the failure of the material will occur when the value of f is changed. In this case, the material is fully voided. The Prediction will not be correct because, originally, the material had to go through three steps for the ductile failure, as already mentioned. It cannot be described as a fully voided material.

As already mentioned, more modifications will be needed to modify the Gurson model, and it can be a great and powerful tool to predict ductile failure, which means it covers the three steps (nucleation, propagation, and coalescence)

To cover the limitations of the Gurson model, the first modification was made by Tveegard (1981), in which they introduced new material constants q_1, q_2, and q_3. The introduction of the new constants improved the Prediction of the Gurson model, and the following equation gives the new modified model:

$$\phi = \left(\frac{\sigma_e}{\sigma_0}\right)^2 + 2q_1 f\cosh(\frac{3q_2\sigma_h}{2\sigma_0}) - (1+q_3 f^2) \hspace{2cm} \textit{Equation 6}$$

The Gurson model only depicts the growth stage of material failure; it has to be expanded to include the nucleation and coalescence stages. As a result, in 1986 [28], Tveegard and Needlman were able to make several modifications to the Gurson model and introduce new parameters, as shown in the modified model of the Gurson model that gave birth to the GTN model, with the definition of the new parameters defined in this section:

The model is defined as follows:

$$\phi = \frac{\sigma_e^2}{\sigma_M^2} + 2q_1 f^* \cosh\left[\frac{tr\sigma}{2\sigma_M}\right] - \left(1 + q_1^2 f^{*2}\right) \qquad \text{Equation 7}$$

In which q_1 is the material constant, $tr\sigma$ is the sum of principal stresses, σ_M is the equivalent flow stress, and f^* is the ratio of effective void volume to the material volume ratio defined as follows:

$$f^*(f) = f_c \quad \text{If } f \leq f_c \qquad \text{Equation 8}$$

$$f^*(f) = f_c + \frac{(1/q_1) - f_c}{f_f - f_c}(f - f_c) \quad \text{If } f \geq f_c \qquad \text{Equation 9}$$

Where f is the voids volume ratio, f_c is the void volume ratio at the beginning of nucleation, f_f is the void volume ratio when a fracture occurs, or σ_M is the equivalent flow stress.

The void growth rate is the sum of existing void growth f_g and the new void nucleation f_n, and the following equation presents it:

$$\dot{f} = \dot{f}_n + \dot{f}_g \qquad \text{Equation 10}$$

Where the components are further formulated as follows:

$$\dot{f}_g = (1 - f)tr\varepsilon^{pl} \qquad \text{Equation 11}$$

$$\dot{f}_n = A\varepsilon_M^{pl} \qquad \text{Equation 12}$$

$$A = \frac{f_n}{S_n\sqrt{2\pi}}\exp\left[-1/2\left(\frac{\varepsilon_M^{pl} - \varepsilon_N}{S_N}\right)\right] \qquad \text{Equation 13}$$

In $tr\varepsilon^{pl}$ the volume plastic strain rate, S_N is the voids nucleation mean quantity, f_n is the volume ratio of the second phase particles (responsible for the voids nucleation), and ε_N is the mean strain at the time of voids nucleation.

So eight parameters have to be defined:

$$\phi = \phi(q_1, q_2, f_0, f_c, f_n, f_f, \varepsilon_N, S_N)$$

The values of q_1 and q_2 are almost constant based on several studies on determining GTN parameters for different parameters, as shown in the table below.

$$q_1=1, q_2=1.5.$$

Table 1 GTN parameters for different materials

References	q_1	q_2	E_N	S_N	f_0	f_c	f_n	f_f	Material
Bauvineau et al. (1996) [33]	1.5	1	-	-	0.002	0.004	-	-	CMn Steel
Decamp et al. (1997) [34]	1.5	1	-	-	0.0023	0.004	-	0.225	CMn Steel
Schmitt et al. (1997) [35]	1.5	1	0.3	0.1	0	0.06	0.002	0.212	Ferritic base Steel
Skallerud and Zhang. (1997) [36]	1.25	1	0.3	0.1	0.0003	0.026	0.006	0.15	CMn Steel
Benseddiq and Imad. (2008) [37]	1.5	1	0.3	0.1	0	0.004-0.06	0.002-0.02	~0.2	

Not only did Tveegard and Needleman try to modify the Gurson model, but various researchers have also tried to develop an extended GTN model to be useful in different complicated situations in the last two decades. Its popularity and success are based on experimental evidence.

In 2008, Nahshon and Hutchinson [38] developed an extended version of the GTN model that deals with shear-induced damage.

In 2014, Zhou et al. [39] introduced new shear damage-related parameters to the GTN model based on experimental results. In 2000, Z.L. Zhang et al. developed a complete Gurson model approach for ductile fracture [40].

2.4. Presentation of some extended GTN models

A significant shortcoming of models based on the Gurson technique is the absence of shear effects in the formulation. This result eliminates the possibility of forecasting the site of shear and failure under low-stress triaxiality circumstances. Under dominant shear stress, the distortion of the cavities and ligaments between the cavities is critical in the progression of the material's

internal deterioration. Thus, to enhance the predictive power of the GTN model at low levels of constraint triaxiality, L. Xue [41], Nahshon, and Hutchinson [38] proposed including a shear mechanism in the law of cavity evolution.

I will start first by giving a general overview of the extension done by L. Xue

The process is based on geometric considerations involving a unit cell construction with a circular vacuum at its center subjected to simple shear stress. According to the author, the progression of shear damage (f_{shear}) depends on the porosity, the corresponding plastic strain, and the Lode angle. This mechanism's rate of change may be mathematically represented as:

$$f_{shear} = q_4 f^{q_5} g_0 \dot{\varepsilon} \varepsilon^p$$
<div align="right">*Equation 14*</div>

q_4, q_5 reflect the material's component parameters.

For issues with two dimensions, $q_4 = 1.69$ et $q_5 = 0.5$, and three-dimensions $q_4 = 1.86$, and $q_5 = 0.33$

The variable f, which denotes porosity, is the equivalent strain and is the parameter that introduces the shear mechanism's reliance on the Lode angle. If it is greater than zero, the shear mechanism is considered. If, on the other hand, it is zero, the shear mechanism does not influence the damage evolution, and only the nucleation and growth mechanisms are active.

The Lode angle function is defined as follows:

<div align="right">*Equation 15*</div>

$$g_0 = 1 - \frac{6|\theta|}{\pi} = 1 - |\bar{\theta}|$$

Where is θ the Lode angle given, and where $|\bar{\theta}|$ is the normalized Lode angle, the load angle is given by the equation below

$$\theta = \tan^{-1}\left\{ \frac{1}{\sqrt{3}}\left[2\left(\frac{s_2 - s_3}{s_1 - s_3} \right) - 1 \right] \right\}$$
<div align="right">*Equation 16*</div>

s_1, s_2, s_3 are the tensor components of deviatoric stresses in the primary plane.

The shear process provided by L. Xue [41] is compatible with the GTN model, which already includes micro-void nucleation and growth mechanisms. Thus, the development of porosity is reinterpreted as follows:

$$f = f_c + f_n + f_{shear}$$

Damage that accumulates in a material reduces all of its elastic qualities. However, this effect is minor compared to the effect of damage on plastic behavior. As a result, the evolution rule of

shearing damage does not account for the term total strain. It is characterized solely in terms of cumulative plastic strain and the pace at which it accumulates.

$$f_{shear} = q_4 f^{q_5} g_0 \, \dot{\varepsilon} \, \varepsilon^p$$

Equation 17

In the next section, I will briefly introduce the extension done by K. Nahshon and J. Hutchinson.

The two scientists, K. Nahshon and J. Hutchinson provided an extra word f_{shear} to characterize the shear mechanism in addition to the one established by L. Xue.

$$f_{shear} = k_w \frac{f w_0(\sigma)}{q} S : \dot{\varepsilon}^p$$

Equation 18

where $w_0(\sigma)$ is a function of the third normalized invariant's stress state ξ. The parameter k_w is a component parameter of the material used in this procedure. The following is the syntax for the parameter.

$$w_0(\sigma) = w(\xi) = 1 - (\xi)^2$$

Equation 19

It is critical to note that $w(\xi)$ it does not allow for exact differentiation of some stress levels, such as the two axisymmetric states represented by:

    a) equal tension between two minor principal stresses (uniaxial tension with $\xi = -1$

    b) equal tension between two principal stresses (biaxial tension $\xi = 1$

    Ultimately, K. Nahshon and J. Hutchinson's alteration is phenomenological. f can be interpreted as either an effective volume fraction of the cavities or a basic damage measure.

2.5. Complete Gurson Model

With the assumption that all voids remain spherical as external loading increases, and by applying Thomason's void coalescence criterion based on the plastic limit load model, this resulted in the so-called Complete Gurson Model (CGM).

The critical void volume fraction (fc) is a material constant in the GTN model. Still, the complete Gurson model is the material's reaction to coalescence.

According to Zhang et al. [40]., the value of fc decreases as the stress triaxiality ratio T rises (Fig. 2). Additionally, Zhang et al. have demonstrated that the initial void volume fraction f0 strongly influences the value of fc.

Stress triaxiality measures the stress in a material at the tip of a crack. It is described as the relationship between the equivalent plastic strain, which reflects the material's plastic deformation, and the hydrostatic stress, which indicates the material's average stress.

Because it can influence the possibility of crack propagation and fracture, stress triaxiality is crucial to understanding fracture mechanics. A ductile fracture, in which the material experiences extensive plastic deformation before failing, can be encouraged by high levels of stress triaxiality.

While brittle fracture, in which the material fails with little to no plastic deformation, can be promoted by low levels of stress triaxiality, which is the opposite, is a possibility.

The GTN model's critical void fraction is crucial because it controls when metals, including microvoids, switch from ductile to brittle failure modes. The material can bend plastically and exhibit ductile behavior when the volume percentage of voids in the material is smaller than the critical void fraction. Yet, the material becomes more brittle and prone to fracture when the volume proportion of voids exceeds the critical void fraction.

The critical void fraction for a given material is normally determined experimentally since it relies on several variables, including the composition of the material, the loading circumstances, and the size and form of the voids.

The critical void fraction in the Gurson-Tvergaard-Needleman (GTN) model is a dimensionless quantity, as it is defined as the ratio of the volume of voids or pores to the total volume of the material.

The complete Gurson model is precise for both non-hardening and hardening materials
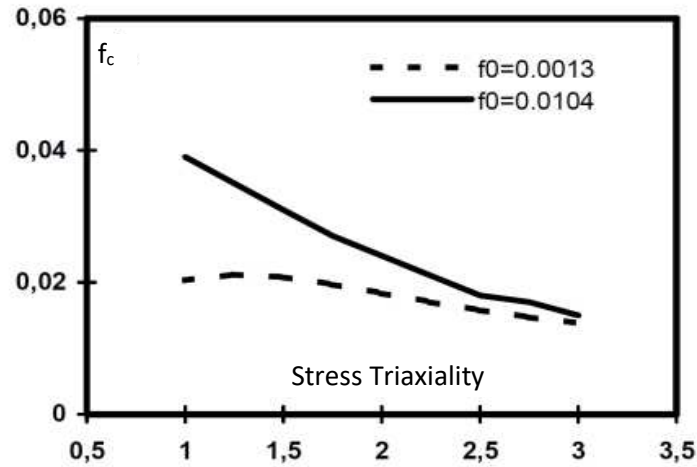
Figure 2. Critical void volume fractions versus stress triaxiality [40]

As explained, the CGM considers the value of the critical void volume fraction as non-constant, or for the GTN model, the value of f_c is a material constant in which the failure occurs when $f \geq f_c$ *(Please see the paragraph regarding the GTN model for more details)*

Following this condition, in the GCM model, the value of f_c is defined by Thomason's plastic limit-load criterion, as shown below [40], which forecasts the beginning of coalescence.

$$f \geq f_c$$

The parameters of the above condition are defined as follows :

α = 0.1

β = 1.2

For the values of (α and β) were fitted by Thomason, the parameter σ_m is defined as the maximum principal stress

Furthermore, the value of r is defined as the void space ratio, and it is given by the equation below :

$$r = \sqrt[3]{\frac{3f}{4\pi} e^{(\varepsilon_1 + \varepsilon_2 + \varepsilon_3)}} \left(\frac{\sqrt{e^{(\varepsilon_1 + \varepsilon_2)}}}{2} \right)^{-1}$$

Equation 20

Regarding the parameters ε1, ε2, and ε3, they represent the principal strains

As mentioned in this thesis, the full focus was given to the GTN model. However, it will be important in further studies or similar studies to use the complete Gurson model.

After the detailed presentation of the GTN model, in the next section, the focus will be given to the artificial neural network as the optimization approach used in this thesis

2.6. Artificial intelligence and optimization methods

2.6.1. Introduction

In recent years, the computer technology used in nuclear reactors has expanded.

The research area of artificial neural networks is attracting researchers and investors in the industry, which leads to providing funding to universities and research institutes to develop ANN applications in many areas [42-44]

Many studies show that the ANN has a very strong ability to learn the input-output relationship of a nonlinear system through training with sufficient data [45-46]

As mentioned in the section related to the GTN model, it is necessary to determine the eight parameters that should have physical meaning.

Respecting the literature, the relationships between the eight parameters create a nonlinear system, so using ANN in determining those parameters might lead to developing an appropriate approach to finding the GTN parameters.

This thesis aims to use the artificial neural network to determine the GTN parameters set for CT, SENT, and pipeline.

Therefore, the next section will be more focused on the basics of ANN, its architecture, and the learning algorithms used for training the network

So as a short conclusion, it is not easy to determine GTN parameters, so it is quite important to find a solution for such an issue by implementing the artificial neural network in determining GTN parameters by paying more attention to the most sensitive GTN parameters. The next section will mainly focus on the literature review on artificial neural networks.

2.6.2. General overview of Artificial neural network

An Artificial Brain Network (ANN) is a mathematical model that simulates biological neural networks in terms of computing [47-49]. It comprises interconnected artificial neurons that use a connectionist approach to interpret data.

The ANN can respond to changes in external or internal data that flow through the network during the learning process. ANN's main rules are assisting machines in completing tasks and

developing self-learning. Artificial neural networks (ANNs) are a key component of machine learning and are used to identify patterns in data. As a result, ANNs are the best answer for data classification, grouping, and Prediction.

In the field of mechanical engineering, the ANN can be used in different fields, as shown below :

- Autonomous Systems: ANNs can be used for autonomous systems, such as self-driving; the neural network can learn from sensor data and make real-time decisions, allowing the system to operate autonomously.
- Manufacturing: ANNs can be implemented in this field in order to perform manufacturing optimization, such as predicting defects in parts or optimizing production processes for improved efficiency.
- Robotics: ANNs can be used in this field to learn a robot arm's movement patterns or predict the outcomes of different control strategies. Energy Systems: ANNs can be used for energy systems, such as predicting energy consumption or optimizing the performance of renewable energy.
- Overall, ANNs offer a powerful tool for mechanical engineers to analyze data, optimize systems, and improve performance across various applications.

There are not many activities that an artificial neural network cannot complete once trained. An artificial neuron was created to simulate the biological function of a neuron in the human brain. A biological neuron is made up of dendrites (inputs), soma (cell body), and axons (outputs), as described in Fig.3[50]
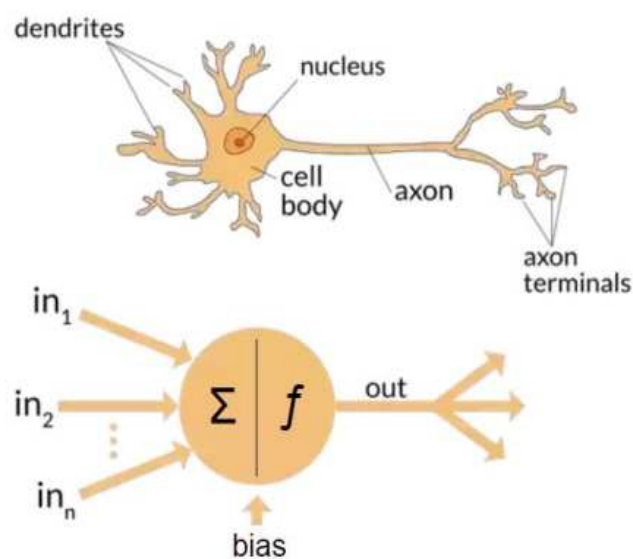
Figure 3. Neuron network and the human brain

The structure of the human brain is reproduced in a very basic fashion while building artificial neural networks. As a result, the mathematical model of an artificial neuron and the structure of a real neuron have certain similarities.

However, important distinctions in the working principles of biological and artificial neurons are beyond this article's scope. Of course, the human brain's structure is not known.

An artificial neural network is a collection of basic neural processors.

2.6.3. Simple mathematical model of a neuron

Through its synaptic connections, the neuron is activated with n inputs, as shown in Fig. 4 [51]
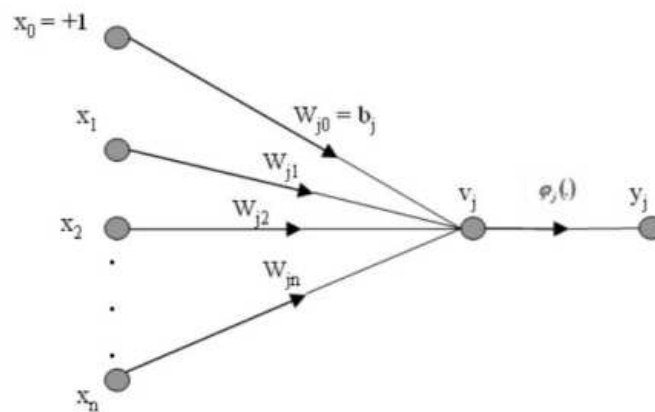
Figure 4. Single neuron description

Each synaptic connection has a weight, a positive or negative value indicating the connection's strength.

To get the induced local field v_j, each input is multiplied by the synaptic connection's weight. The weighted inputs are added along with an externally supplied bias.

On a directed graph, bias is represented by a synaptic weight with a constant input of +1. Then, on the local induced field of the neuron, an activation or squashing function φ_j is applied to v_j of the neuron, which leads to the output yj of neuron j.

The activation function reduces the output range to a certain interval.

These parameters shown in Fig. 4 are defined mathematically as follows :

n is the number of input data

The input vector x_i :

$$E = 1/n \sum_{j=1}^{n} (F_{ij} - Rij)$$

<div align="right">Equation 21</div>

The weight vector :

$$w_{ji} = \left[w_{j1}, ... w_{jn} \right]$$

<div align="right">Equation 22</div>

The induced local field v_j :

<div align="right">Equation 23</div>

$$v_j = \sum_{j}^{n} w_{ji} x_i$$

The bias b_j:

$$b_j = w_{j0} x_0$$

<div align="right">Equation 24</div>

The output parameter is defined as y_j :

$$y_j = \varphi(v_j)$$

<div align="right">Equation 25</div>

2.6.4. Learning Styles

There are two main learning models.

- Supervised Learning

A training example consisting of an input and the desired output is provided to the network in supervised learning. The network's synaptic weights are then changed to minimize the discrepancy between the actual network output and the intended output. [52]

Supervised learning is distinguished by how it trains computers to classify data accurately or predict outcomes using labeled datasets. The model modifies its weights as input data is fed into it until the model has been properly fitted, which takes place as part of the cross-validation process. Such as classifying spam in a different folder from the email; supervised learning assists enterprises in finding scalable solutions to several real-world issues.

- General overview of the process of supervised learning

A training set is used in supervised learning to instruct models to produce the desired results. This training dataset has the right inputs and outputs, enabling the model to develop over time. The loss function verifies the algorithm's correctness, and iterations are made until the error is sufficiently reduced.

When using data mining, supervised learning may be divided into two issues: regression and classification.

In order to accurately classify test data into different categories, the classification uses an algorithm. It identifies particular entities in the dataset and tries to determine how those things should be defined or labeled.

Regression is used To comprehend the relationship between dependent and independent variables; It is frequently used to produce estimates for a company's sales revenue.

The most known regression algorithms include linear, logistic, and polynomial regression.

- Different algorithms for Supervised learning

Various computing methods and algorithms are applied during supervised machine-learning operations.

The most popular learning techniques are briefly explained below [53], often calculated using software like R, Python, or MATLAB :

✓ Simple Bayes: A classification method known as Naive Bayes adopts the idea of Class Conditional Independence from the Bayes Theorem. This means that each predictor has an equal impact on the outcome and that the existence of one feature does not affect the presence of another in the probability of a certain result. Multinomial Nave Bayes, Bernoulli Nave Bayes, and Gaussian Nave Bayes are the three varieties of Nave Bayes classifiers.

✓ Linear regressive: To predict future outcomes, linear regression is frequently employed to determine the relationship between a dependent variable and one or more independent variables. Simple linear regression is used when there is only one independent variable and one dependent variable. It is called multiple linear regression as the number of independent variables rises. It attempts to plot a line of best fit for each type of linear regression, which is determined using the least squares method. When shown on a graph, this line is straight in contrast to other regression models.

✓ Rational regression: While logistical regression is used when the dependent variable is categorical or has binary outputs, such as "true" and "false" or "yes" and "no," linear regression is used when the dependent variable is continuous. Even though both regression models aim to identify the relationships between the data inputs, logistic regression is mostly employed to address binary classification issues, such as spam identification.

✓ Narrowest-neighbor first: The KNN algorithm, also called K-nearest neighbor, is a non-parametric algorithm that groups data points according to their proximity and correlation with other accessible information. This approach assumes that related data points can be discovered closely. It then assigns a category based on the most general category or average after attempting to determine the distance between data points, typically by Euclidean distance. Data scientists favor it because of how simple it is and how quickly calculations are completed. However, as test datasets get larger, the processing times are longer, which makes them less desirable for classification jobs. KNN is frequently employed in image recognition and recommendation systems.

- Unsupervised Learning

There is no intended outcome in this scenario. The network's synaptic weights are adjusted until the network's output is a suitable representation of the input data. [52]

In addition, unsupervised learning analyzes and groups unlabeled datasets using machine learning algorithms. These algorithms identify hidden patterns or data clusters without the assistance of a human. It is the best option for exploratory data analysis, cross-selling tactics, consumer segmentation, and picture identification because of its capacity to find similarities and differences in information.

- The three most effective methods for neural networks

✓ Neural network for classification

A neural network can classify a pattern or dataset into a preset class. By employing the Feedforward Networks

✓ Neuronal Prediction Network

A neural network can be taught to generate predicted results from a given input—for instance, stock market forecasting.

✓ Neural Association Network

Train the Neural Network to remember the particular pattern. The network links the noise pattern with the memory's nearby one or discards it when offered. For instance, Hopfield Networks does grouping, classification, and other tasks.

2.6.5. Main ANN algorithms

The arrangement of neurons in layers and the pattern of synaptic connections between them inside and between layers are referred to as "architecture" in neural networks.

A layered network has an input layer of source nodes, an output layer of computational nodes and neurons, and one or more hidden layers of neurons between the input and output levels. Depending on the nature of connections between neurons, there are two primary groups of neural network designs.

➢ Feed-Forward Neural Networks

Feed-forward neural networks were chosen as an example of an artificial neural network since they are the most common and are utilized in a wide range of applications.

As the name suggests, artificial neural networks are modeled after their biological counterparts, the brain and the nervous system. A biological brain's structure and information processing methods are completely distinct from those of a traditional digital computer. The biological brain is significantly more sophisticated and superior to traditional computers in many aspects, with the human brain serving as an ideal example.

The ability of a biological brain to perform the adaptative learning that a traditional computer lacks is its most important point of differentiation. Conventional computers execute predetermined tasks based on the "programs" or "software" installed. A "neuron" is the fundamental unit of a neural network. One may think of a neuron as a processing element. Neurons in a neural network are linked by "synaptic weights," or "weights" for short. Each neuron in a network receives "weighted" information from the neurons to which it is connected via these synaptic connections and creates an output by processing the weighted sum of these input signals (which can be either external inputs from the environment or other neurons' outputs) through an "activation function." The network is referred to as a "feed-forward neural network" if there is no "feedback" from the outputs of the neurons towards the inputs throughout the network. Otherwise, Neural networks are typically organized into "layers." Feed-forward neural networks can be divided into "single-layer" or "multi-layer" categories depending on how many layers there are.

Fig. 5 [54] shows a fully linked single-layer feed-forward neural network. There are two layers in this structure, counting the input layer. However, it is not counted because there is no calculation in the input layer.

The output layer receives input signals via the weights, and the neurons compute the output signals.
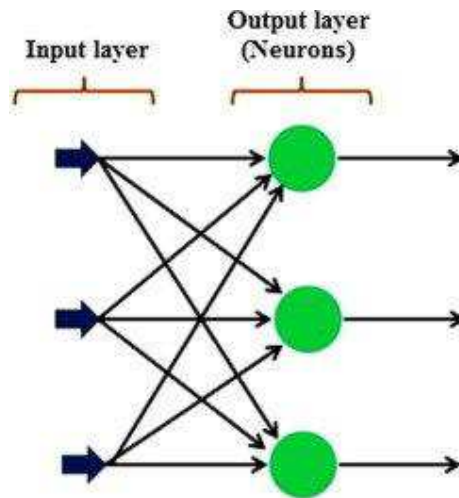
Figure 5. Singe layer network

Regarding the multi-layer feed-forward neural network, there is (at least) one layer of "hidden neurons" between the input and output layers as opposed to a single layer in a single-layer network.

The role of hidden neurons is to make a meaningful relation between the network output and external input. The network can retrieve higher-order statistics thanks to one or more hidden layers.

Because there are three input neurons, three hidden neurons, and two output neurons in the example network shown in Fig. 6 [54], there is only one hidden layer. The network is known as a 3-3-2 network. Because every neuron in each layer is coupled to every other neuron
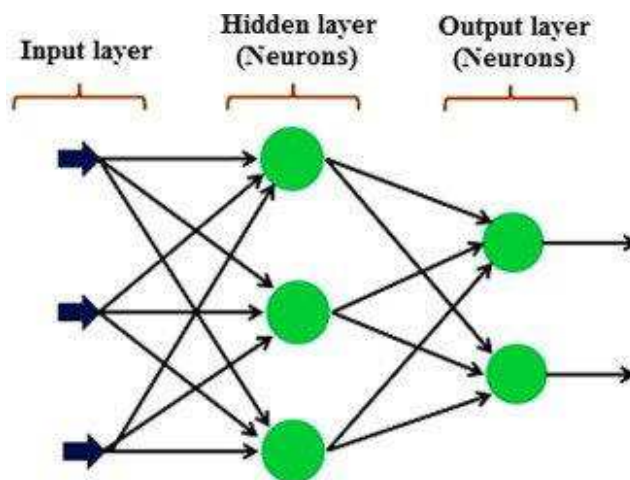
Figure 6 multi-layers network

➢ Recurrent Neural Networks

the network is regarded as a "recurrent neural network" if there is feedback or a synaptic link from the outputs to the inputs (either their inputs or the inputs of other neurons).

In other words, an artificial neural network that employs sequential or time series data is known as a recurrent neural network (RNN). Well-known programs like Siri, voice search, and Google Translate include these deep learning algorithms. They are frequently employed for ordinal or temporal issues, such as language translation and speech recognition. \

Recurrent neural networks (RNNs) use training data to learn like feed-forward.

They stand out due to their "memory," which allows them to affect the current input and output using data from previous inputs.

Recurrent neural networks' outputs depend on the previous parts in the sequence, unlike typical deep neural networks, which presume that inputs and outputs are independent. Unidirectional recurrent neural networks cannot account for future events in their forecasts, even though they would be useful in deciding the output of a particular sequence. [55]

The RNN has a "memory" that retains all calculations-related data based on what was already mentioned. It executes the same action on all the inputs or hidden layers to produce the output, using the same settings for each input. Contrary to other neural networks, this decreases the complexity of the parameter set.

• Difference between FNN and RNN

The way that RNNs and feed-forward neural networks channel information gives them their names.

Information only flows in one direction in a feed-forward neural network—from the input layer to the output layer via the hidden layers. The network receives the information without any delays. Feed-forward neural networks are poor at making predictions because they do not recall the information they receive.

A feed-forward network has no concept of time order because it considers the current input. It cannot recall anything from the past outside its schooling.

The information in RNN loops back on itself.

It takes into account both the current input and the lessons it has learned from prior inputs when making a decision.

The Figures below [55] will show how the data flow between FNN and RNN,
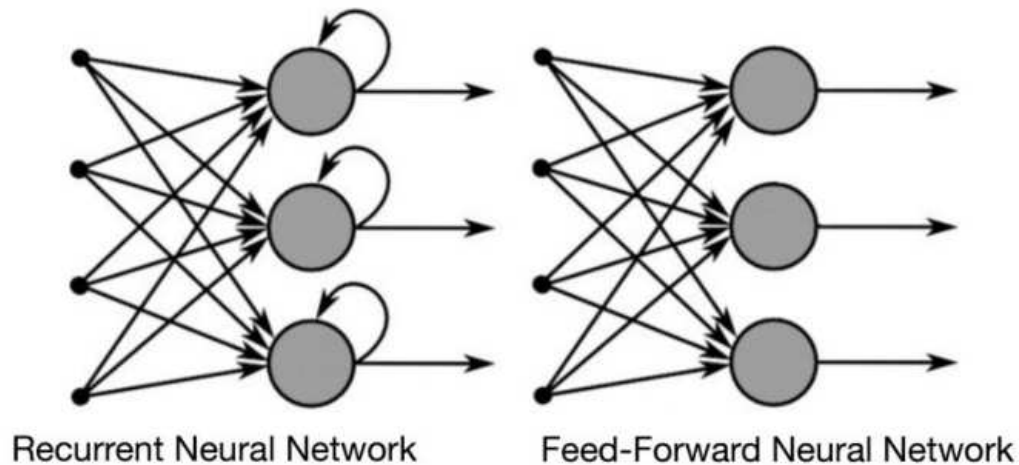
Figure 7. RNN vs. FNN

In this next section, I will focus on the Main training methods used for feed-forwards networks because it related to the main optimization method (backpropagation algorithm) used in this thesis

2.7. Main training methods used for feed-forwards networks

2.7.1. Gradient Descent Algorithm

Finding a local minimum or maximum of a given function is done using the iterative first-order optimization process known as gradient descent.

The gradient descent algorithm technique is frequently used in machine learning.

This algorithm is typically taught at the start of almost all machine learning courses because of its significance and simplicity of implementation, and it is frequently utilized in a variety of fields, including management engineering (robotics, chemical, mechanical)

The gradient descent algorithm aims to reduce the supplied function (say, cost function).

The Cost Function is a function that evaluates how well a model performs given a set of data. The Cost Function quantifies and displays the mistake as a single real number between the predicted and expected values.

The cost function increases and improves machine learning efficiency by allowing it to discover the local or global minimum and minimize error. Until the cost function approaches zero Fig. 8 [56-57], it continues to iterate in the negative gradient direction. The model will stop learning after reaching this point of the sharpest drop. Even while the cost and loss functions are often assumed to be the same, there is a slight distinction between the two. A cost function determines

the average error over the entire training set. In contrast, a loss function refers to the error of a single training sample. This small distinction between the two functions concerns the error that occurs during the training of machine learning models.
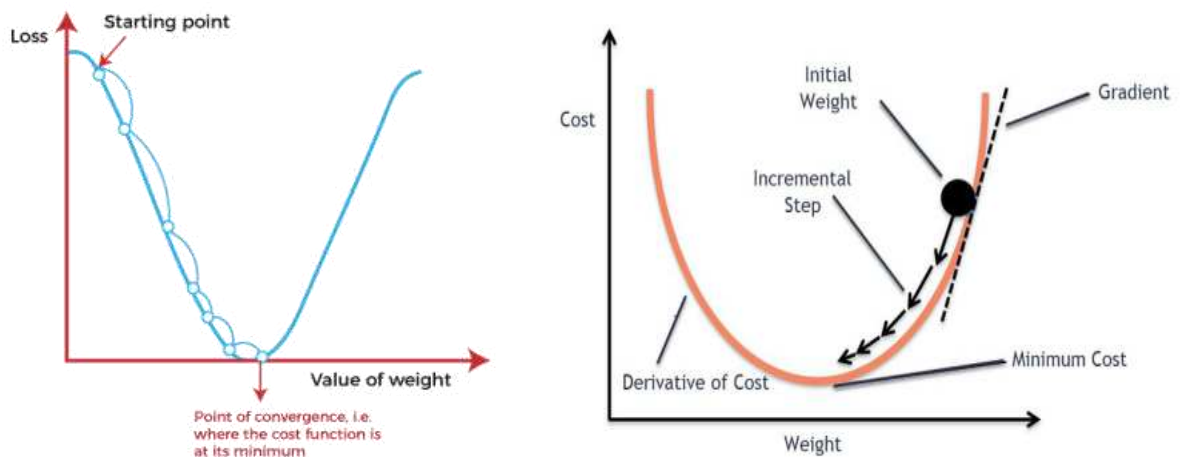
Figure 8. Gradient descen funcion

2.7.2. Back propagation algorithm

The backpropagation algorithm was developed by Bryson and Ho [58] and modified by Werbos [59]. Much research has made modifications to make the algorithm more understandable. In 1986, three researchers published two papers [60] and [61] (Ronald Williams, David Rumelhart, and Geoffrey Hinton) related to the backpropagation algorithm.

That research discusses various neural networks in which Backpropagation works far quicker than prior ways of learning, allowing neural nets to tackle previously unsolvable problems.

The backpropagation method is now the backbone of neural network learning.

It is important to highlight that the backpropagation algorithm is a quick, basic, and straightforward programming method.

It is a typical approach that works well in most cases. In addition, it does not need any particular statement of the functions to be taught.

➢ The architecture of the Backpropagation algorithm

The network's synaptic weights are initially assigned random values during training. After that, the network is given a training example at each iteration. An input and its corresponding target form the basis of a training example. Simulation data is used to generate training examples.

The network generates an output and compares it to the target by processing the input. The difference between the target and the output determines the error. The training algorithm adjusts the network's synaptic weights proportionally to the error. The training process aims to reduce the error below a predetermined value iteratively and necessitates a training set consisting of many training examples. [62-64].

In other words, the main goal of Backpropagation is to minimize the error between the output and the target by optimizing the weights.

The analysis of Fig. 9 [65] and Fig. 10[55] will better understand the backpropagation algorithm and help us summarize the back propagation's main steps

- Calculate the error; what is the difference between the model's output and the real output?
- Minimum error—Determine whether or not the gap has been minimized.
- Update the parameters: If the gap is significant, the parameters should be updated (weights and biases).
- Check the error once again after that. Repeat the procedure until the mistake is reduced to a bare minimum. The model is ready to provide a prediction.
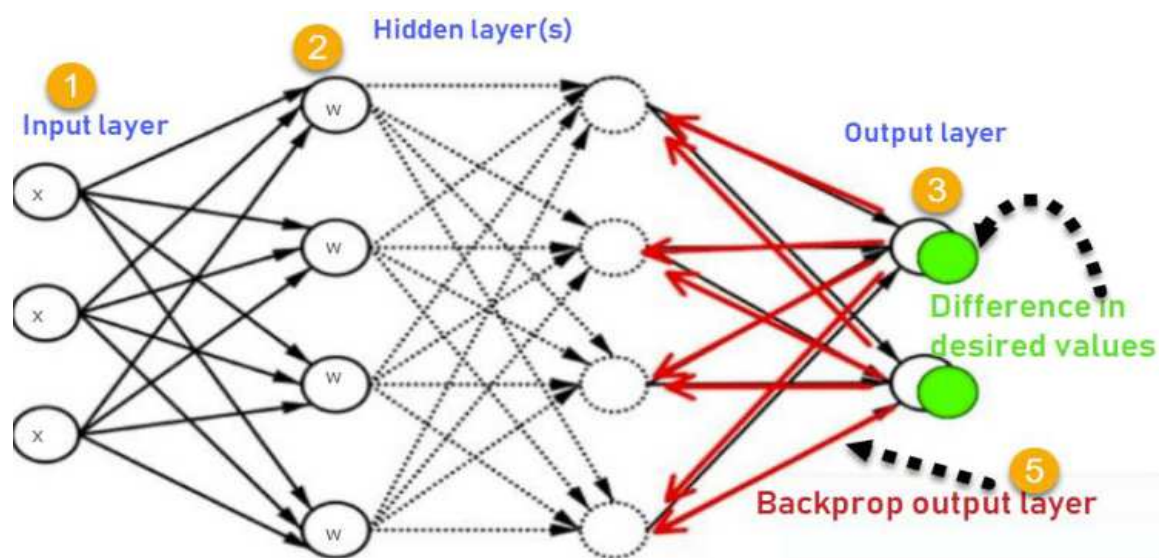
Figure 9. Backpropagation algorithm
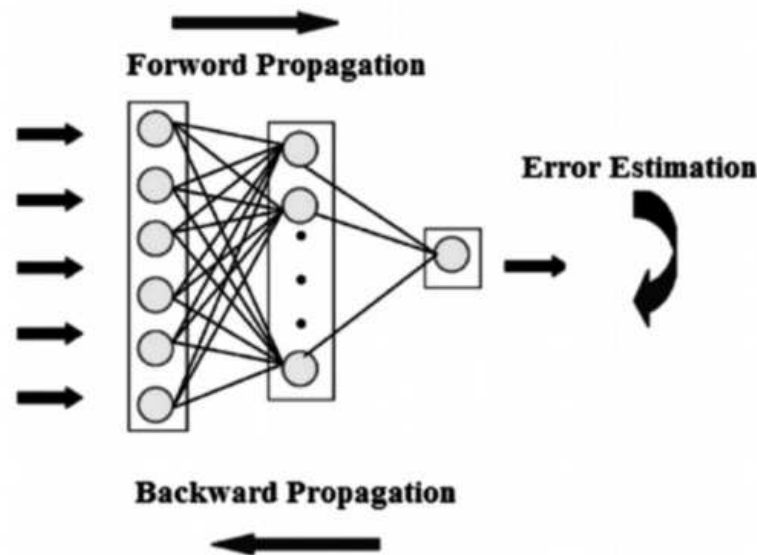
Figure 10. Backpropagation vs. Feed-forward propagation

Every input to the network is multiplied by the weights on the connections between neurons, then summed before using an active function to generate an output.

The backpropagation technique reduces the error between the output and the goal by propagating the error back into the network.

According to the amount of the initial error, the weights on each of the connections between the neurons are altered.

After that, the input data is sent forward again, resulting in new output and error.

The method is repeated until the error is reduced to an acceptable level.

Each neuron has a sigmoid function and is completely linked to the following layer's neuron, or the sigmoid function is defined as $F_{ij} = \dfrac{1}{1+e^{-x_{ij}}}$ in which is the output of a neuron I was given an input pattern j, and xij is the total input to the ANN, the backpropagation method requires the derivative of the output function to the total input to update the weights. As a result,

$$\frac{\partial F_{ij}}{\partial^{x_{ij}}} = F_{ij}(1 - F_{ij})$$

<div align="right">Equation 26</div>

The training is stopped once the error reaches an acceptable level.

A backpropagation neural network has a simple design that consists of H layers of processing neurons for the coming inputs, which are the outputs of the preceding layer. The result of each processing neuron on the n_{th} layer is fed into every neuron on the $n+1_{th}$ layer. The last layer

generates estimated outputs, and the layers between the input and output are the hidden layers (f

The main part of the Backpropagation is the calculation of the mean squared error (E), which is presented as follows:

$$E = 1/n \sum_{j=1}^{n} (F_{ij} - Rij)$$

n is the number of predictions, Fij is the output data (predicted result), Rij is the target value, and the Backpropagation aims to minimize the E value.

In the next chapter, I will be proceeding with the main part of the thesis, which is the experimental part

RESEARCH AND RESULTS

This section details my study and findings on determining GTN parameters, and it is divided into numerous theses. I used many tools and procedures in each thesis previously mentioned in the research methodology and literature review background parts.

3.   Experimental, Simulation, ANN, and Results.

3.1. Introduction

Before dealing with the experimental process presentation, I will present the different steps of the work in the flowchart below :
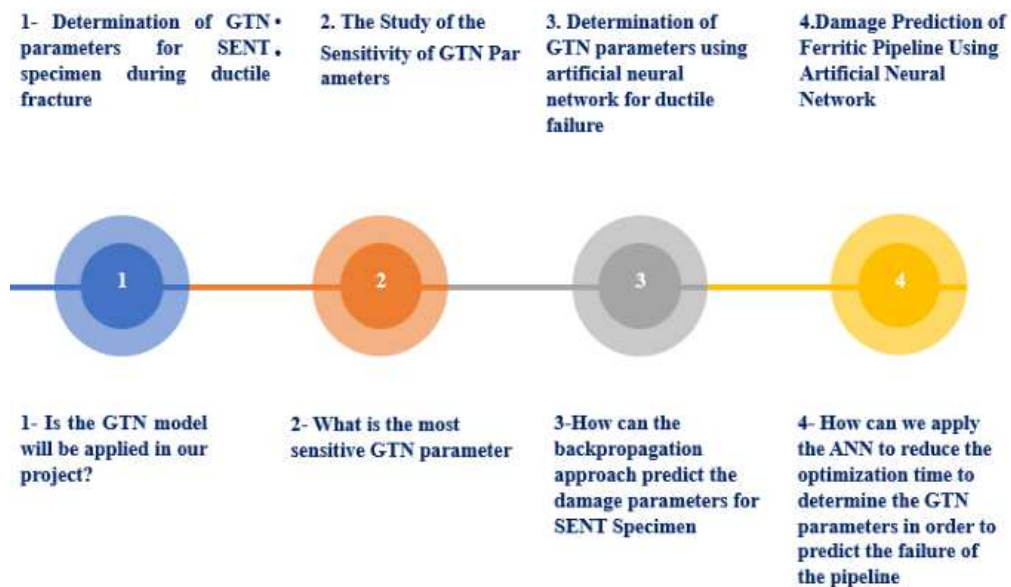
Figure 11: Flowchart presents the main steps of the thesis

- The thesis' journey is shown in the flowchart, Fig. 11.

- First Step: Proving the validity of the GTN model in our project (Using CT and SENT specimens)

- Second step: Study the sensitivity of GTN parameters because the same set of parameters could lead to the same results (Using NT specimen)

- Third Step: After finding that the GTN model can be implemented in the thesis, I introduce the ANN approach to see it's applicability, which was done using the SENT specimen. (Using CT and SENT specimens)

- Fourth Step: After proving the validity of the GTN model and ANN in this thesis, it was necessary to move to the next step, which is the prediction of the failure of the pipeline using the direct method (Using the Mockup FP1)

- Fifth Step: The introduction of the ANN model to optimize the time consumed during the determination of GTN parameters for the pipeline (Using NT, Mockup FP1 and FP2)

3.2. Presentation of the experimental data.

First of all, it is really important to mention that the material used during this study is ferritic steel 15NiCuMoNb5; the detailed component of the material was provided by EDF (Electricite du France) France [67].

Table 2 Material components

	C	Si	Mn	P	S	Cr	Mo	Ni	Al	Sn	Cu	N	Nb	O
EDF	0.140	0.310	0.940	0.009	0.020	0.400	0.350	1.140	0.015	0.013	0.620	0.013	0.030	0.003

Tensile tests were conducted at 20°C on cylindrical tensile test samples to assess the material's stress-strain constitutive law (Appendix 1).

At 20°C, notched tensile (NT) specimens were also fracture tested; the radius of the tensile specimen in this work is 2 mm, as shown in the Figure below:
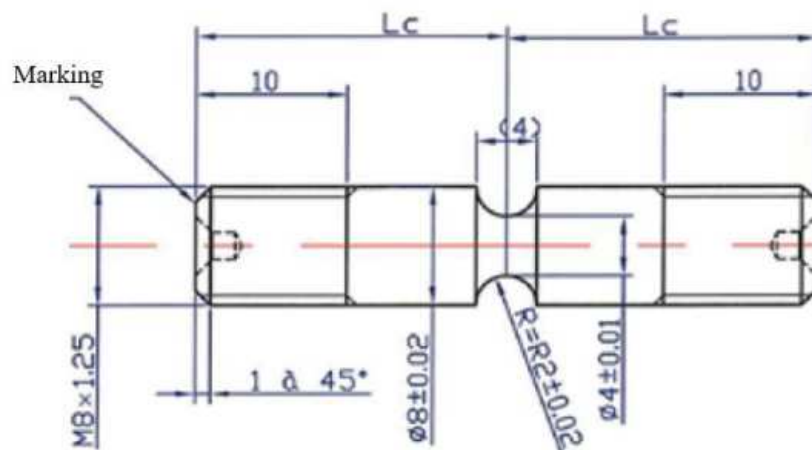
Figure 12. Experimental data of the NT sample

Then, at 20°C, a tearing test was conducted on a side-grooved CT 18881 sample (Appendix 2),

The single-edge notched tension (SENT) fracture toughness test specimen experiments results

are presented in (Appendix 3)

The CT and SENT specimens' geometries are demonstrated in Fig. 13 and 14.

The specimen's fatigue-crack length was 27.8 mm.
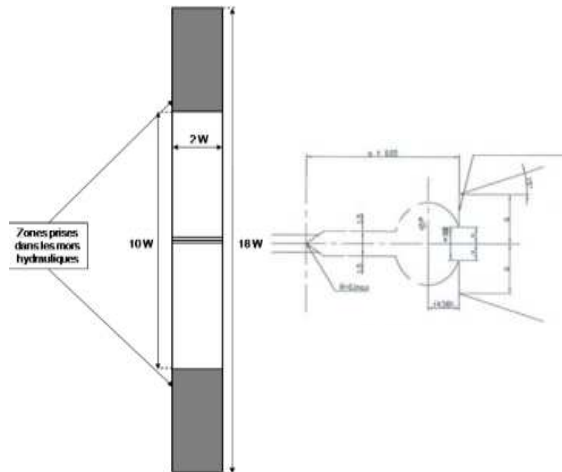
Figure 13 Geometry of SENT specimen   **Figure 14 Geometry of the CT specimen**
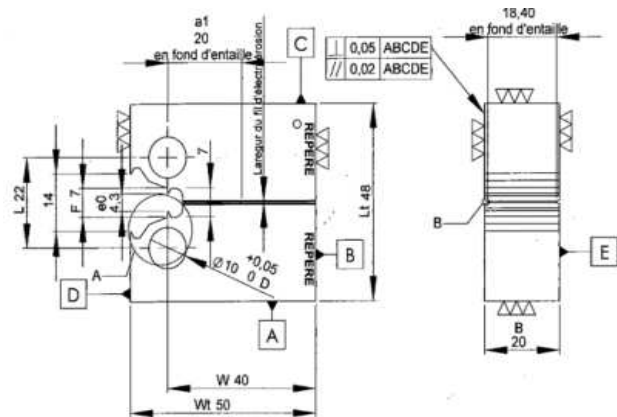
Regarding the four-point bending test on pipes, two large-scale experiments, FP1 and FP2, were
planned on mock-ups consisting of ferritic pipes on the EDF 4-point bending test facility
developed during the former STYLE project [66] Fig.15 and Table 2
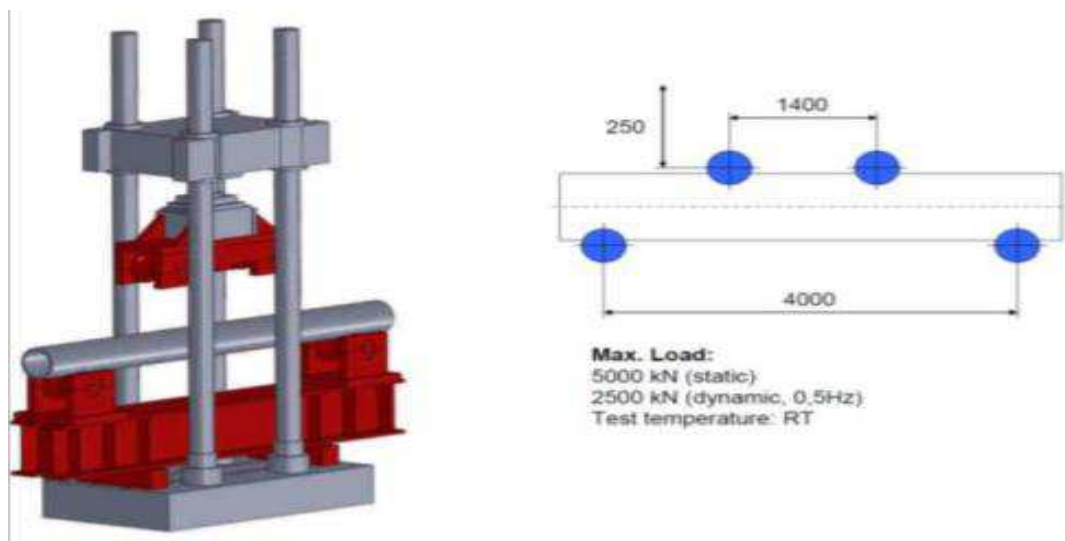
Figure 15 4PB frame for testing mock-ups for ferritic steel

Table 3 Geometries of the two mock-ups [66]

			FP1	FP2
Thickness(mm)			30	30
Crack depth(mm)			-	0.5
Crack angle(º)			30	30
Crack shape			Through-wall crack	Inner surface crack
inner(mm)			318	318
outer(mm)			378	318

All tests shall be undertaken at room temperature unless the material has strong ductile tearing development in the radial and (or) circumferential directions.

Each mock-up is instrumented appropriately to give the relevant data for analysis and validation: load, displacement, crack opening, pipe deflection, etc.

Several significant objectives include detecting the commencement of ductile crack formation and quantifying fracture growth during the trials.

Framatome GmbH supplied a representative pipe segment constructed of 15NiCuMoNb5 steel from which three component-scale mock-ups will be produced and tested Fig. 17.

However, in this study, I will focus on the mock-up FP1 as the primary objective is to shorten the time required for GTN parameters prediction using an artificial neural network, but I will also use the mock-up FP2 to confirm the optimization approach used in the mock-up FP1

Fig. 16 [66] presents the initial crack shape for the mock-up FP1.
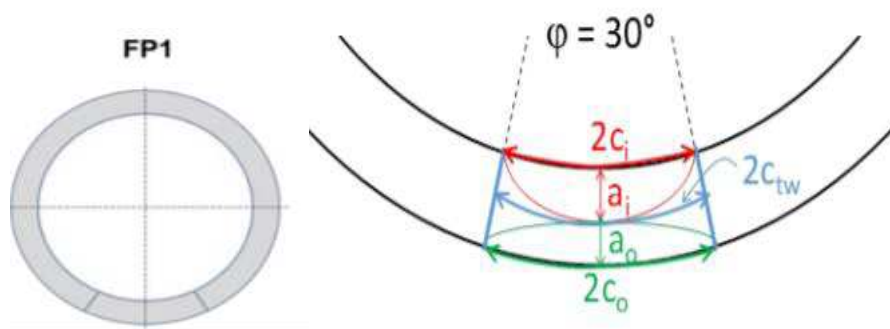
Figure 16 Initial flaw shapes of mock-ups FP1

The four-point bending test is detailed in [67]
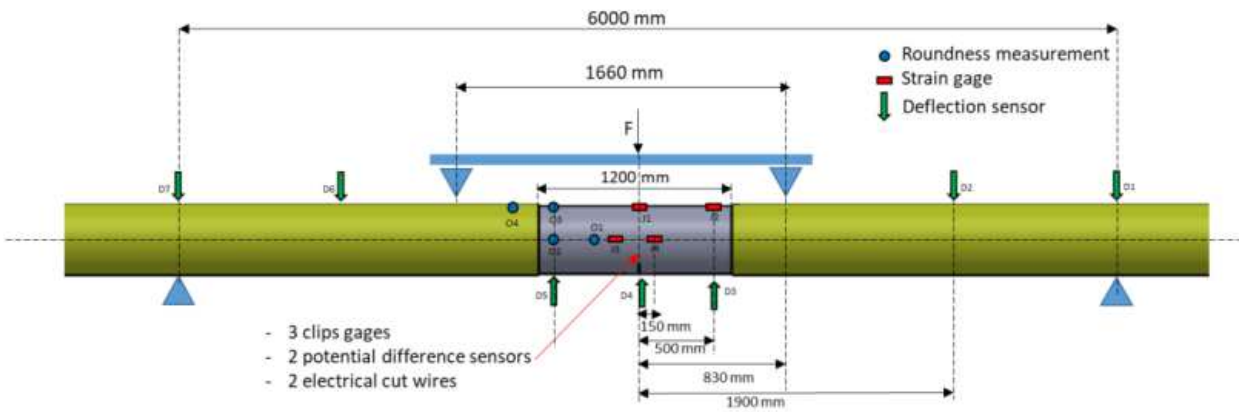
Figure 17 Geometry of the mock-up FP1 [66]
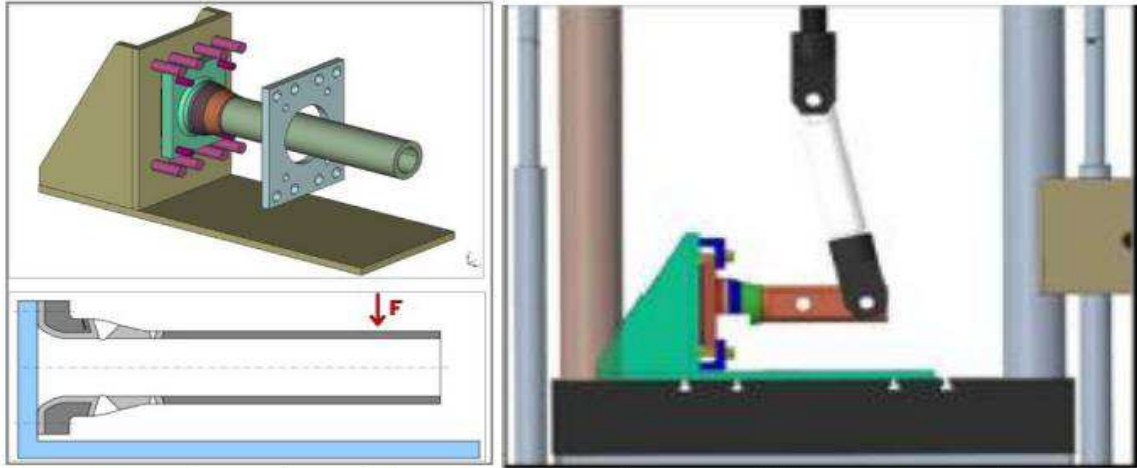
Figure 18 Design of the experimental set-up of the nozzle mock-up [66]

Figure 19 Four bending tests in reality [66]

Fig. 19 shows the real picture of the mock-up FP1 during the experiment

Figure 20 The mock-up FP1 during the experiment [66]

Fig. 20 shows the experimental results that show the pipeline's failure.

Comparing the experimental and simulation results will ensure that my approach is correct during the pipeline protection.

I will highlight the values of the maximum load and COD (crack opening displacement) and compare them to the simulation.
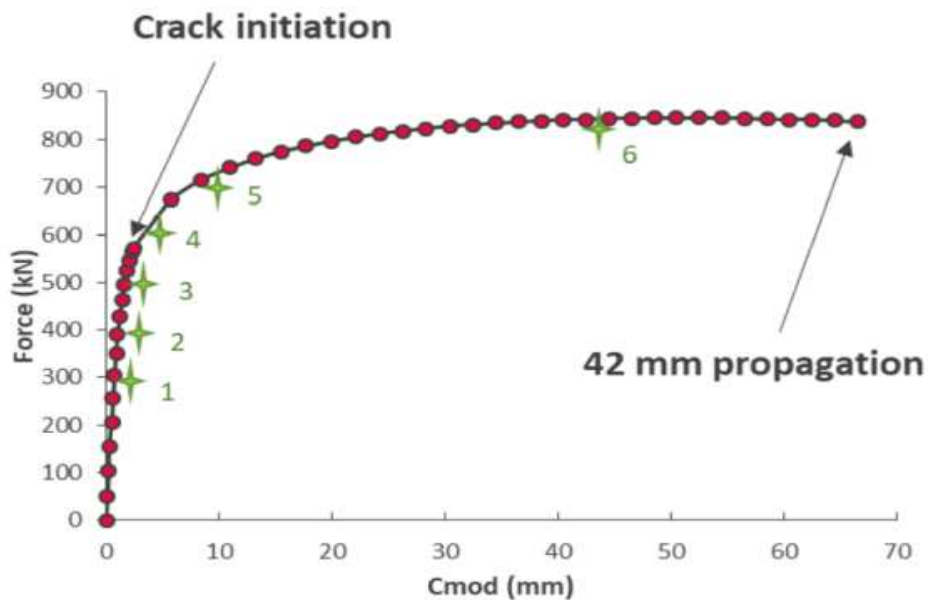
Figure 21 Measurement of the main experiments

45
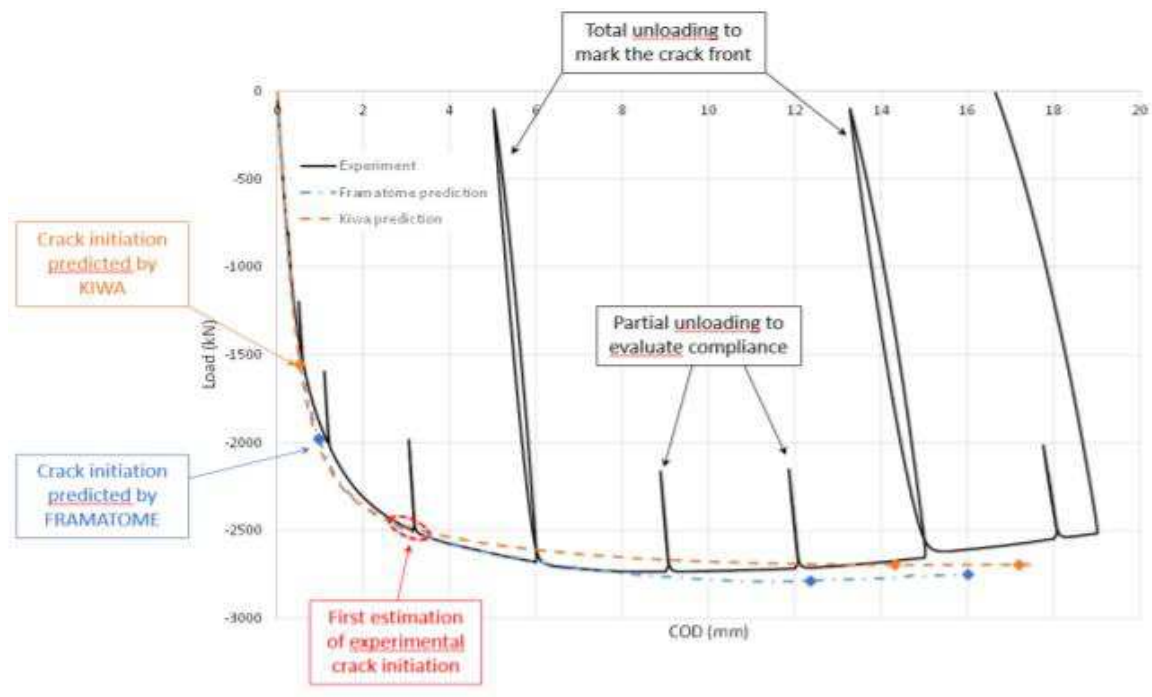
Figure 22 Load vs. COD for FP1

Nevertheless, before starting the prediction process and the main calculation, I noticed in the literature review that many researchers tried to modify the GTN model and give initial values of the GTN parameters. As already mentioned, the values of the GTN parameters are not fixed, and it is quite hard to determine them. For this reason and others, it is wise first to study the sensitivity of the GTN parameters and determine the most sensitive parameter. The results will help us focus more on determining GTN parameters and not choosing random values.

4.   The study of the sensitivity of GTN parameters

Before calculating GTN parameters, it is important to determine the most sensitive parameters because they will influence the upcoming work. As already mentioned, it is necessary to determine eight GTN parameters, which is crucial to use the GTN model. It is hard to find one set of parameters as long as they depend on each other.

To answer this question regarding sensitivity, Yassine and Szavai [68] and Zhang et al. [40] did a detailed study to check the most sensitive GTN parameters. However, Yassine and Szavai used different geometries to study the GTN parameter sensitivity.

The next section will mainly focus on the sensitivity of GTN parameters based on two CT and NT specimens.

I will take the following steps to investigate the sensitivity of GTN parameters and how changing each one affects the results:

- Conduct a small-scale test on Notch tensile specimens (diameter 10 cm) to get experimental data (Appendix 1
-) and the stress-strain curve.
- Perform the Finite Element Simulations of the Notch specimen. The reason for choosing Notch tensile specimens is that the simulation will take 5 to 10 minutes. I can simulate just a quarter of the specimen due to the axisymmetry.
- Run simulations to investigate the effect of each parameter.
- Conduct a small-scale test on CT specimens to provide experimental (Appendix 2) data and obtain the stress-strain curve. Carry out the CT Specimen Finite Element Simulations.
- Check if the most sensitive parameters will be similar between the NT and the CT specimens, leading us to infer the sensitivity change between different geometries.

4.1.1. NT and CT specimens presentation

To determine the most sensitive GTN parameters in the results, I used the Notch tensile specimens and Compact tension specimen data. The main goal is to see the most sensitive parameters with the geometry change.

According to the literature (Table 1) (Bauvineau et al. (1996); Decamp et al. (1997); Schmitt et al. (1997); Skallerud and Zhang (1997); Benseddiq and Imad (2008)), I got the initial values of GTN

The identification of the GTN parameters that I had intended to explore was accomplished by repeating the simulation numerous times until the simulation results suited the experimental data.

f_0 =Initial void volume fraction= 0.003

f_n=the new voids nucleation = 0.3

f_c=the voids volume ratio at the beginning of nucleation = 0.007

f_f =is the voids volume ratio when a fracture occurs = 0.35

S_N =the voids nucleation mean quantity = 0.005

ε_n =strain at the time of voids nucleation = 0.065

I took advantage of the symmetry and created a 2D FEM model for just a quarter of the Notch and CT specimens, as illustrated in Fig. 23 and 24.
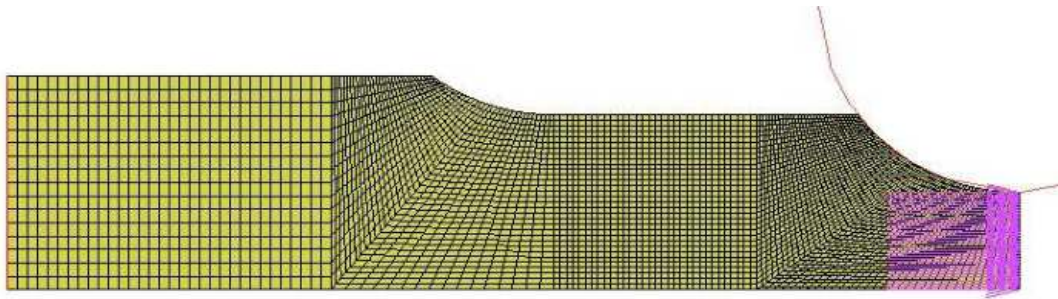
Figure 23 Notch Specimen simulation
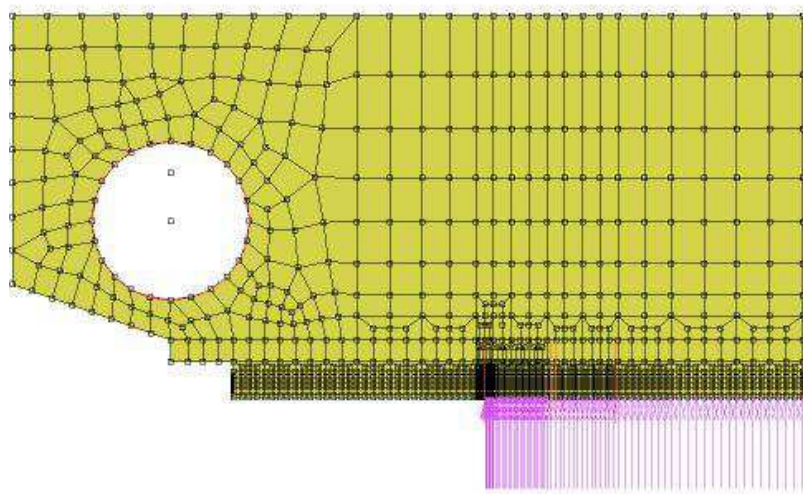
Figure 24 CT Specimen Simulation

4.1.2. Study of the sensitivity of GTN parameters.

I started with the notched specimen to see how the GTN parameters impact the findings. I ran 20 simulations for each parameter, changing one parameter's value while keeping the others constant.

After identifying the parameters sensitive to tiny modifications, I will see if the most sensitive parameters in the notched specimen have the same impact on the CT specimen.

As previously stated, I decided to deal with six parameters because the values of q1 and q2 are nearly set, as in Table 1.

I ran 120 simulations in total, with 20 runs for each parameter. The results of Force vs. Crack Opening Displacement (COD) for notch specimens are displayed in the Figures below.

$f_0 = 0.003$ (I made the variation of the parameter by this value ± 0.0003)

$f_n = 0.3$ (I made the variation of the parameter by this value ± 0.03)

$f_c = 0.007$ (I made the variation of the parameter by this value ± 0.0007)

$f_f = 0.35$ (I made the variation of the parameter by this value ± 0.035)

$S_N = 0.005$ (I made the variation of the parameter by this value ± 0.0005)

$\varepsilon_n = 0.065$ (I made the variation of the parameter by this value ± 0.0065)

The curves shown in the Figures below, from Fig. 25 to Fig. 34, display the force versus crack opening displacement (COD) for different variations of the GTN model parameter.

Each curve (color) represents a specific behavior of the material to changes in the GTN parameter.
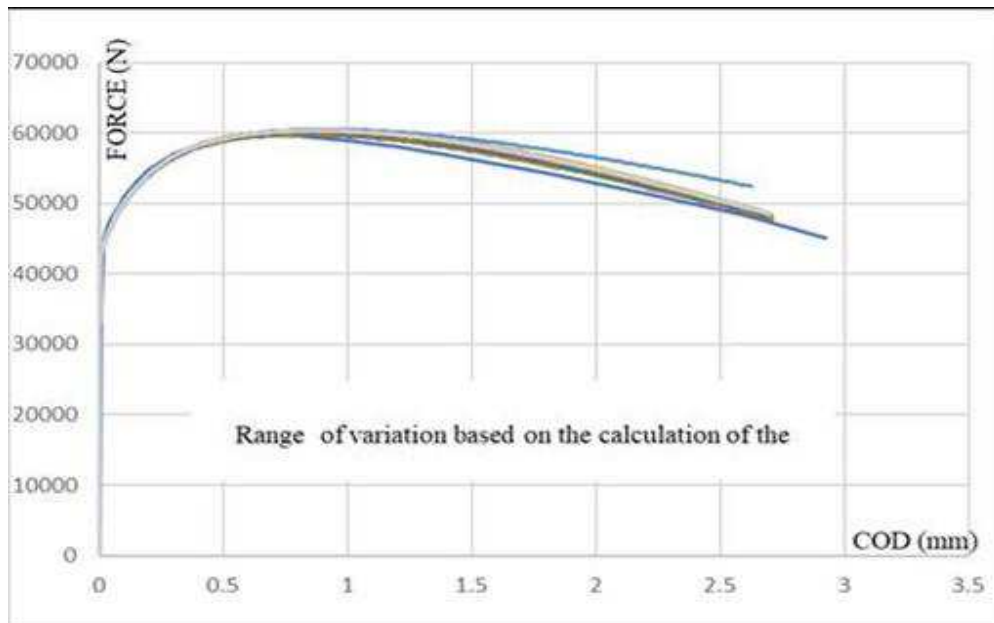
Figure 25 The variation of the Initial void volume
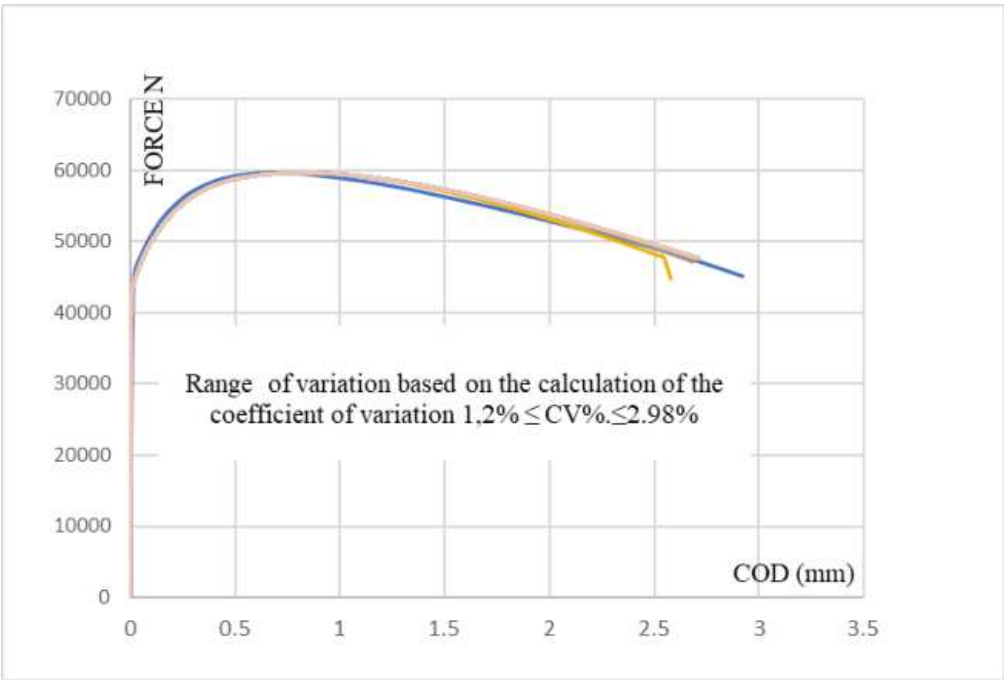
Figure 26 The new voids nucleation
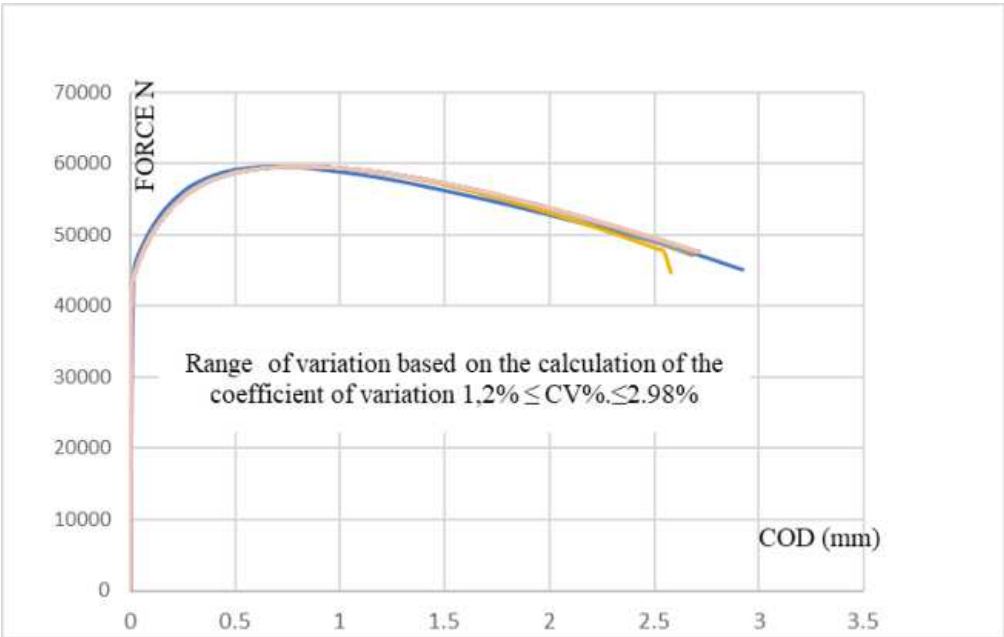
Figure 27 The variation of the voids volume ratio at the beginning of nucleation f$_c$
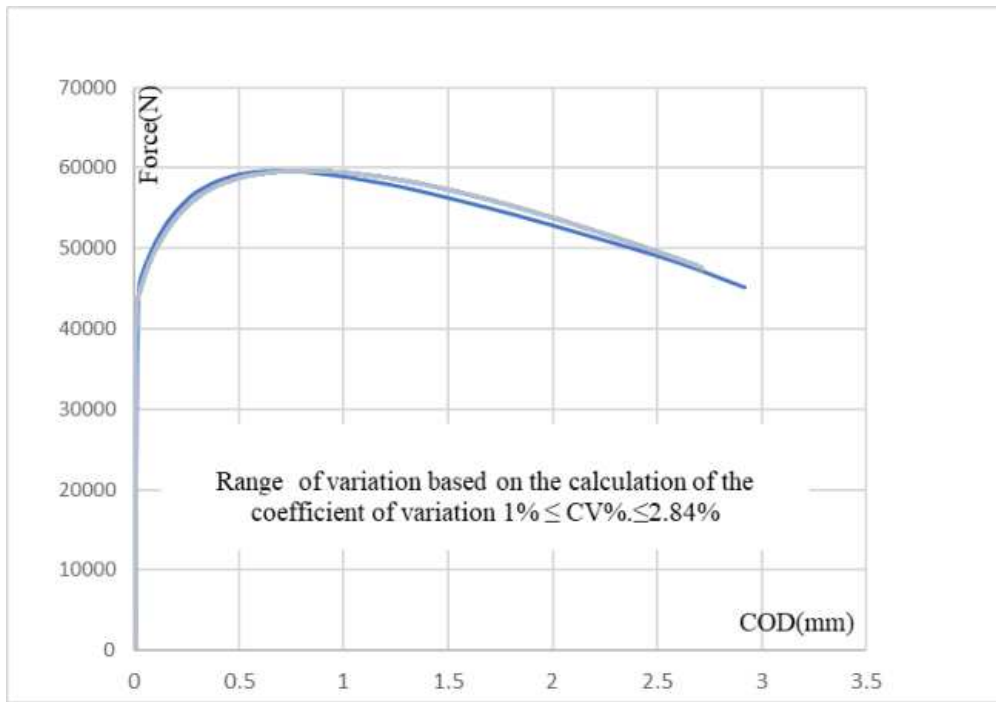
Figure 28 The change of voids volume ratio when the fracture occurs
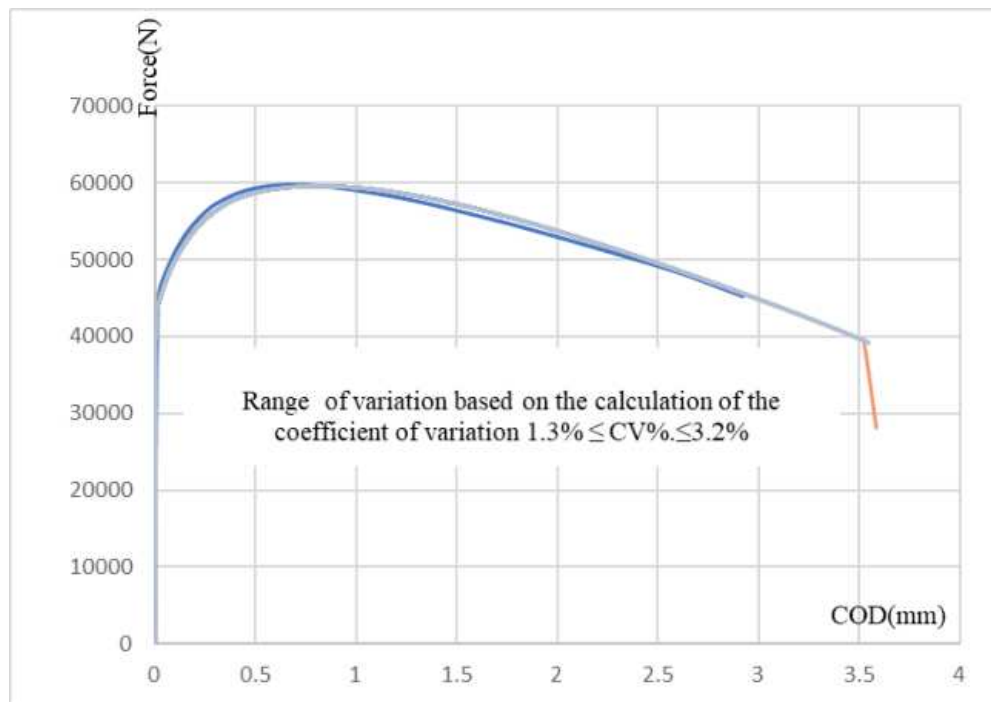
Figure 29 Strain at the time of voids nucleation ε_n
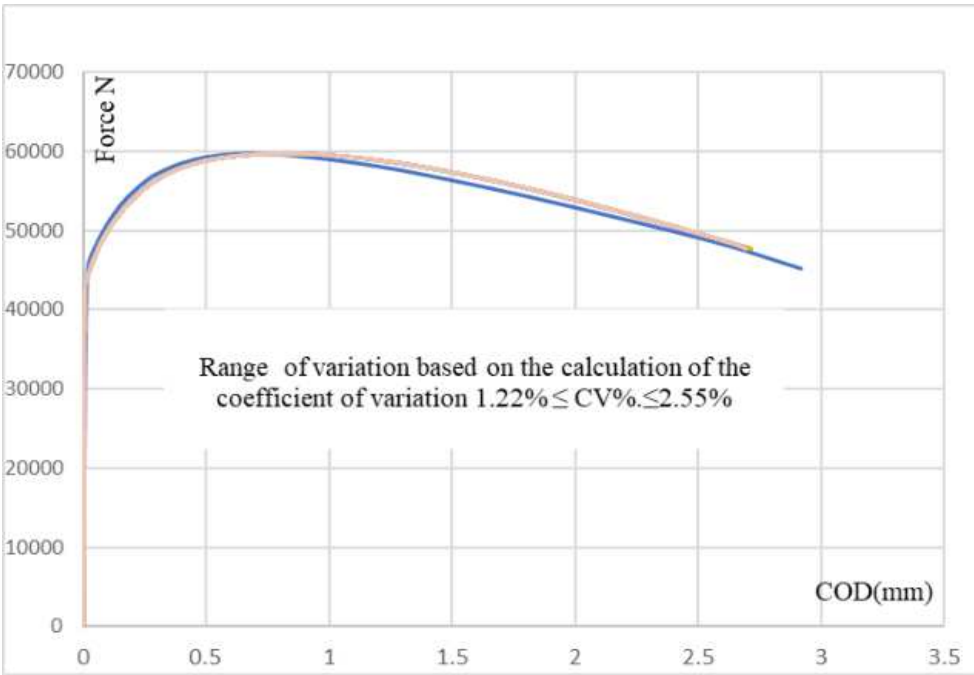
Figure 30 The voids nucleation mean quantity S_n
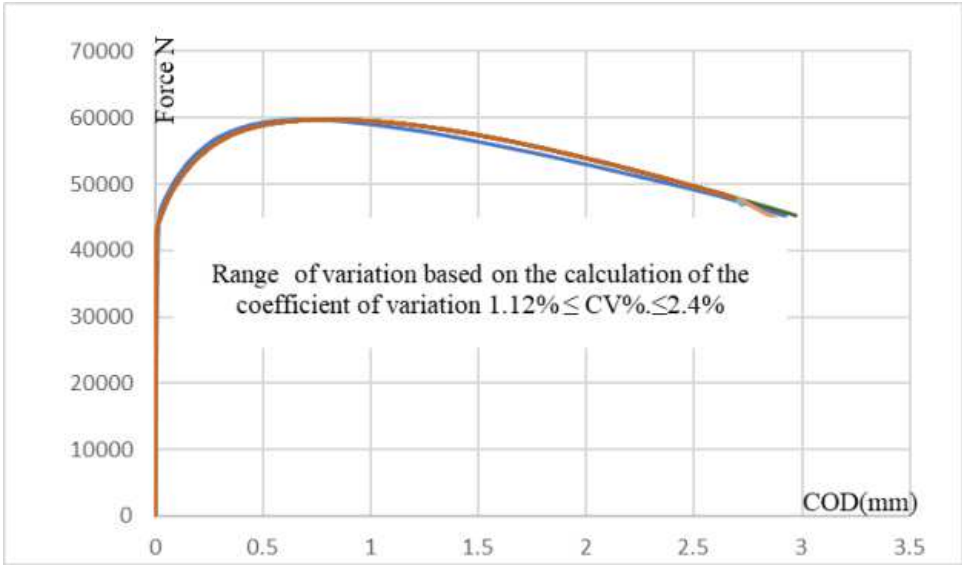
Figure 31 New voids nucleation f_n

As can be seen in the findings, the initial void volume fraction f_0 is the most sensitive parameter to a slight change in its values for NT and CT Specimens.

I may deduce that the exact value of f_0 must be determined with more precision. It must have physical significance and respect the values listed in Table 1.

The difference in the stress-strain curve is quite small for f_c, f_f, f_n, and Sn.

It appears that changing the values of the f_c, f_f, f_n, and Sn values has no macroscopical effect on failure prediction for NT

When the value of f_f is less than the value of f_c, no simulation may be started.

As I have done for the NT specimen, I will determine the sensitive parameters for the CT specimen. I performed ten simulations for each parameter, each taking six hours.

The figures below will present just the three sensitive parameters (f_0, ε_n, and S_n) for the CT specimen; no influence was recorded for the rest of the parameters. So no added value will be added to analyze them. (f_0, f_n, and f_c)

The Force vs. Crack Opening Displacement (COD) results for CT specimens for the most sensitive parameters are shown in the graphs.
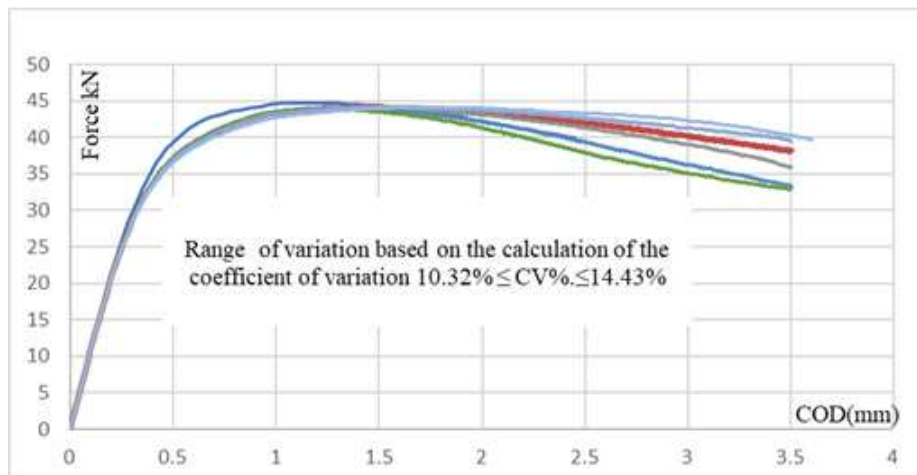
Figure 32. Initial void volume fraction f0
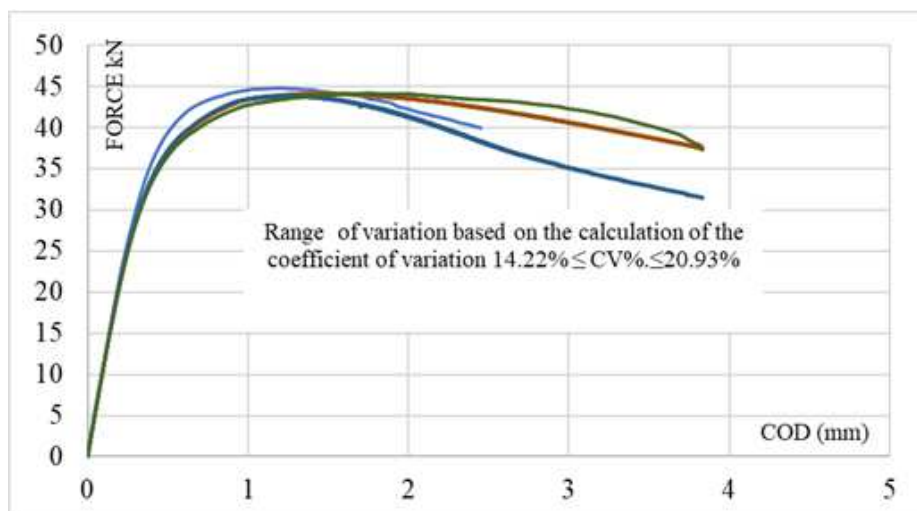
Figure 33. The voids nucleation means the quantity
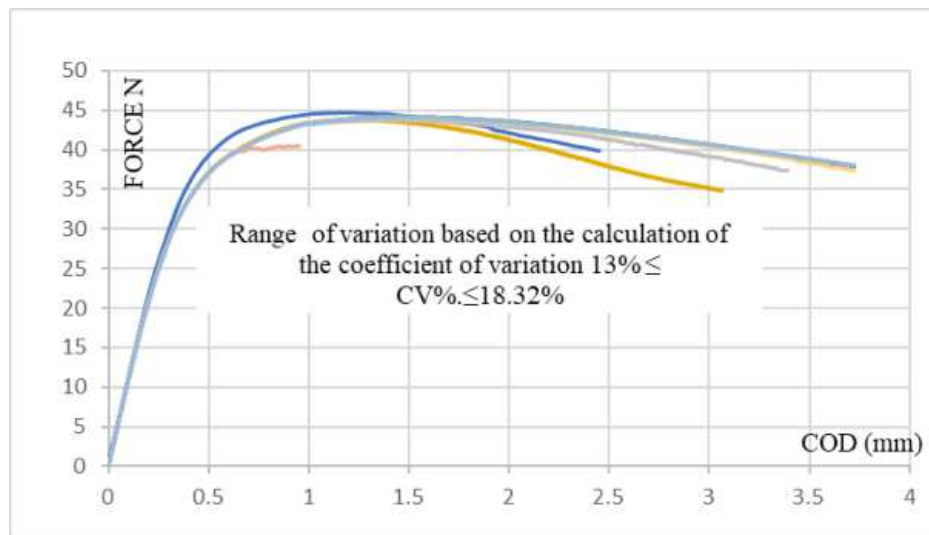
Figure 34. Strain at the time of void nucleation

By examining the curves, it is clear that changing the parameter f_0 impacts the findings, especially when compared to those obtained with the notched specimen. It is obvious now that the parameter f_0 becomes more sensitive to tiny changes in the case of CT specimens.

As a first conclusion, it is clear that the sensitivity of strain at the time of void nucleation and the voids nucleation means the quantity becomes noticeable due to the geometry and the change in the applied load; for the NT specimen, the change of the two parameters does not show a huge variation.

More studies must be done to check the variation of parameters compared to other geometries. A microscopic study should check the variation of the most sensitive parameters.

The Gurson parameters, as shown in Table 1, are not set in stone and change depending on the type of material. I may also find a new set of parameters that work like the experience. However, they differ in fracture initiation and propagation at the microscopic level.

According to the findings of this investigation, the most sensitive metrics are f_0, ε_n, and S_n.

Based on the results found after analyzing the sensitivity of GTN parameters, I will proceed with the Prediction of GTN parameters based on the direct method.

After determining the most sensitive parameters that will be included in future studies that will help us to determine the GTN parameters in a precise manner, the next step is to start the application of GTN parameters and predict the failure of the pipeline.

However, before reaching the Prediction of the failure of the pipe, it is important to check the validity of the GTN model on the material used in this work and how the model will be efficient. For this reason, I decided to predict the failure of the single-edge notched tension (SENT) specimen to test the model's validity.

4.2. Application of GTN model to predict the failure of SENT

The Gurson–Tvergaard–Needleman (GTN) model commonly forecasts material breakdown using laboratory specimens.

It is difficult and time-consuming to identify the GTN parameters directly.

The GTN model is based on ductile fracture micro-mechanical behavior, which includes void nucleation, growth, and coalescence.

The most common method for determining GTN parameters combines experimental and Finite element modeling results. However, it is time-consuming because I must repeat the simulations until the simulation data fits the experimental data at the specimen level (axisymmetric tensile bar and CT specimens).

However, other methods for determining GTN parameters, such as artificial neural networks and swarm particle optimization, aim to determine the parameters quickly.

Based on the fracture toughness test of the CT specimen, I derive the GTN parameters for the SENT specimen in this section.

The SENT specimen was chosen because it may represent the pipe under both uniaxial and biaxial stress situations. Clement Soret and colleagues (2015) [69].

4.2.1. Determination of GTN parameters from CT specimen test result.

To anticipate the SENT specimen's ductile failure, I must first establish the GTN parameters, which may be done by following these steps:

- Use Finite Element Simulations to conduct a 3D examination

- Use Finite Element Simulations to conduct a 3D examination

- The GTN parameters are determined by combining the experimental and FEM results.

Fracture toughness test modeling
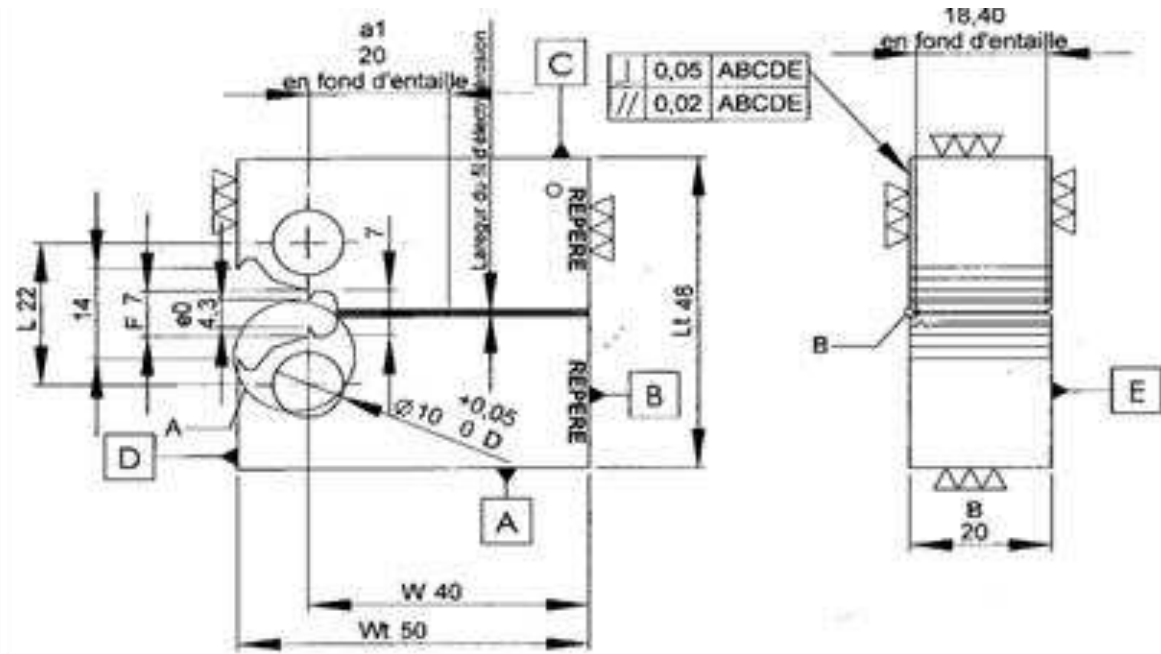
Figure 35 CT speicmen geometrie

The fracture toughness test data is being used to calculate the GTN parameters for the SENT specimen. These experiments used compact tension (CT) specimens Fig. 35.

Based on the literature, I obtained starting values of GTN parameters for steels, as in Table 1.

I took advantage of the symmetry and created a 3D FEM model for half of the CT specimen, as shown in Fig. 36. The FEM model has 58,103 nodes and 51,512 elements.

Because the gradient of strain and stress is intense near the crack tip, because the upper part of the specimen is not, I will proceed to mesh refining near the crack tip, which saves more computing time. The mesh size in front of the pre-crack tip is 0.125 mm by 0.0625 mm, and the mesh is composed of axisymmetric quadratic elements with eight nodes. Fig. 37 shows that the fracture has moved inside the specimen and a contour plot of the void volume fraction.

The measured force (kN) vs. Crack opening displacement (mm) measurement and the FEM simulations are presented in Fig. 38. The starting crack of a0/W = 0.61 was employed in the simulations. As a result, COD measurements were taken on the CT specimens' knife-edge characteristics in the mouth. Different sets of GTN settings were used in the simulations.

With the exception of simulation 2, practically all of the simulated force-COD curves are in acceptable agreement with the experimental data up to the peak load. As can be seen from the curves, the best match in the post-peak stage may be found in simulations 1 and 8 Fig. 39.

Furthermore, as shown in Fig. 37, the GTN model predicts fracture start and propagation for the CT specimen well.
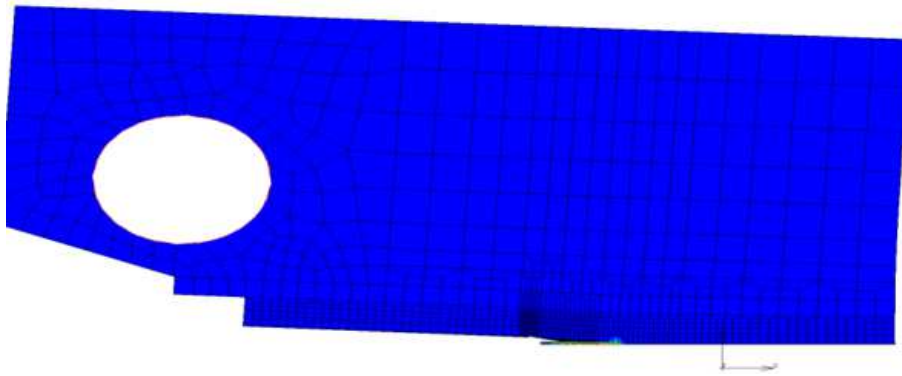
Figure 36 FEM of CT specimen
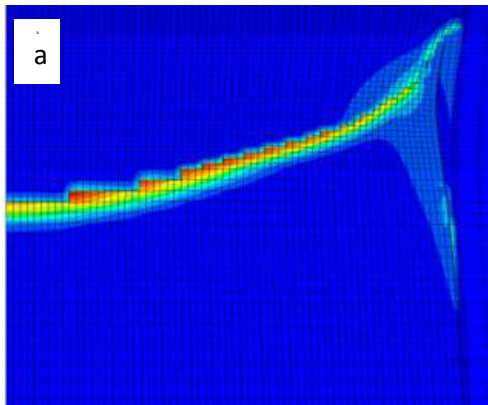
Figure 37 (a) The contour plot of the void volume fraction of the deformed specimen ; (b) The crack Propagation of the CT specimen
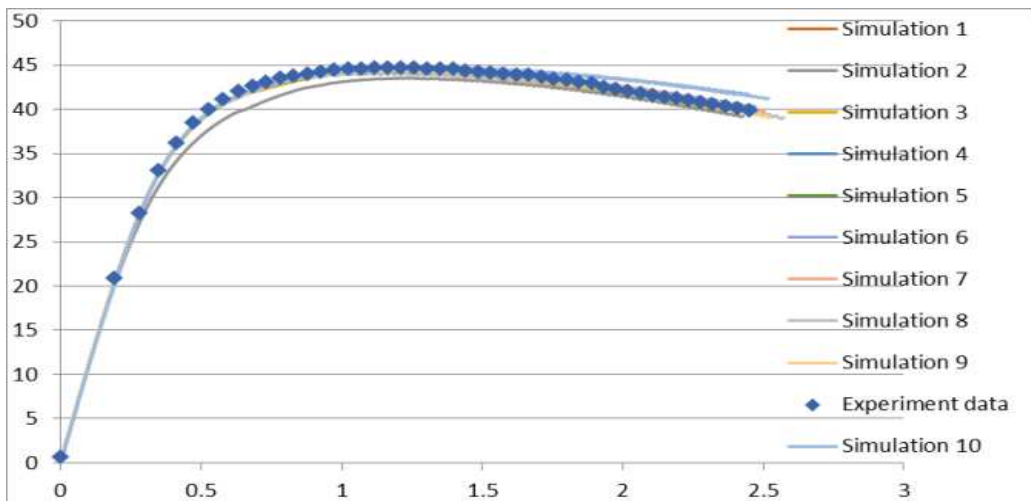
Figure 38 Force-COD curves of 10 simulations
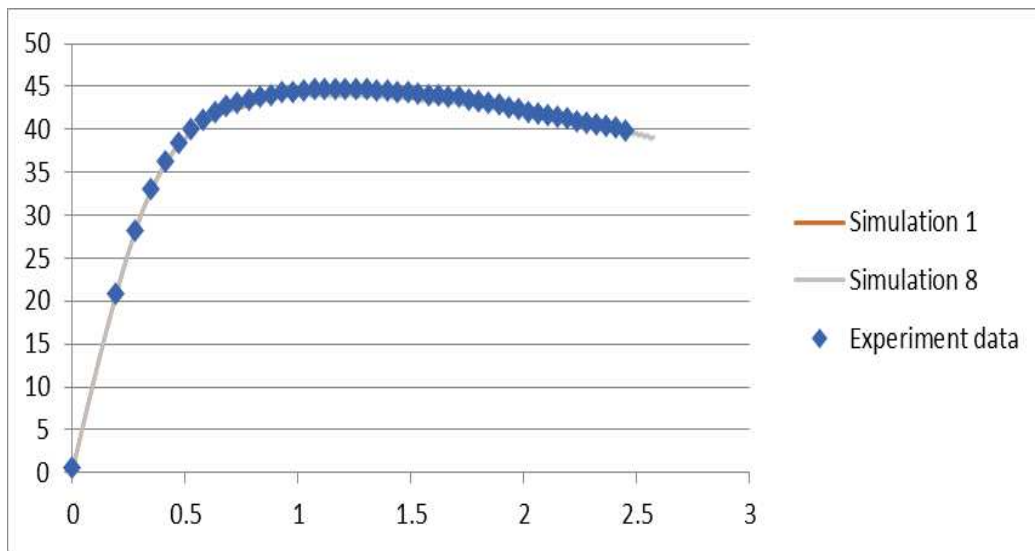
Figure 39 Force-COD curves of simulations 1 and 8

Table 4 presents the summary of GTN parameters found during the different simulations.

Table 4 Table of GTN parameters for different Simulations

	Initial Void Volume Fraction	Critical Void Volume Fraction	Failure Void Volume Fraction	Mean Strain for Nucleation	Standard Deviation	Volume Fraction for Void Nucleation
Simulation 1	**0.003**	**0.07**	**0.35**	**0.65**	**0.005**	**0.3**
Simulation 2	0.003	0.2	0.3	0.3	0.05	0.06
Simulation 3	0.0032	0.22	0.35	0.3	0.05	0.05
Simulation 4	0.0015	0.12	0.35	0.3	0.05	0.08
Simulation 5	0.001	0.15	0.3	0.22	0.05	0.05
Simulation 6	0.001	0.17	0.32	0.25	0.05	0.05
Simulation 7	0.001	0.1	0.33	0.17	0.05	0.024
Simulation 8	**0**	**0.045**	**0.27**	**0.2**	**0. 45**	**0.05**
Simulation 9	0.001	0.1	0.33	0.165	0.05	0.025
Simulation 10	0.001	0.1	0.33	0.2	0.05	0.025

By comparing the actual and simulated fracture propagation in Fig. 37. I can remark that the crack propagation is similar between the experiment and the simulation. I can predict fracture propagation using the GTN parameters used in simulations 1 and 8.

By examining the GTN parameters used in simulations 1 and 8, I found that the values used in simulation 8 are the ones that are closest to the literature data in Table 1, which means that I will predict the failure of the SENT specimen based on the GTN parameters that I got in the simulation 8.

4.2.2. Prediction of Crack propagation for SENT specimen

I will use the SENT specimen to test the validity of the GTN parameters that I discovered from CT simulations. (The experimental data of the SENT specimen will be mentioned in appendix 3)

The dimensions of the SENT specimen are shown in Fig. 38, and I employ axisymmetry, as I did for the CT simulation, and create a 3D model just for the 1/4 of the specimen.

The FEM model has 75,461 nodes and 68,160 elements in total.

To eliminate the influence of the mesh's sensitivity on the findings, the mesh size in front of the pre-crack tip Fig. 41 is the same as the CT specimen (0.125 mm x 0.0625 mm). The mesh is made up of axisymmetric quadratic elements with eight nodes.

In Fig. 41, the fracture has progressed inside the specimen, and the contour plot of the void volume fraction of the deformed specimen is displayed.

I perform a FEM simulation using the GTN parameters obtained in simulation 8. The results reveal that the simulation curve matches and agrees well (Fig. 43.

Furthermore, as shown in Fig. 42b, the GTN model accurately predicts fracture start and propagation, demonstrating the model's validity once more.
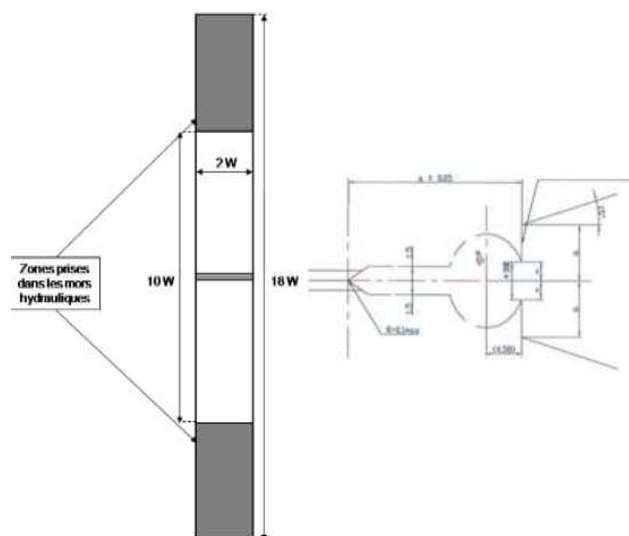
Figure 40. Dimension of SENT specimen

Figure 41 The 3D FEM of the SENT specimen
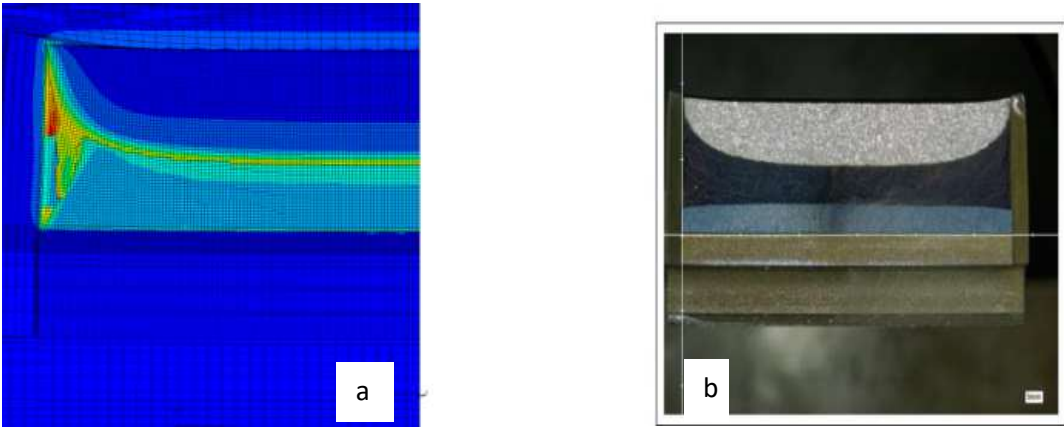
Figure 42 (a) the contour plot of the void volume fraction of the deformed specimen ; (b) The crack propagation in the SENT specimen
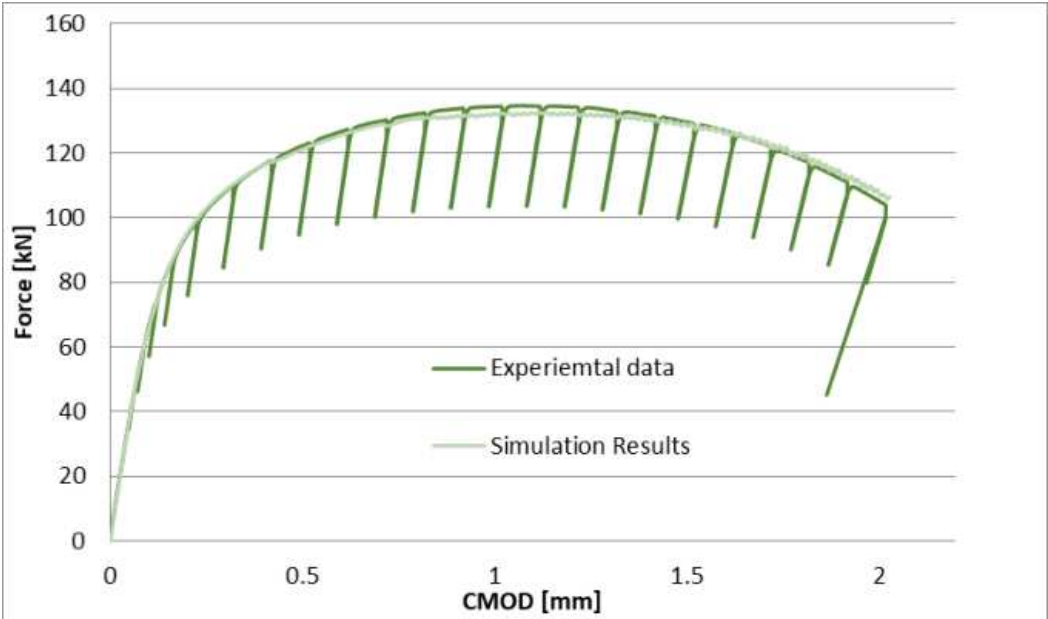
Figure 43 Force-COD curve

In the next part, I will present the Prediction of the failure of a SENT sample, but this time by using an artificial neural network.

This study checks the validity of the chosen approach, which will be used in the Prediction of the pipeline's failure.

4.2.3. Prediction of failure of SENT specimen based on Artificial Neural Network

Traditionally, the backpropagation approach entails determining the parameters that minimize the difference between a finite element method-predicted force and the experimental response.

The biggest disadvantage of this strategy is that it takes excessive time, especially when several tests are utilized.

I use the ANN model instead of FEM simulations during the optimization loop to overcome this limitation. Only the finite element simulations of the experimental tests under consideration are employed in training the ANN models. Because the ANN model's projected reaction is virtually instantaneous, several tests may be run simultaneously to find the material parameters.

The optimization strategy aims to reduce the time needed to identify the GTN parameters, which normally involve illogical attempts. To do this, I intend to create an optimization model that uses the GTN parameters as the input layer and the force (load) as the output layer. I intend to accelerate and improve the predictability of the process by building a neural network that predicts the GTN parameters.

I aim to minimize errors when using uploaded data to train a neural network and construct a connection between the input and output layers. Then by using experimental data as the output data, I will utilize the backpropagation algorithm to forecast input parameters (GTN parameters).

The network topology, transfer function, and learning method influence the design of a neural network.

Back propagation-trained multilayer perception is one of the most common and adaptable types of neural networks. It can handle non-linear models with excellent accuracy. The architecture of the ANN model is shown in Fig. 44. It has three layers: the input layer, the concealed layer, and the output layer. Each neuron in the hidden layer receives the following total outputs from all of the neurons in the input layer:

$$V_j = \sum_i^n W_{ij} x_i + b_j \qquad \qquad \textit{Equation 28}$$

where

V_j presents the input to the j_{th} neuron in the hidden layer,

n refers to the total number of neurons in the input layer,

W_{ij} is the weight from the i_{th} neuron in the input layer to the j_{th} neuron in the hidden layer,

x_i is the input to the i_{th} neuron in the input layer,

and bj is the threshold value of the jth neuron in the hidden layer.

The output of a neuron in the hidden layer is calculated by applying the potential input to a transfer function.

The sigmoid function shown in (11) is the transfer function between the input and hidden layers.

$$y_i = F(V_j) = \frac{1}{1+e^{-V_j}}$$

Equation 29

For the output layer, the output σ_k of the neuron k is given by the relation below:

$$\sigma_k = \sum_{j}^{m} W_{jk} y_j + b_k$$

Equation 30

Where

m number of neurons in the hidden layer,

W_{jk} is the connection weight from the i_{th} neuron in the hidden layer to the k_{th} neuron in the output layer, y_j is the output from the j_{th} neuron in the hidden layer, and h_k is the threshold value of the k_{th} neuron in the output layer. Hamdi & Haykel (2010) [70]]
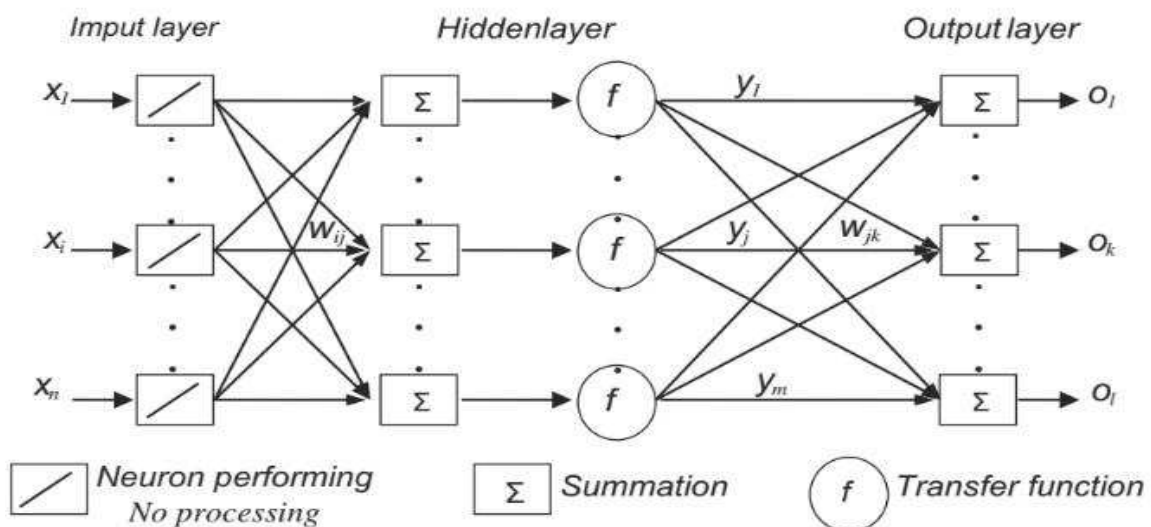
Figure 44 Multilayer perceptron

4.2.4. Methodology and results

I decided to predict just three GTN parameters to study the validity of GTN parameters and use the same optimization approach with the six parameters.

To estimate the SENT specimen's ductile behavior, I must first establish the GTN parameters, which may be done by following these steps:

- Conduct small-scale experiments (CT, SENT) to collect experimental data.

- Conduct 3D Numerical Simulations and create a database for neural networks.

- Using a mix of experimental and FEM data and an Artificial Neural Network, estimate the GTN parameters.

- The software used during the optimization approach is MATLAB 2019 [71]

CT Specimen modelling

The fracture toughness test data is used to generate the GTN values for the SENT specimen. These tests were carried out on compact tension (CT) specimens, as illustrated in Fig. 35, with their dimension also shown.

I made the model using symmetry and created a 3D FEM model for only half of the CT sample. Fig. 45 The Finite element model has 58,103 nodes and 51,512 elements.

So because fracture propagates and the stress is very strong around the crack tip, unlike the upper part of the specimen, I would proceed to mesh optimizing near the crack tip, saving more computing time.

The mesh size in front of the pre-crack tip is 0.125 mm 0.0625 mm, and the mesh is composed of axisymmetric quadratic elements with eight nodes.

In Fig. 46, the crack has spread inside the specimen, and the contour plot of the void volume ratio of the deformed sample is displayed.
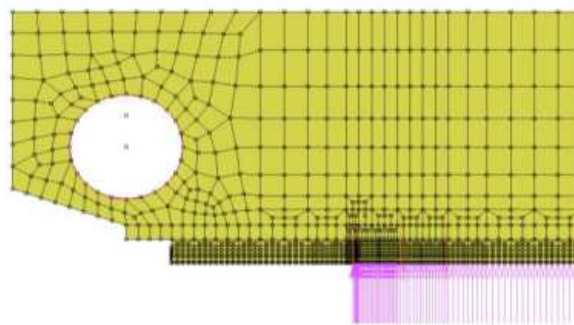
Figure 45 FEM of CT Specimen
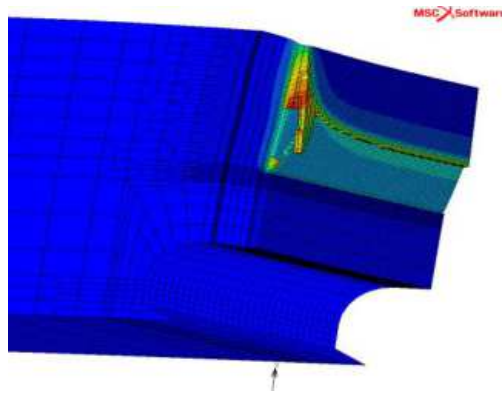
Figure 46 Contour plot of the void volume fraction of the deformed specimen

4.2.4.1. ANN and the creation of the database

Twenty simulations for CT specimens were performed to generate the database essential to train the ANN; for each simulation, I used a different set of GTN parameters,

The trained ANN model for the CT test has 48 input neurons, 60 hidden neurons, and three output neurons (48-60-3).

The input layer's neurons represent the response force F, and the output layer represents the GTN parameters (f_0, f_c, and f_f); these data are generated from the simulations.

After training the neural network, I could predict the three GTN parameters by applying the backpropagation approach; in other words, the trained neural network will predict the GTN parameters based on the experimental data of the SENT specimen.

f0=0.001, fc=0.0052, and f_f=0.2027 are the GTN parameters determined by utilizing the ANN.

The script shown in appendix 5 presents the algorithm of the backpropagation approach used to predict the GTN parameters.

4.2.4.2. Prediction of Crack propagation for SENT specimen

I will examine the SENT specimen to verify the correctness of the GTN parameters determined using CT Simulations.

The dimensions of the SENT specimen are presented in Fig. 47. Like the CT simulation, I will apply axisymmetry and create a 3D model of just 1/4 of the specimen; the FEM model comprises 75,461 nodes and 68,160 elements. To eliminate the influence of the mesh's sensitivity on the findings, the mesh size in front of the pre-crack tip is the same as the CT specimen (0.125 mm 0.0625 mm). The mesh is built of axisymmetric quadratic elements with eight nodes. The contour map of the deformed specimen's void volume percentage in Fig. 48 illustrates how the fracture has propagated into the specimen.

I do a FEM simulation using the GTN parameters obtained by the ANN; the results indicate that the simulation curve closely matches the actual curve and that they agree well (Fig. 49). Additionally, as seen in Fig. 48, the GTN model accurately predicts crack extension, demonstrating the model's validity once again.
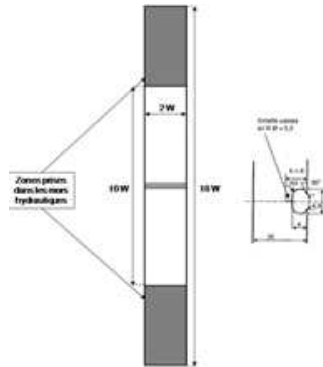
Figure 47 Dimensions of SENT specimen
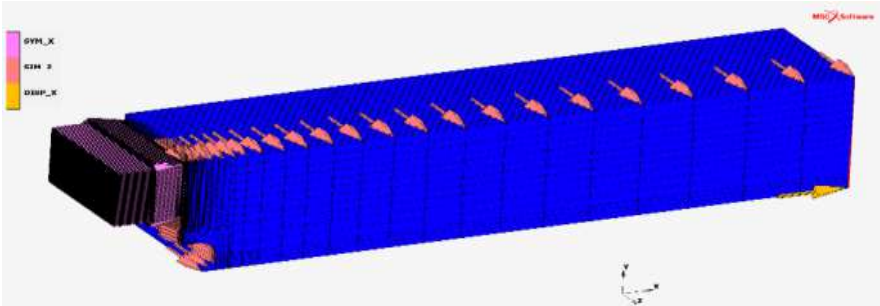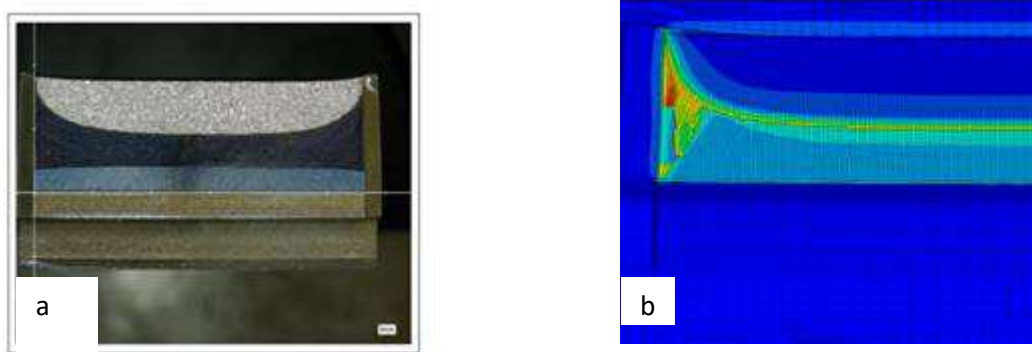

**Figure 48 (a) the contour plot of the void volume fraction of the deformed specimen ; (b) The crack propagation in the SENT specimen**
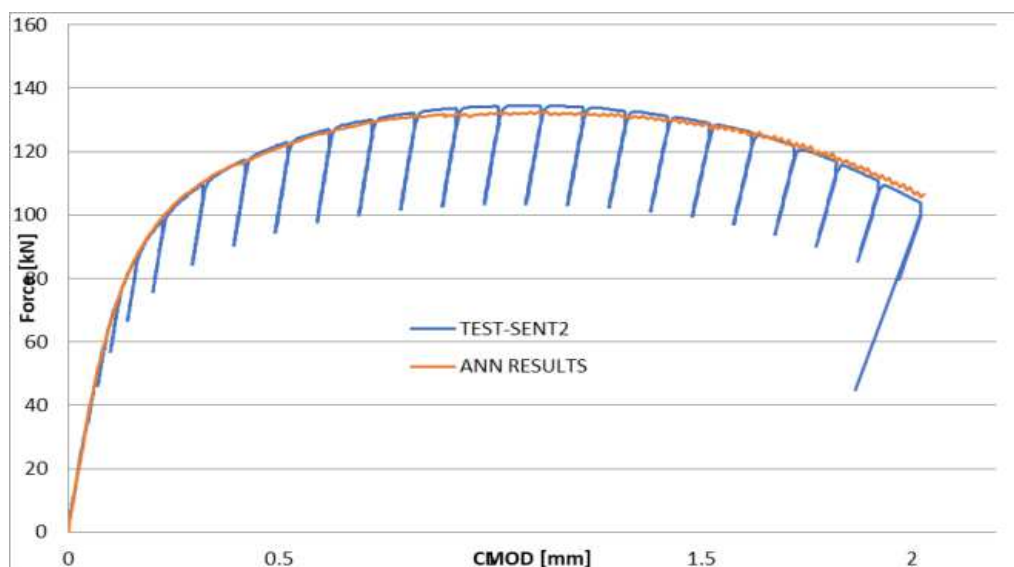
Figure 49 Force-COD curve

By analyzing the curve above, it is obvious that ANN estimates the correct values of GTN parameters used to predict the failure of the SENT specimen.

By comparing the experimental and simulation results, I can conclude from the curve analysis that the onset of ductile tearing is correctly predicted: 115 kN (simulation) versus 118 kN reported in the experimental data. The maximum projected load is 138 kN, and the experiment's highest force is 136,7 kN,

In other words, I was able to approve the validity of the backpropagation approach in this study, and I will be able to use it in the prediction of the failure of the pipeline.

4.2.5. Prediction of Failure of Ferritic pipeline using direct Method.

The pipe's four-point bending test was reproduced with a through-wall fracture defect Fig. 50
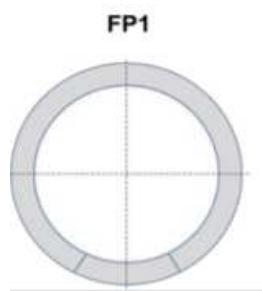
Figure 50 through wall fracture

Only a quarter of the pipe was meshed to reduce the computation time required due to the high number of elements Fig. 51.
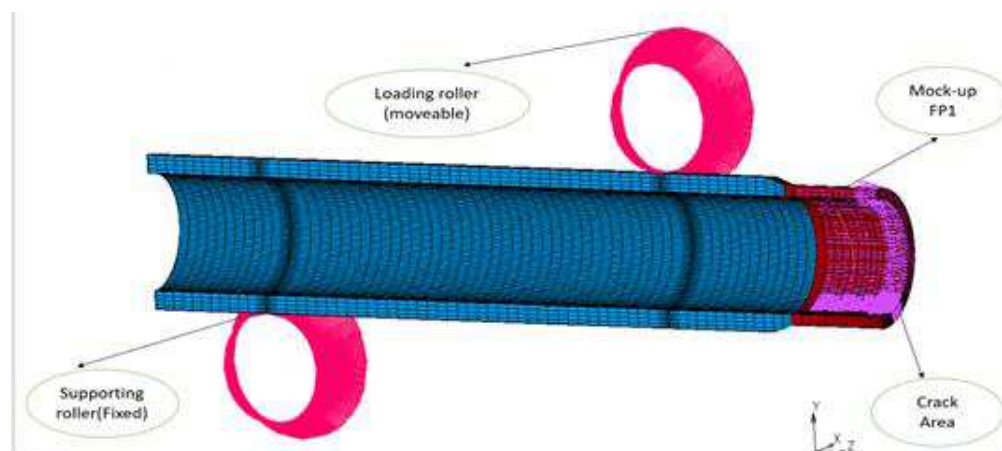
Figure 51 FEM of the quarter of the pipeline

The GTN model is only considered in a condensed region for time consumption Fig. 52.
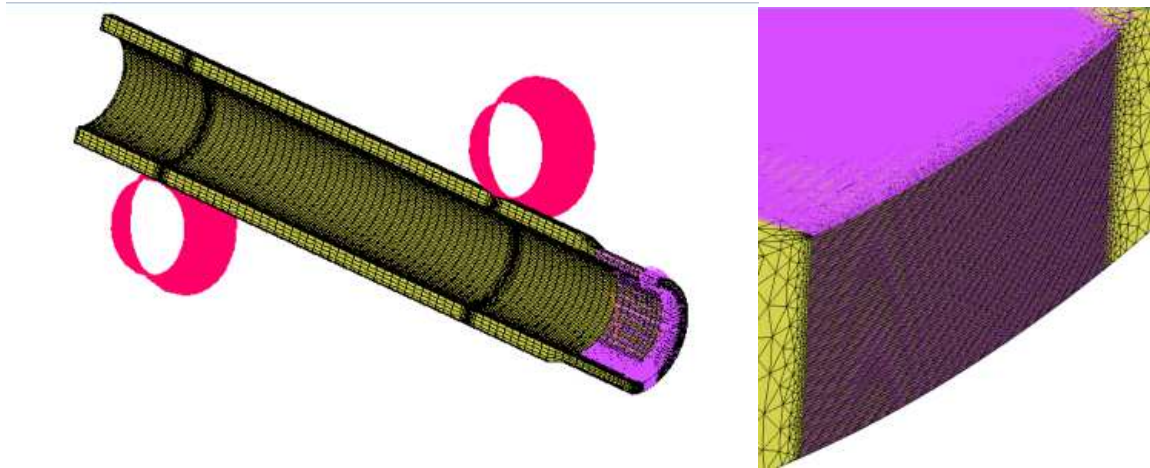
Figure 52 mesh near the crack tip

The dimensions of the Mockup FP1 are already mentioned in Table 3; to reduce the computation time, I decided to model just half of the mockup, thanks to the axisymmetry.

The FEM model has 104193 nodes and 248038 elements in total. (The experimental data of the FP1 are mentioned in Appendix 4).

To eliminate the influence of the mesh's sensitivity on the findings, the mesh size in front of the pre-crack tip is the same as the CT specimen and the SENT, as already mentioned previously (0.125 mm 0.0625 mm). The mesh is made up of axisymmetric quadratic elements with eight nodes.

I perform a FEM simulation using the GTN parameters only on the crack propagation area, which is the most sensitive part of the model.

To determine the correct set of GTN parameters, I had to repeat the simulations with a different set of GTN parameters and compare the simulation results with the experiment; the correct set of GTN parameters is the set of parameters that leads to a correct prediction of the experimental results.

Due to the huge amount of elements in the model, it took around two days of computing for one simulation.

So to get the correct set of GTN parameters, I had to do around 15 simulations; with basic math calculation, it took around 30 days of computation,

The set of GTN parameters was almost the same as the one found for the SENT specimen, which approves the assumption that the SENT specimen is a good representative of the pipeline. After

15 Simulations, the set of GTN parameters that lead to the correct assumption of experimental results is presented below :

- $f_0 = 0$, fc $= 0.0045$, $f_f = 0.26$, $f_n = 0.06$, $S_n = 0,44$ and $\varepsilon_n = 0.2$

The ferritic mock-up is modelled to have an elastic behaviour (E=203 GPa).

In Fig. 53 (Force vs. Crack opening displacement) below, I see that the GTN model predicts the pipeline's failure very well. It leads us to the right prediction of the crack propagation; in addition, the initiation and maximum load are also well predicted.
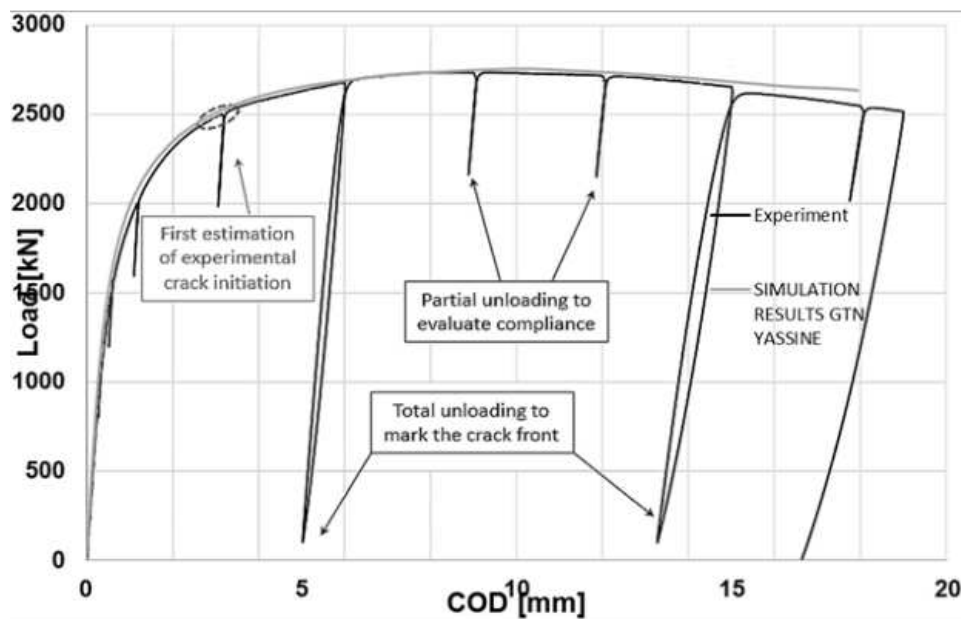
Figure 53 Force vs. Crack opening displacement

I can conclude from the curve analysis that the onset of ductile tearing is correctly predicted: 2255 kN (simulation) versus 2240 kN reported in the experimental data. The maximum projected load is 2741.624 kN, which will occur at a CMOD of 22 mm. The experiment's highest force is 2808 kN, which occurs at a CMOD of 23.42 mm.

After using the direct method, I noticed that the GTN model was a strong and practical tool. However, it took us 30 days to find the right set of parameters, hence the need to find an alternative, complementary way to predict the GTN parameters quickly. For this reason, I have integrated artificial intelligence into the simulation process and reduced the duration of the 30 days to 6 hours.

The next section will describe in detail the work done and the optimization process used to determine the GTN parameters that will be used to predict the failure of the pipe in a short time.

4.2.6. Prediction of failure of the pipeline using the ANN approach

As mentioned in the literature review, ANN was used in many fields to improve productivity and quality.

The purpose of using the artificial neural network is to optimize the time consumed during the prediction of failure of GTN parameters.

In the last section, I was able to approve that the GTN tool is a useful tool to predict the failure of the pipeline, but it took 30 days; it is important to highlight that in the last section, I used just the quarter of the specimen to reduce the computing time, so I can conclude that for complicated and sophisticated equipment the simulation period will be much longer than three days. Hence, finding another alternative to cover the gap and reduce the time consumed in predicting the GTN parameters was necessary.

4.2.6.1.   Simulation and application of ANN work.

I will use the backpropagation approach in this part, as in section 3.3.4.

- To estimate the PIPELINE ductile behavior, I must first establish the GTN parameters, which may be done by following these steps:

  - Conduct small-scale experiments (NT) to collect experimental data.

    Make the Finite Element Simulations of the Notch specimen; the reason behind choosing Notch tensile specimens is that the simulation will take just 5 to 10 min and I can simulate just a quarter of the specimen due to the axisymmetry

  - Conduct 3D Numerical Simulations and create a database for neural networks.

  - Using a mix of experimental and FEM data and an Artificial Neural Network, estimate the GTN parameters.

The illustration below gives a general overview of the prediction process of GTN parameters.
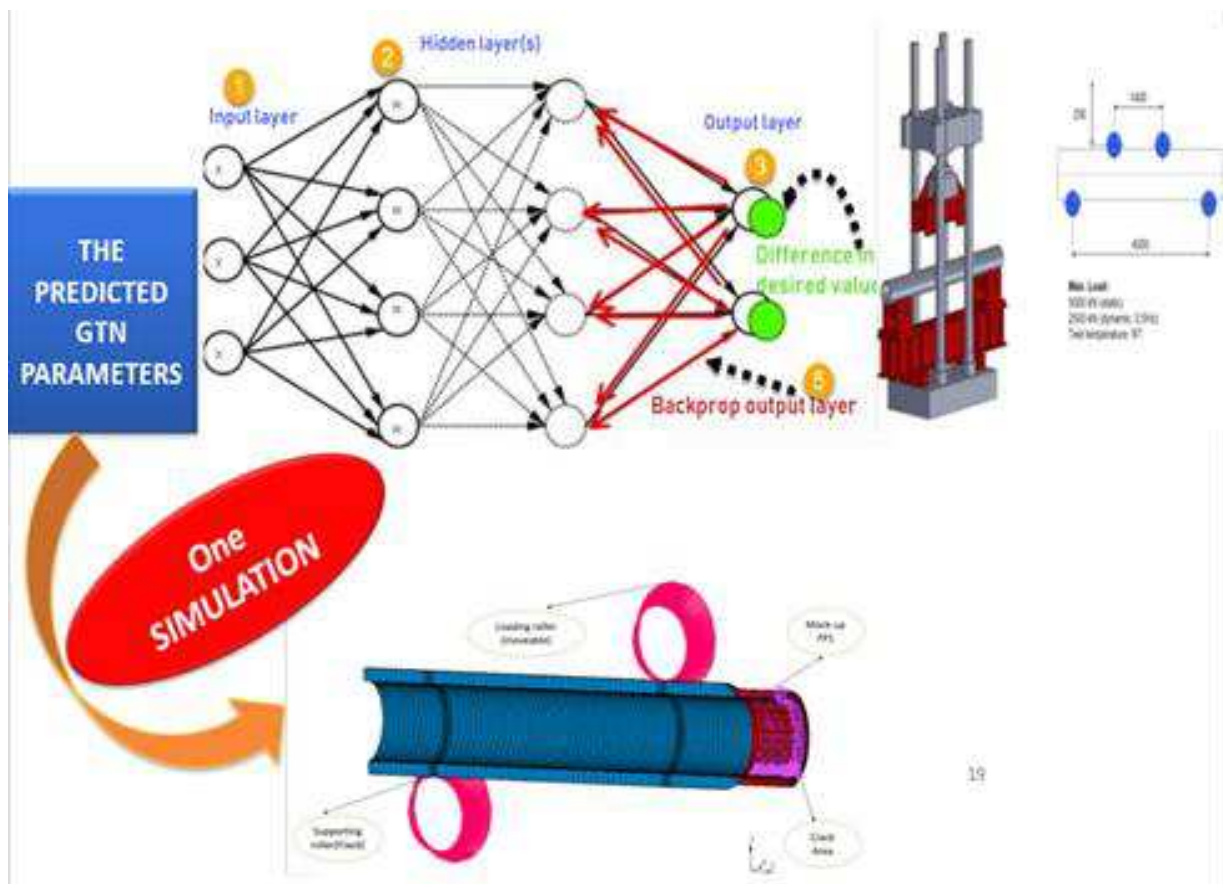
Figure 54. Prediction of the failure of the PIPELINE

Creating accurate GTN parameters for pipeline failure simulations involves multiple steps.

The approach begins with generalizing the neural network database based on NT specimen simulation. This entails gathering information from NT specimens, which gauge a material's ability to withstand fracture and applying it to create a generalized neural network database.

The process's succeeding phases will be built upon this database.

The next step is to run the backpropagation process.

Backpropagation is a widely used optimization algorithm in machine learning that involves updating the weights of a neural network to minimize the error between the predicted output and the actual output.

In this case, I use the backpropagation process to predict the GTN parameters (material properties related to ductile fracture) based on the experimental data of the pipeline that I implemented into the output layer of the neural network.

During the training phase, the backpropagation process propagates the error signals from the output layer to the neural network's input layer.

Once I have obtained the GTN parameters, I must verify their accuracy in predicting pipeline failure. I use the MARC Mentat software to simulate the pipeline's failure based on the GTN parameters I obtained to achieve this.

This simulation shows whether the GTN parameters I obtained are sufficient for accurately predicting pipeline failure.

Overall, the process involves using data from NT specimens to train a neural network, using the backpropagation algorithm to predict GTN parameters based on experimental data of the pipeline, and verifying the accuracy of the GTN parameters by simulating pipeline failure using MARC Mentat software.

4.2.6.2. NT Specimen modeling

The simulation and geometry of the NT specimen are indicated in Fig. 55; the reason behind choosing the NT specimen is the short time of computation, which leads us to generate a significant database to train the neural network.

To find the GTN parameters using ANN, I made 60 simulations of the NT specimen.

The database was generated in 300 minutes, and each simulation took around 5 minutes.

The simulations were done with a different set of GTN parameters based on the data in Table 1.
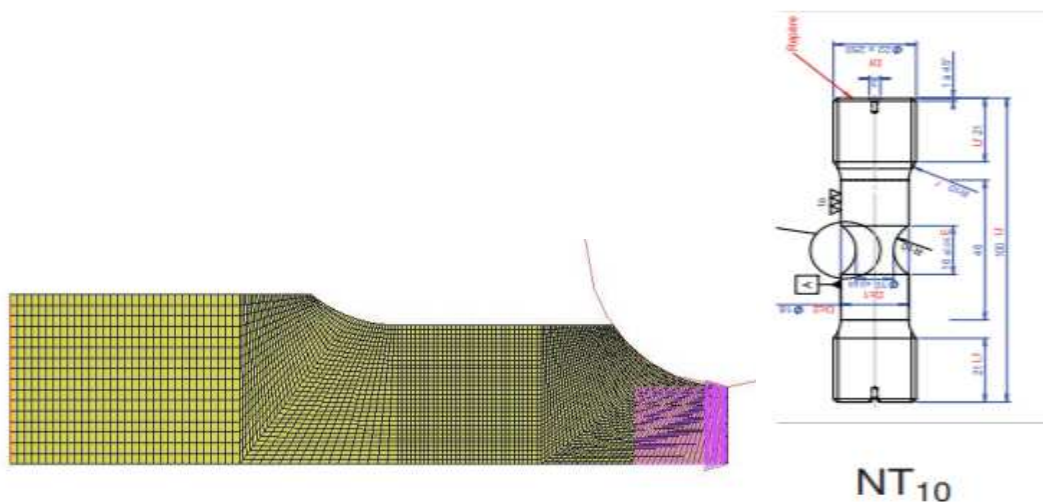
Figure 55. notch specimen and simulation

The mesh size in front of the pre-crack tip is 0.125 mm 0.0625 mm, and the mesh is composed of axisymmetric quadratic elements with eight nodes.

4.2.6.3. ANN and the creation of the database

As mentioned, sixty simulations for NT specimens with different GTN parameters were performed to generate the database essential to train the ANN.

The trained ANN model for the CT test has 200 input neurons, 75 hidden neurons, and six output neurons (200-75-6). The displacements of a reference point chosen in the specimen's border corresponding to the provided values of the response force F are represented by the neurons of the input layer, and the GTN parameters to be identified are represented by the neurons of the output layer (f_0, f_c, f_f, f_n, S_n and ε_n).

I estimated the GTN parameters after training the Neural Network based on the NT simulation data until I reached the point that the neural network proceeded as a simulation tool, which led to the GTN parameters prediction.

The next step is to enter the experimental data of the pipeline, and the neural network will do the job and predict the GTN parameters corresponding to the pipeline in a few minutes.

f_0=0, f_c=0.0045, f_f=0.25, f_n= 0.05, S_n = 0,45 and ε_n = 0.2 are the GTN parameters determined using the ANN.

In appendix 6, I do present the script behind the ANN model.

4.2.6.4. Prediction of Crack propagation for pipeline specimen

 The main step now is to predict the pipeline's failure based on the GTN parameters in the last paragraph.

The dimensions of the Mockup FP1 are already mentioned in experiment part 6; to reduce the computation time, I decided to model just half of the mockup; *I used axisymmetry.

The FEM model has 104193 nodes and 248038 elements in total.

To eliminate the influence of the mesh's sensitivity on the findings, the mesh size in front of the pre-crack tip is the same as the CT specimen and the NT as already mentioned previously (0.125 mm 0.0625 mm), and the mesh is made up of axisymmetric quadratic elements with eight nodes.

I do a FEM simulation using the GTN parameters obtained by the ANN; the results indicate that the simulation curve closely matches the actual curve and that they agree well Fig. 56

.
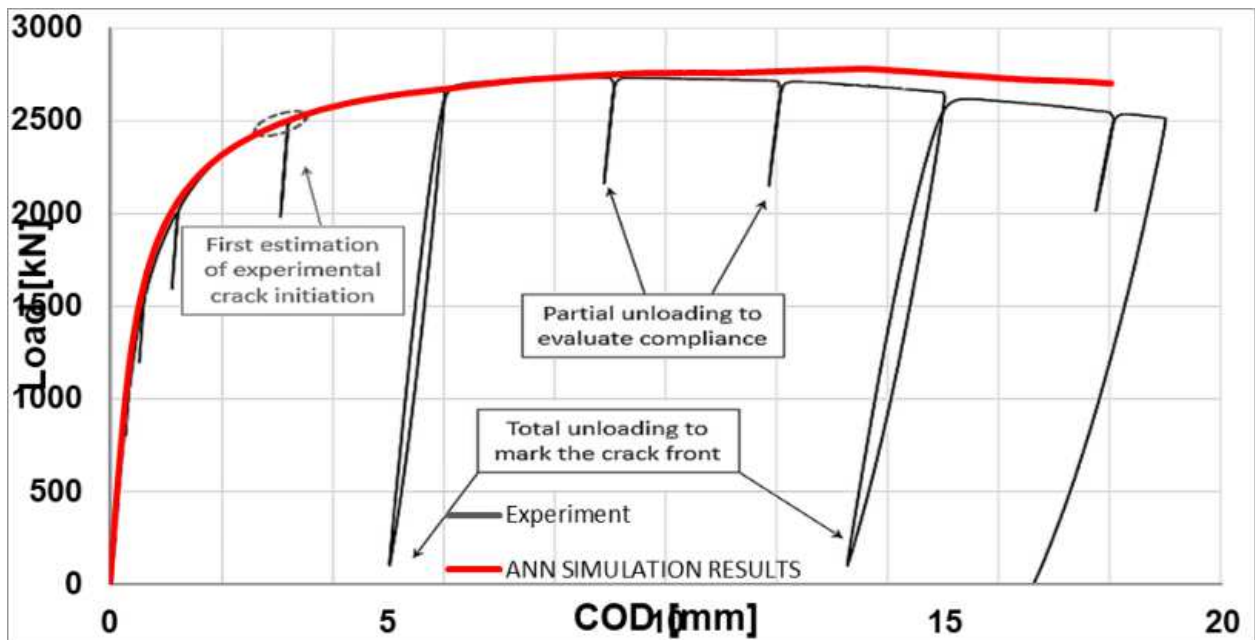
Figure 56. experimental and simulation results

By analyzing the curve above, it is obvious that ANN estimates the correct values of GTN parameters used to predict the failure of the SENT specimen.

It is noticeable that the curve found by ANN is not fully fitting the experimental data, especially at the end of the curve; this phenomenon is related to the database used to train the network.

I decide to run a Statical comparison between the ANN and direct method for FP1.

1. Descriptive statistics: The mean, median, standard deviation, and range for the load force results obtained from the direct method and the artificial neural network method are shown in the table below:

Method	Mean	Median	Standard Deviation	Range
Direct	50.82	51.29	3.01	14.55
ANN	50.50	50.44	3.19	13.91

2. Normality testing: I performed The Shapiro-Wilk test to check the normality of the data. The results indicate that the load force results obtained from both methods are normally distributed (p > 0.05).

I first computed the load force results for the direct and ANN techniques before doing the Shapiro-Wilk test.

The Shapiro-Wilk test was employed in this study to check the normality of the load force data produced using the direct technique and the ANN approach. I concluded that the data were normally distributed and I found that the p-value is higher than 0. 05.

In the next step I decided to study the accuracy of the ANN, direct method with the experimental data by using MAE, RMSE and the R2.

- Mean Absolute Error (MAE): The MAE is a metric that assesses the standard deviation between expected and observed values. It is derived by averaging the absolute disparities between the values that were anticipated and those that occurred. The model performs better in terms of prediction when the MAE is lower.

- Root Mean Squared Error (RMSE): The RMSE is a metric that assesses the average squared variation between the expected and actual values. The average of the squared discrepancies between the expected and actual values is considered in its calculation. The model performs better in terms of prediction the smaller the RMSE.

- the R2 value (s) is an indicator of how much of the variance in the dependent variable can be predicted by the independent variable. Higher values indicate stronger prediction skill; it ranges from 0 to 1. The R2 value of 1 indicates that the model perfectly fits the data, while an R2 value of 0 indicates that the model does not explain any of the variability in the data.

At the end I found that the Artificial Neural Network (ANN) technique outperformed the Direct method in forecasting the GTN results. In comparison to the Direct approach, the ANN model had significantly lower Mean Absolute Error (MAE), Root Mean Squared Error (RMSE), and R-squared values. In comparison to 12.958 and 16.128 for the Direct technique, the MAE and RMSE values for the ANN method were 6.853 and 8.195, respectively. With the ANN and Direct approaches, the R-squared values were 0.962 and 0.855, respectively. Therefore, the ANN method is recommended for future GTN parameters predictions.

Based on these results, it can be concluded that there is no significant difference between the load force results obtained from the direct method and the artificial neural network method.

To confirm the validity of GTN parameters found in the previous study, I decided to predict the failure of another mockup

The second Mock-up will have the same geometry and loading as the first mockup, which I already mentioned previously but will have irregularly shaped initial flaws for the first mockup, the crack introduced through-wall FP1, but for the second mockup, the initial defect was in surface fractures FP2 Fig. 57 The crack is introduced in all cases using EDM and fatigue pre-cracking.

Figure 57 initial crack defect FP2

The geometry of the second mockup is presented in table 2.

The ferritic mockup is modeled in Fig. 58 to have an elastic behavior (E=203 GPa).
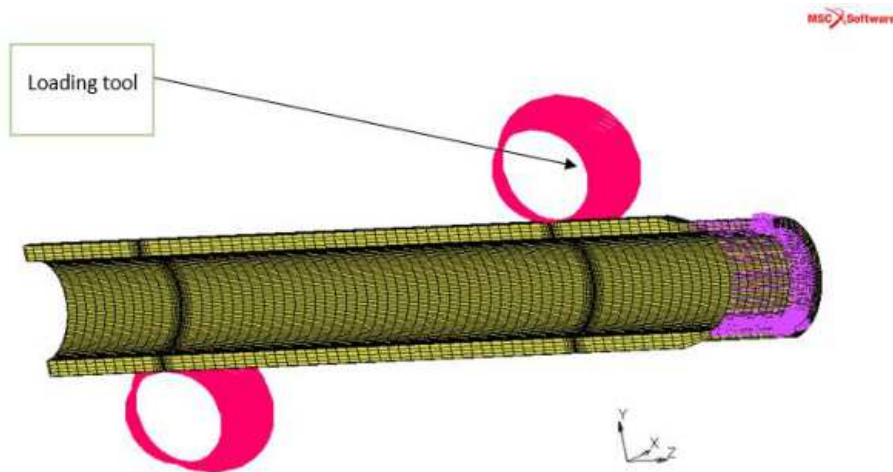
Figure 58 Simulation of the second mockup

Based on what I found in the previous section regarding the FP1 mockup, I will use the same trained model to determine the GTN parameters that will be used to predict the failure of the second pipeline FP2. I will need to use the corresponding experimental data for FP2.

In Fig. 60 (Force vs. Crack opening displacement) below, the GTN model predicts the pipeline's failure very well. It leads us to the right prediction of the crack propagation, especially at the cleavage initiation.

The crack initiation for the mockup FP2 is presented in the Figure below
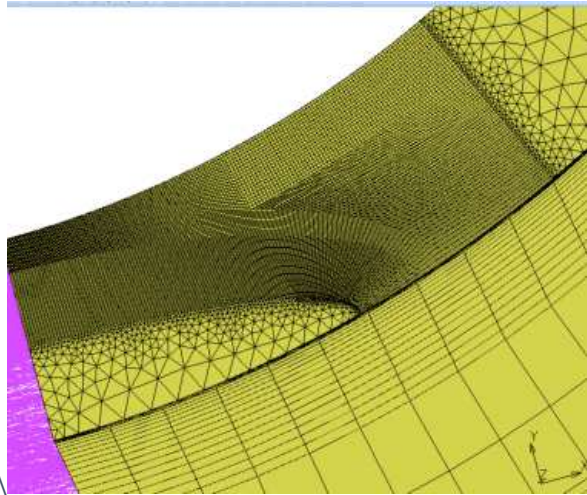
Figure 59 crack initiation

It is important to highlight that the initiation and maximum load are well predicted.

I can conclude from the curve analysis that the onset of ductile tearing is correctly predicted: 2660 kN (simulation) versus 2705 kN reported in the experimental data. The maximum projected load is 2840 kN, and the experiment's highest force is 2840 kN,
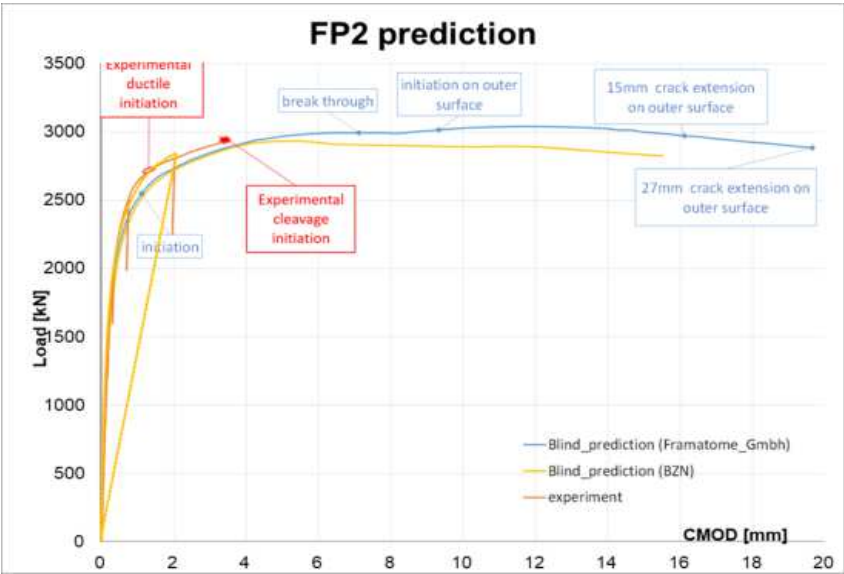
Figure 60 Load vs. Crack opening displacement of fp2

Remarks and Interpretation :

- The GTN model is a practical tool that can be used in the nuclear industry to improve the realibility of the failure prediction of real components that is essentially needed in nuclear industry to improve its safety without over conservatism.

- The backpropagation algorithm was a robust optimization tool that reduced prediction time from 30 days to six hours. This improvement can be attributed to the developed optimization approach. While the direct method is a standard approach for determining GTN parameters, this method can involve arbitrary numbers and require multiple simulations to obtain a suitable set of parameters. In contrast, the developed optimization approach enabled us to derive a precise set of GTN parameters from a single pipeline simulation, thereby saving significant time and computational resources. Specifically, when dealing with unsymmetric geometries with intricate dimensions, the direct method can be highly inefficient, requiring several months to derive the correct set of parameters. The optimization approach overcomes this limitation by enabling GTN parameter prediction for complex geometries solely based on simulating NT specimens made of the same material

- An increase in the training data will be needed to face the convergence issue and find more precise predictions.

- Due to the critical area from which I take the specimen for fracture toughness tests, the specimen size is a critical obstacle. The subsidized specimens can be used instead of normal-sized specimens to overcome such issues.

- One of the critical issues of the GTN model is the number of parameters that we need to find. They depend on the type of the material and the load conditions, making it critical to find the exact set of GTN parameters.

- Predicting the pipeline's maximum load and crack propagation was crucial, which is the main purpose of avoiding pipeline failure.

- Lately, the tendency is toward applying the complete GTN model, which was not the purpose of this thesis, but the same calculation can be done using the complete GTN model.

In the next chapter, I will give a general overview of the subsidized specimen and determine the J-R curves; further studies will be done to predict the failure of the pipeline using the subsidized specimen.

5. General overview of the subsidized specimen and determination of J-R curves

5.1. Introduction

Nowadays, fracture mechanics has been employed for decades, and procedures for standard-sized specimens are well established.

Because it was created primarily to evaluate massive structures against brittle failure, standardized specimens are currently rather large.

However, these standard specimens are impractical in many circumstances due to the size constraints imposed by the experimental material or the component under consideration.

These examples include determining local qualities and evaluating the mechanical properties of newly produced materials under laboratory circumstances.

As a result, new techniques utilizing much smaller specimens must be developed. Processes utilizing smaller specimens must be offered, with their validity limitations and relationship to standardly acquired results, to provide a solution for a wide range of applications.

Mechanical properties, such as fracture toughness for brittle fractures, are determined using standard standards (ASTM E1820, E399). These standards state that specimen size restrictions are required for testing. The conditions cannot be met in rare circumstances, such as with irradiated specimens or restricted material sources.

It is important to highlight that the sub-size specimens do not meet the size criteria of the standard ASTM E1820 (2011).

Employing small-size or even miniature mechanical specimens is becoming increasingly common due to the potential to optimize material usage, particularly where material availability is a concern or space inside irradiation facilities is restricted.

The purpose of this section is to test non-standard specimen sizes and explain the fracture mechanism using the finite – element and the GTN model; in addition, it will be possible to ensure that the size will not affect the prediction process, which might lead to further studies to predict the failure of PIPELINE using small scale specimen.

This section of the Ph.D. studies is part of a European project called FRACTESUS (Fracture mechanics testing of irradiated RPV steels using sub-sized specimens); FRACTESUS is approved as a project in the EURATOM Work Programme 2019-2020 in the section NFRP-04: Innovation for Generation II and III reactors. The project frames the overall H2020 program to

improve nuclear safety continually, security, and radiation protection, notably contributing to the long-term decarbonization of the energy system in a safe, efficient, and secure way. FRACTESUS also adheres to the three H2020 priorities: Excellent science, Industrial leadership, and Societal challenges [72].

Small-scale specimens are crucial in examining the characteristics of irradiated materials. The use of tiny specimens has several advantages. Across most cases, just a tiny amount of material may be irradiated in a reactor under ideal temperature, neutron flux, and dosage. A tiny amount of irradiated material may also make specimen handling simple. Smaller specimens contain less radioactive material, reducing worker exposure and trash disposal.

On the other hand, the utilization of tiny specimens raises many obstacles. These difficulties are related to adequate consideration for structural parameters and the transferability of tiny specimen data to the actual structures of interest. The most often used sample shape in surveillance programs is the Charpy V-notch specimen.

Any fracture toughness specimen made from the broken standard Charpy specimens may be used to evaluate reactor pressure vessels.

The most frequent specimen shape used in nuclear safety programs is the Charpy V-notch specimen.

The Mini-CT specimen approach has the benefit of having the same cross-section (10x10 mm) as a regular Charpy specimen, allowing it to be created from a simple slice of a damaged Charpy specimen.

5.2. Geometries and simulation

Materials from both eastern and western-type reactor pressure vessels are included in the test matrix. Included are plates, forgings, and weld metals. Low-alloy steels that have been purposefully enriched in copper, phosphorus, nickel, and manganese have chemical compositions that range from fairly pure.

Steels that have been irradiated, annealed, and re-irradiated are included, albeit most of the materials are unirradiated. According to earlier tests, the reference temperature T0 for unirradiated materials ranges from -134°C to +8°C, while the irradiated materials have even higher T0 values.

The chemical properties of the material used in the project are presented in the Table below.

Table 5 List of materials to be used in FRACTESUS [72].

Material	Type	Cu [wt%]	P [wt%]	Ni [wt%]	Mn [wt%]	Fluence [E19 n/cm²]	T0 [°C]
15Kh2MFAA	BM	0.05	0.01	0.1	0.49	0	-104
15Kh2MFAA	BM	0.05	0.01	0.1	0.49	I_1 = 20 (E > 0.5MeV) (at 270°C)	TBD
15Kh2MFAA	BM	0.05	0.01	0.1	0.49	I_1A (Annealed at 470°C)	TBD
15Kh2MFAA	BM	0.05	0.01	0.1	0.49	I_1A I_2 = 20 (E > 0.5MeV) (at 270°C)	TBD
A533B (JRQ)	BM	0.14	0.018	0.83	1.39	0	-71
A533B LUS (JSPS)	BM	0.24	0.028	0.43	1.52	0	+8
ANP-4	BM	0.05	0.006	0.84	0.85	4 (at 280°C-286°C)	-78
SA 533 B1 (MVE)	BM	0.041	0.005	0.632	1.42	0	-119
SA508 Cl.3	BM	0.04	0.008	0.93	1.37	0	-43
10KhMFT	WM	0.11	0.047	0.14	1.16	IA	-11.6
10KhMFT	WM	0.11	0.047	0.14	1.16	1.6 (I) (at 270°C)	74.4
73W	WM	0.31	0.005	0.6	1.55	0	-64
73W	WM	0.31	0.005	0.6	1.55	1.5 (E>1MeV) (at ~288°C)	34
ANP-5	WM	0.22	0.015	1.11	1.14	0	-38

The geometry of the mini CT specimen (W=8, a0/W=0.5, *B*=4 mm) is presented in Fig. 61.
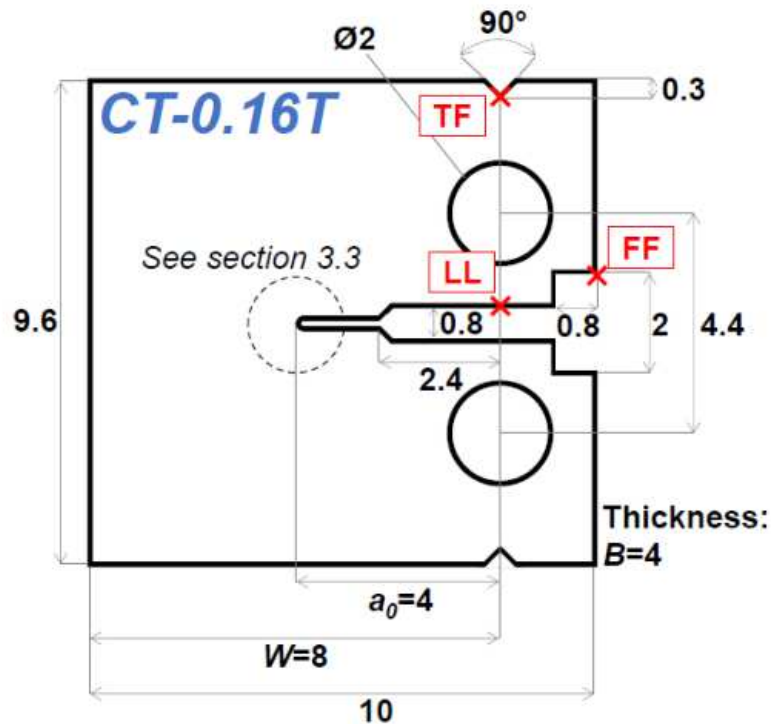
Figure 61 Mini CT specimen

As long as the local approach will be used in this study, the refinement of the mesh size near the crack tip will be crucial, as shown in the Figure below.

A refined zone size is chosen before the crack tip; the number of elements in this refined zone is 50 along the X-axis. Each element in this refined zone contains 12 radial elements along the quarter circle of radius five μm that describes the crack tip.
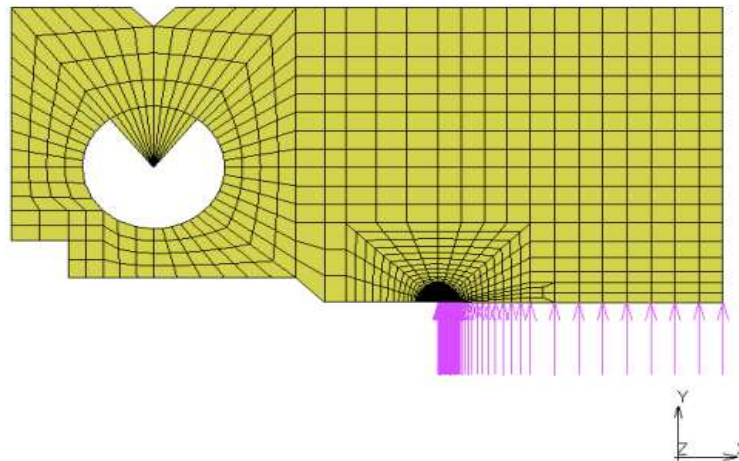
Figure 62 mini CT specimen
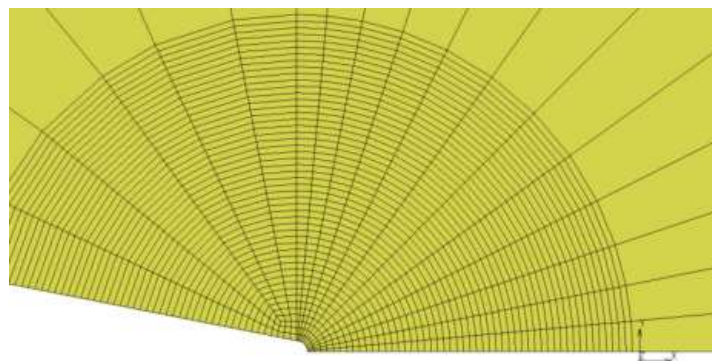
Figure 63 meshing near the crack tip

The type of material used in this work is RPV steel.

The simulations were carried out in MSC marc software utilizing an elastic-plastic material model with multi-linear hardening and viscous stabilization for all continuum elements. The mesh is composed of axisymmetric quadratic elements with eight nodes.

Because of the axisymmetry, I created a 3D FEM model for half of the MCT specimen, as shown

in Fig. 63, The FEM model has 18078 nodes and 14,952 elements.

The geometry of the Large specimen (1T-CT) is presented conforming to ASTM E1921 standard {73], specimen geometry is as follows: W=50.8 mm, a0/W=0.5, B=0.5, W=25.4 mm.

The Isotropic elasticity parameters of the large and mini CT specimens data can be found in Appendix 7.

The geometry of the large specimen is presented in the Figure below.
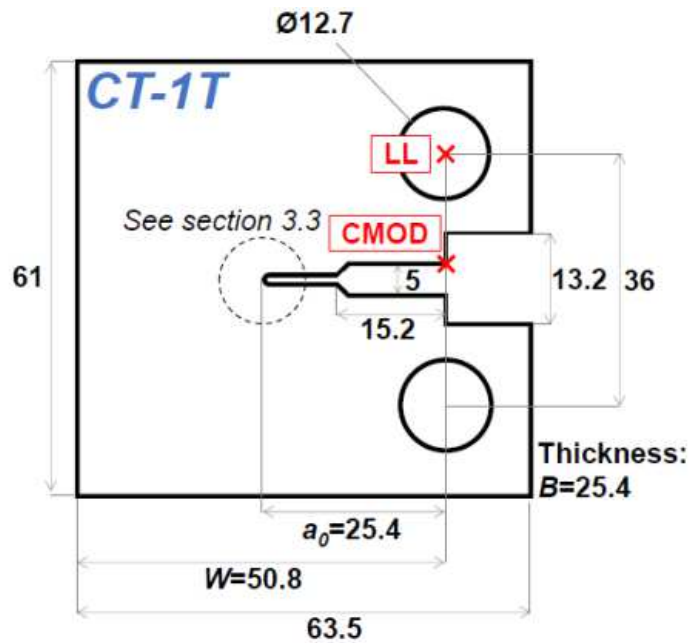
Figure 64 Large-scale specimen

To avoid the mesh sensitivity, the same parameters of the mesh size near the crack tip were also used for the large specimen like the subsidized specimen,
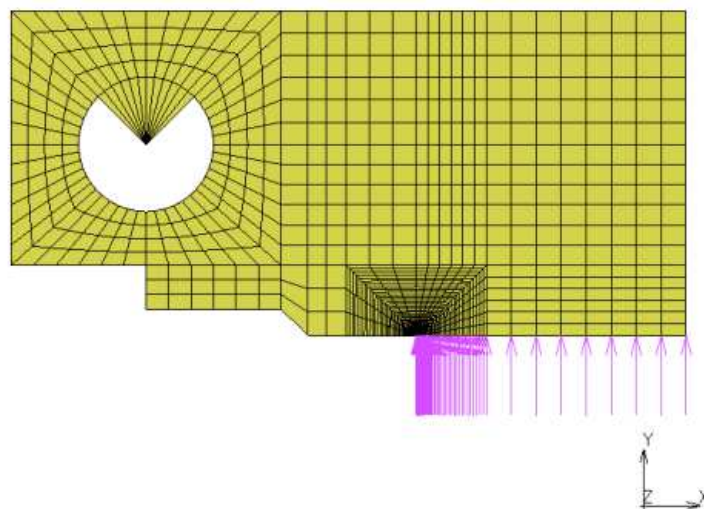
Figure 65 Large CT specimen

5.3. Determination of J-R curves for the mini CT and large CT specimen.

The crack length at the appropriate loading level must be known to determine the J-R curve.

There are essentially two methods: single-specimen and multiple-specimen.

The multiple specimen test method involves loading many "similar" specimens to varying levels and visually measuring the achieved crack lengths at the fracture surface. In the instance of the single-specimen approach, three commonly used single-specimen test procedures were created with fracture lengths monitored during the test to acquire a complete range of crack lengths for J-R curve determination from a single specimen.

The elastic unloading compliance method is the most frequently employed among the single-specimen approaches. Another approach is the electrical potential drop, the normalization method in ASTM 1820 [74].

As it is difficult to determine the J-R curve experimentally, new options for doing so are being investigated. A numerical simulation is one of these options.

A suitable model representing the material's actual behavior after damage (the crack propagation) is required to produce a trustworthy J-R curve.

The GTN model allows for the numerical simulation of crack formation, the calculation of crack length increment, and the simulation of load-line displacement, which makes it possible to determine the J integral.

The GTN model was implemented as a subroutine in the finite element method program Marc Mentat.

The next step is to use MARC Mentat to determine and compare the J-R curve with the experimental data for the mini CT and large specimen.

The following parameters got applied: Poisson's ratio = 0.3 and E= 202563 MPa Young's modulus.

The curves below show that results found using the simulation fit the experiments very well, except in the case of the Mini CT specimen, a slight difference is shown at the simulation.
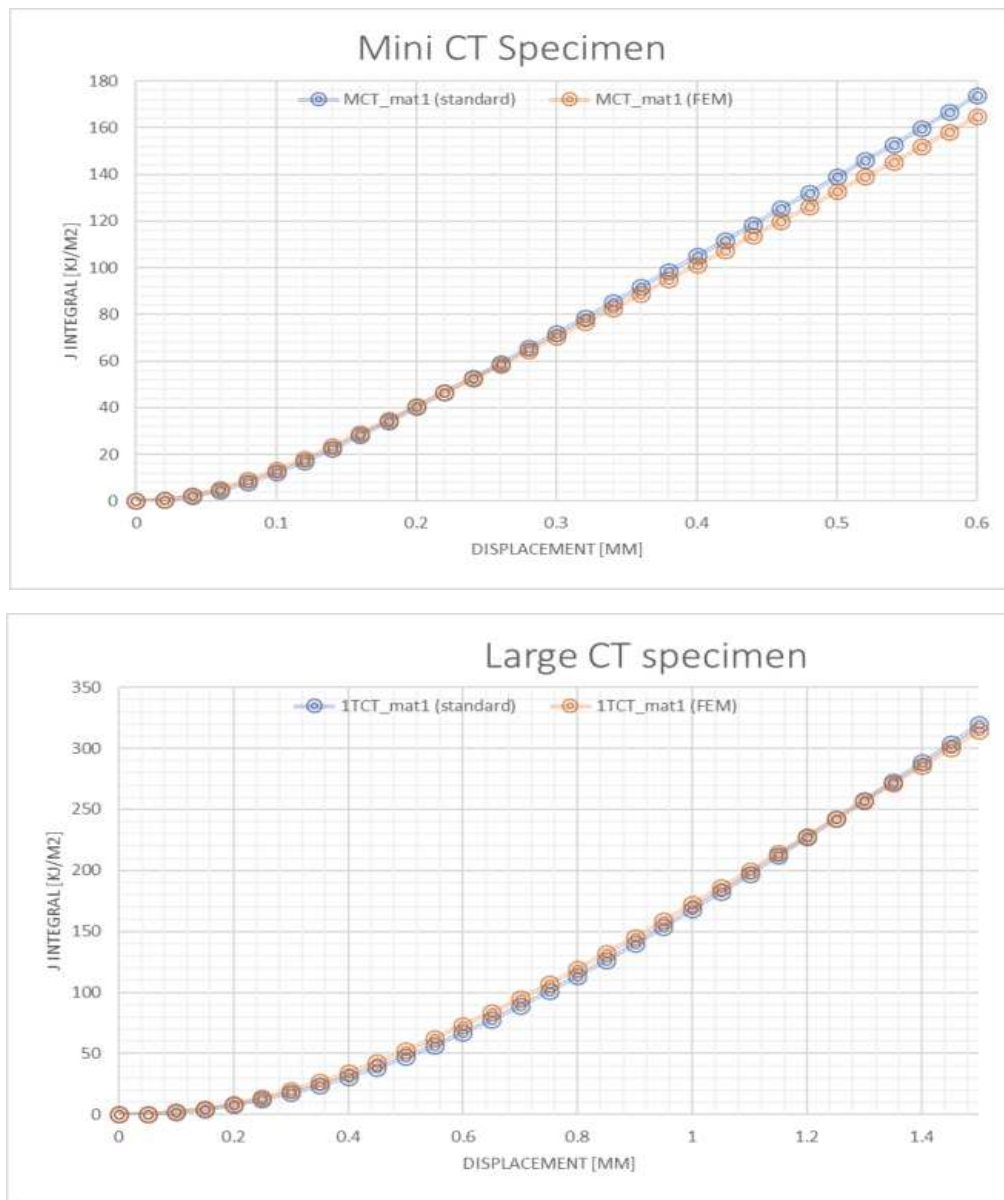
Figure 66 J-R curves for small-scale and large-scale specimens

Remarks :

As already mentioned, this thesis will not focus on the small-scale specimen. However, it will open the doors for further studies on this topic and how to implement the artificial neural network in determining GTN parameters based on small-scale specimen.

As already shown before, the time consumed by using large NT species was 6 hours. With the scale specimen, the duration will be shorter. The general overview related to the small-scale specimen was to show the importance of the specimen size in a critical area such nuclear field.

6.   Main conclusions and future work :

➢ The GTN model is a great and strong tool that can be used in the field of nuclear safety to predict the ductile failure of the pipelines used in the nuclear power plants

➢ To show the validity of the GTN model in my studies, I decided to start by predicting the failure of the SENT specimen, and the results show the possibility of using the model in this research.

➢ To be able to use the GTN model, it is important to determine eights parameters; based on the previous studies, the values of two parameters are almost fixed (q1 and q2); the problem is with the determination of the other six parameters, which basically should not be random values. Still, they should respect the values found in the literature review (TABLE 1); during this thesis, I studied the sensitivity of GTN parameters to find the most sensitive parameters, which could affect the determination process of GTN parameters.

➢ Finding the parameters that are the most sensitive would be advantageous since it would enable us to avoid big changes in their values and prevent their significant influence on the results.

➢ The direct method of determining GTN parameters is the combination of the experimental and finite element results; this method was used to predict the failure of the SENT specimen and pipeline; after analyzing the results, I got two main conclusions:

   • The first one is the efficiency of the GTN model; I could predict the failure of the SENT specimen and the pipeline.

   • The second conclusion is the time consumed during the determination of GTN parameters, and it was a huge disadvantage because I needed 30 days to predict GTN parameters, which is a long time because of a simple reason that during the simulation, We used just the quarter of the sample, so for more sophisticated equipment where it is not possible to apply the axisymmetric, the time consumed will take months instead of days or hours

➢ Based on the two conclusions mentioned above, it was necessary to find a solution for the time consumed during the determination of GTN parameters; that is why I decided to include the artificial neural network in the process, the results that I found show that the

backpropagation approach was a magical solution, to determine GTN parameters in 6 hours instead of 30 days.

➢ More studies must be done with other geometries to study the backpropagation approach and confirm its validity.

➢ Based on the backpropagation approach, I would suggest a detailed study with different specimens to predict GTN parameters and determine pipeline failure and other sophisticated equipment.

NEW SCIENTIFIC RESULTS – THESES

T1- The validation of the GTN model was crucial to its use in this work. Using the direct method, I achieved a perfect fit between the predicted results and experimental data using the GTN model. However, I had to deal with the issue of sensitivity, which required a detailed study of the variation in the effect of the parameters to slight changes in their values. To address this, I conducted 120 simulations and demonstrated how the parameters behave, which will be valuable for future researchers in this field, as a new result based on this study I concluded that the main sensitive parameters are f_0, ε_n, and S_n [P1] [P2] [P3] [P4]

T2- This study presents a novel optimization approach for determining GTN parameters based on backpropagation, which was found to significantly reduce the calculation time from 30 days to just 6 hours. The results of this approach provide accurate values of GTN parameters and enable accurate predictions of crack behaviour in pipelines, which is of paramount importance for improving nuclear safety guidelines in the industry. Overall, our study contributes to the development of more efficient and accurate methods for predicting GTN parameters and crack behaviour, with potential applications in various industries.[P5] [P6]

T3- The ANN method is found to have outperformed the Direct method with significantly lower MAE, RMSE, and higher R-squared values. Therefore, the ANN method is recommended for future GTN parameters predictions.

REFERENCES

[1]   Harris, A. (1986). Titanic —a Royal Mail Ship. Science, 231(4740), 783-783. doi: 10.1126/science.231.4740.783-d

[2] Lay-Ekuakille, A., & Telesca, V. (2020). Flow distribution imaging and sensing for leaks in pipelines using decimated signal diagonalization. *Measurement: Sensors Volumes 7–9, October 2020, 100014*

[3] Hu, Z., Tariq, S., & Zayed, T. (2021). A comprehensive review of acoustic-based leak localization method in pressurized pipelines. *Mechanical Systems and Signal Processing Volume 161, December 2021, 107994*

[4] Oh, S. W., Yoon, D. B., Kim, G. J., Bae, J. H., & Kim, H. S. (2018). Acoustic data condensation to enhance pipeline leak detection. *Nuclear Engineering and Design*, *327*, 198–211. https://doi.org/10.1016/J.NUCENGDES.2017.12.006

[5] Muñoz, J. A., Khelfa, T., Komissarov, A., & Cabrera, J. M. (2021). Ductility and plasticity of ferritic-pearlitic steel after severe plastic deformation. *Materials Science and Engineering: A*, *805*, 140624. https://doi.org/10.1016/J.MSEA.2020.140624

[6] Qiang, B., & Wang, X. (2019). Ductile crack growth behaviors at different locations of a weld joint for an X80 pipeline steel: A numerical investigation using GTN models. *Engineering Fracture Mechanics*, *213*, 264–279. https://doi.org/10.1016/J.ENGFRACMECH.2019.04.009

[7] Kingklang, S., & Uthaisangsuk, V. (2018). Plastic deformation and fracture behavior of X65 pipeline steel: Experiments and modeling. *Engineering Fracture Mechanics*, *191*, 82–101. https://doi.org/10.1016/J.ENGFRACMECH.2018.01.026

[8] Keim, V., Nonn, A., & Münstermann, S. (2019). Application of the modified Bai-Wierzbicki model for the prediction of ductile fracture in pipelines. *International Journal of Pressure Vessels and Piping*, *171*, 104–116. https://doi.org/10.1016/J.IJPVP.2019.02.010

[9] Shen, F., Münstermann, S., & Lian, J. (2020). Investigation on the ductile fracture of high-strength pipeline steels using a partial anisotropic damage mechanics model. *Engineering Fracture Mechanics*, *227*, 106900. https://doi.org/10.1016/J.ENGFRACMECH.2020.106900

References

[10]   Soret, C., Madi, Y., Gaffard, V., & Besson, J. (2017). Local approach to fracture applied to the analysis of a full size test on a pipe containing a girth weld defect. *Engineering Failure Analysis*, *82*, 404–419. https://doi.org/10.1016/J.ENGFAILANAL.2017.07.035

[11]   Keshavarz, A., Ghajar, R., & Mirone, G. (2014). A new experimental failure model based on triaxiality factor and Lode angle for X-100 pipeline steel. *International Journal of Mechanical Sciences*, *80*, 175–182. https://doi.org/10.1016/J.IJMECSCI.2014.01.007

[12]   Oikonomidis, F., Shterenlikht, A., & Truman, C. E. (2014). Prediction of crack propagation and arrest in X100 natural gas transmission pipelines with a strain rate dependent damage model (SRDD). Part 2: Large scale pipe models with gas depressurisation. *International Journal of Pressure Vessels and Piping*, *122*(1), 15–21. https://doi.org/10.1016/J.IJPVP.2014.07.001

[13]   Alaswad, A., Benyounis, K. Y., & Olabi, A. G. (2016). Optimization Techniques in Material Processing. *Reference Module in Materials Science and Materials Engineering*. https://doi.org/10.1016/B978-0-12-803581-8.04004-2

[14]   Shikalgar, T. D., Dutta, B. K., & Chattopadhyay, J. (2020). Analysis of p-SPT specimens using Gurson parameters ascertained by Artificial Neural Network. *Engineering Fracture Mechanics*, *240*, 107324. https://doi.org/10.1016/J.ENGFRACMECH.2020.107324

[15]   Xu, W. Z., Li, C. B., Choung, J., & Lee, J. M. (2017). Corroded pipeline failure analysis using artificial neural network scheme. *Advances in Engineering Software*, *112*, 255–266. https://doi.org/10.1016/J.ADVENGSOFT.2017.05.006

[16]   Pérez-Pérez, E. J., López-Estrada, F. R., Valencia-Palomo, G., Torres, L., Puig, V., & Mina-Antonio, J. D. (2021). Leak diagnosis in pipelines using a combined artificial neural network approach. *Control Engineering Practice*, *107*, 104677. https://doi.org/10.1016/J.CONENGPRAC.2020.104677

[17]   Wen, K., He, L., Liu, J., & Gong, J. (2019). An optimization of artificial neural network modeling methodology for the reliability assessment of corroding natural gas pipelines. *Journal of Loss Prevention in the Process Industries*, *60*, 1–8. https://doi.org/10.1016/J.JLP.2019.03.010

[18]   El-Abbasy, M. S., Senouci, A., Zayed, T., Mirahadi, F., & Parvizsedghy, L. (2014). Artificial neural network models for predicting condition of offshore oil and gas pipelines. *Automation in Construction*, *45*, 50–65. https://doi.org/10.1016/J.AUTCON.2014.05.003

[19]   Abbassi, F., Belhadj, T., Mistou, S., & Zghal, A. (2013). Parameter identification of a mechanical ductile damage using Artificial Neural Networks in sheet metal forming. *Materials & Design*, *45*, 605–615. https://doi.org/10.1016/J.MATDES.2012.09.032

[20]   https://cordis.europa.eu/project/id/754589

[21]   https://www.mscsoftware.com/fr/product/marc

[22]   Barenblatt, G. I. (1959). The formation of equilibrium cracks during brittle fracture. General ideas and hypotheses. Axially-symmetric cracks. *Journal of Applied Mathematics and Mechanics*, *23*(3), 622–636. https://doi.org/10.1016/0021-8928(59)90157-1

[23]   J. B. Hunt. Fracture mechanism of semi-brittle steels in torsion (1958). Journal of the mechanics and physics of solids, v. 6, no. 4, July 1958, p. 321–326 + i plate. (1959). *Wear*, *2*(3), 241. https://doi.org/10.1016/0043-1648(59)90020-1

[24]   McClintock, F.A., 1968. A criterion for ductile fracture by the growth of holes. J. Appl. Mech. 35, 363–371.

[25]   Rice, J.R., Tracey, D.M., 1969. On the ductile enlargement of voids in triaxial stress fields. J. Mech. Phys. Solids 17, 201–217

[26]   Needleman, A., Tvergaard, V., 1984. An analysis of ductile rupture in notched bars. J. Mech. Phys. Solids 32, 461–490.

[27]   Gurson, A.L, 1975 Plastic Flow and Fracture Behavior of Ductile Materials Incorporating Void Nucleation, Growth and Interaction. Ph.D. Thesis,

[28]   Rousselier, G., 1981. Finite deformation constitutive relations including ductile fracture damage.

[29]   G.Rousselier, 1987. Ductile fracture models and their potential in local approach of fracture. Nuclear Engineering and Design, 105, pp. 97-111.

[30]   Zhang, Z., & Zhang, Z. L. (n.d.). *A complete Gurson Model mechanics of solar silicon wafer View project Anti-icing or icephobic surfaces View project A complete Gurson Model*. https://www.researchgate.net/publication/267194773

[31]   ROUSSELIER, G. (2001). The Rousselier Model for Porous Metal Plasticity and Ductile Fracture. *Handbook of Materials Behavior Models*, 436–445. https://doi.org/10.1016/B978-012443341-0/50049-1

References

[32]   Samal, M. K., & Shah, P. K. (2013). On the Application of Rousselier's Damage Model to Predict Fracture Resistance Behavior of Zircaloy Fuel Pin Specimens. *Procedia Engineering*, *55*, 710–715. https://doi.org/10.1016/J.PROENG.2013.03.319

[33]   Bauvineau L, Burlet H, Eripret C, Pineau A (1996) Modelling ductile stable crack growth in a C-Mn steel with local approaches. J Phys IV France 06(C6):C6-33–C36-42

[34]   Decamp K, Bauvineau L, Besson J, Pineau A (1997) Size and geometry effects on ductile rupture of notched bars in a CMn steel: experiments and modelling. Int J Fract 88(1):1–18

[35]   Schmitt W, Sun DZ, Blauel JG (1997) Damage mechanics analysis (Gurson model) and experimental verification of the behaviour of a crack in a weld-cladded component Nuclear Engineering and Design Volume 174, Issue 3, 5 October 1997, Pages 237-246

[36]   Skallerud B, Zhang ZL (1997) A 3D numerical study of ductile tearing and fatigue crack growth under nominal cyclic plasticity. Int J Solids Struct 34(24):3141–3161.

[37]   Benseddiq N, Imad A (2008) A ductile fracture analysis using a local damage mod-el. Int J Press Vesel Pip [85(4):219–227

[38]   Nahshon, K., & Hutchinson, J. W. (2008). Modification of the Gurson Model for shear failure. *European Journal of Mechanics - A/Solids*, *27*(1), 1–17. https://doi.org/10.1016/J.EUROMECHSOL.2007.08.002

[39]   Zhou, J., Gao, X., Sobotka, J. C., Webler, B. A., & Cockeram, B. v. (2014). On the extension of the Gurson-type porous plasticity models for prediction of ductile fracture under shear-dominated conditions. *International Journal of Solids and Structures*, *51*(18), 3273–3291. https://doi.org/10.1016/J.IJSOLSTR.2014.05.028

[40]   Z.L. Zhang *, C. Thaulow, J. édegard A complete Gurson model approach for ductile

[41]   L. Xue, « Constitutive modeling of void shearing effect in ductile fracture of porous materials,» Engineering Fracture Mechanics, vol. 75, pp. 3343-3366, 2008.

[42]   R. Zemouri, et al Intelligence artificielle : quel avenir en anatomie patholo-gique ? Neural network : A future in pathology? Annales de Pathologie Vol-ume 39, Issue 2, April 2019, Pages 119-129

[43]   M.Remzi et al Réseaux neuronaux artificiels pour la prise de décision en cancérologie urologiqueArtificial neural networks for decision making in urologic oncology Annales d'Urologie Volume 41, Issue

[44]   F.Brunellea   Intelligence artificielle et imagerie médicale : définition, état des lieux et perspectivesArtificial intelligence and medical imaging: Definition, state of the art and perspectives Bulletin de l'Académie Nationale de Méde-cine Volume 203, Issues 8–9, November–December 2019, Pages 683-687

[45]   S. S. Haykin, Neural networks and learning machines vol. 3: Pearson Upper Saddle River, NJ, USA:, 2009.

[46]   S. Shanmuganathan and S. Samarasinghe, Artificial Neural Network Model-ling vol. 628. Cham, Switzerland: Springer, 2016.

[47]   S. S. Haykin, Neural networks : a comprehensive foundation: Tsinghua Uni-versity Press, 2001.

[48]   S. Kumar, Neural networks : a classroom approach: Tata McGraw-Hill Educa-tion, 2004.

[49]   D. W. Patterson, Artificial neural networks : theory and applications : Prentice Hall PTR, 1998.

[50]   https://medium.com/@adamaya.sharma_iot18/artificial-neural-network-a-replica-of-brain-46aa15486938

[51]   S. Haykin. Neural networks ; a comprehensive foundation, 2nd Edition. Pren-tice-Hall, Upper Saddle River, NJ, 1999

[52]   Taylor J.G. Neural networks. Unicom Ltd., Oxon, UK, 1995

[53]   https://www.ibm.com/cloud/learn/supervised-learning

[54]   Turkson, R. F., Yan, F., Ali, M. K. A., & Hu, J. (2016). Artificial neural network applications in the calibration of spark-ignition engines : An overview. In *Engineering Science and Technology, an International Journal* (Vol. 19, Issue 3, pp. 1346–1359). Elsevier B.V. https://doi.org/10.1016/j.jestch.2016.03.003

[55]   (https://builtin.com/data-science/recurrent-neural-networks-and-lstm)

[56]   https://blog.clairvoyantsoft.com/the-ascent-of-gradient-descent-23356390836f

[57]   https://www.javatpoint.com/gradient-descent-in-machine-learning

[58]   Bryson, A. E., Ho, Y, -C., Applied Optimal Control, Blaisdell, 1969

[59]   Werbos, P., Beyond Regression: New Tools for Prediction and Analysis in the Behavioral Sciences, Ph.D. thesis, Harvard University, 1974.

References

[60]   Rumelhart, D. E., Hinton, G. E., and Williams, R. J., "Learning Internal Repre-sentations by Back-Propagating Errors", Nature, No. 323 : pp.533-536, 1986

[61]   Rumelhart, D. E., Hinton, G. E., and Williams, R. J., "Learning Internal Repre-sentations by Error Propagation", Parallel Distributed Processing: Explora-tions in the microstructure of Cognition edited by Rumelhart, McClelland and the PDP Research Groups Vol.1, pp. 216-271, MIT Press, Cambridge Mass., USA, ISBN: 0- 262-18120-7, 1986

[62]   Mohammed et al ANN backpropagation prediction model for fracture toughness in microalloy steel International Journal of Fatigue Volume 24, Is-sue 9, September 2002, Pages 1003-1010

[63]   Premalatha et al Prediction of solar radiation for solar systems by using ANN models with different back propagation algorithms Journal of Applied Re-search and Technology Volume 14, Issue 3, June 2016, Pages 206-214

[64]   M.Yazdanmehr et al Mechanical behavior modeling of nanocrystalline NiAl compound by a feed-forward backpropagation multi-layer perceptron ANN Computational Materials Science Volume 44, Issue 4, February 2009, Pages 1231-1235

[65]   https://www.guru99.com/backpropogation-neural-network.html

[66]   Moinereau, D., et al, "STYLE project: a large scale ductile tearing experiment on a cladded ferritic pipe", Proceedings of ASME 2014 PV&P Conference, paper PVP2014-28077

[67]   Dominique et al Experimental support to European project ATLAS+ Transac-tions, SMiRT-25 Charlotte, NC, USA, August 4-9, 2019 Division II

[68]   Yassine, C., & Szabolcs, S. (2020). The study of the sensitivity of GTN parameters. *Procedia Structural Integrity*, *28*, 1930–1940. https://doi.org/10.1016/j.prostr.2020.11.016

[69]   Clement Soret, Yazid Madi, Jacques Besson, Vincent Gaffard, (2015). Use of the sent specimen in pipeline design.20th JTM - EPRG European pipeline research group, Par-is, France. 34 p

[70]   Hamdi Aguir, Haykel Marouani (2010) Gurson-Tvergaard-Needleman parameters identification using artificial neural networks in sheet metal blanking International Journal of Material Forming 3:113-116 · April

[71]   https://ch.mathworks.com/products/new_products/release2019a.html

[72]   https://fractesus-h2020.eu/mission-statement

[73]   ASTM International, West Conshohocken (PA, USA), ed., ASTM E1921-19a, Standard Test Method for Determination of Reference Temperature, To, for Ferritic Steels in the Transition Range, (2019).

[74]   https://www.astm.org/Standards/E1820

LIST OF PUBLICATIONS RELATED TO THE RESEARCH FIELD

1. Chahboub Yassine & Dr. Szabolcs Szavai Determination of GTN parameters for SENT specimen during ductile fracture PROCEDIA STRUCTURAL INTEGRITY (2452-3216) : 16 pp 81-88 (2019)

2. Chahboub Yassine et al, Determination of GTN parameters of sent specimen during ductile fracture Tendon : Tamás Kékesi (Metallurgy of non-ferrous metals Tamás Kékesi) ME / FMME / Energy and Quality Institute (eds.) MultiScience - XXXIII. MicroCAD International Multidisciplinary Scientific Conference : Miskolc, Hungary 23.05.2019. - 24/05/2019 Miskolc-University City : ME, pp 1-10 Paper B-10. (2019)

3. Chahboub Yassine & Dr. Szabolcs Szavai The Study of the Sensitivity of GTN Parameters PROCEDIA STRUCTURAL INTEGRITY (2452-3216) : 28 pp 1930-1940 (2020)

4. Chanboub, Yassine & Dr. Szabolcs Szavai (2021) A Back Propagation módszer alkalmazása a GTN paraméterek meghatározásában - The Application of Back Propagation Approach in the Determination of GTN Parameters. GÉP, 72 (1-2). pp. 80-82. ISSN 0016-8572

5. Chahboub Yassine & Dr. Szabolcs Szavai Determination of GTN Model Parameters Based on Artificial Neutral Network for a Ductile Failure Journal of Mechanical, Civil and Industrial Engineering : 2 1 pp 1-5 (2021)

6. Chahboub Yassine & Dr. Szavai Szabolcs Damage Prediction of Ferritic Pipeline Using Artificial Neural Network Procedia Structural Integrity Volume 42, 2022, Pages 1025-1032

APPENDICES

1.

Appendix 1 : Experimental data of the notch specimen

Delta d	F
[mm]	[kN]
0	0
0.01	34.83534
0.02	45.18026
0.04	47.24188
0.06	48.61351
0.08	49.78671
0.1	50.86936
0.15	53.10072
0.2	54.75775
0.25	56.0959
0.3	57.12562
0.4	58.46837
0.5	59.24279
0.6	59.60572
0.7	59.68639
0.8	59.5714
1	58.95754
1.2	58.06949
1.4	56.94097
1.8	54.33155
2.2	51.3945
2.6	48.26352
2.92	45.17356

Appendix 2 : Experimental data for the CT 1881 Speicmen

CMOD	Force								
[mm]	[kN]								
0	0								
0.03841	4.29404	0.629462	41.482	0.915826	43.8268	1.203236	44.5434	1.491388	44.032
0.076844	8.54808	0.640438	41.6352	0.926864	43.8816	1.21427	44.6422	1.502426	44.1632
0.11532	12.69356	0.65142	41.7804	0.937892	43.9608	1.225388	44.5082	1.513582	43.9436
0.153853	16.67794	0.662406	41.9174	0.948934	44.01	1.236418	44.6284	1.524614	44.095
0.192457	20.469	0.673396	42.0476	0.959962	44.0884	1.247534	44.5012	1.535772	43.8806
0.231142	24.0362	0.68439	42.1712	0.971014	44.1146	1.258574	44.5928	1.546808	44.0212
0.269912	27.3104	0.695388	42.2828	0.982054	44.1676	1.269684	44.4864	1.55795	43.8568
0.308752	30.219	0.706438	42.2894	0.993112	44.185	1.280714	44.6106	1.568996	43.9754
0.347706	32.688	0.71746	42.3558	1.004164	44.2102	1.291848	44.4384	1.580146	43.7838
0.386828	34.7616	0.728476	42.4322	1.015202	44.2744	1.302872	44.5812	1.591194	43.8996
0.426108	36.4976	0.739494	42.5122	1.02626	44.2908	1.313998	44.4324	1.602354	43.684
0.465524	37.9748	0.750516	42.5788	1.037296	44.357	1.325026	44.568	1.613402	43.7994
0.47646	38.1768	0.761534	42.6606	1.048354	44.3744	1.336162	44.3878	1.624546	43.6344
0.487346	38.487	0.772544	42.7582	1.059394	44.4374	1.347184	44.5452	1.6356	43.7404
0.49823	38.8044	0.783554	42.8572	1.07046	44.441	1.358326	44.3548	1.646744	43.5744
0.509126	39.1038	0.79457	42.9462	1.081494	44.5174	1.36935	44.5054	1.657802	43.67
0.520028	39.3872	0.805584	43.0406	1.092584	44.45	1.3805	44.293	1.668956	43.4788
0.530938	39.6552	0.816604	43.1226	1.103626	44.5184	1.391524	44.4526	1.680016	43.5702
0.541858	39.9072	0.827622	43.213	1.114706	44.495	1.402674	44.2382	1.69116	43.418
0.552786	40.144	0.838646	43.2884	1.125754	44.539	1.413704	44.385	1.702222	43.5028
0.563722	40.367	0.849664	43.3796	1.136834	44.515	1.424848	44.195	1.713386	43.2932
0.574664	40.5786	0.86069	43.4512	1.147876	44.582	1.435878	44.341	1.724438	43.4116
0.585612	40.779	0.871712	43.5374	1.158968	44.5306	1.447034	44.1142	1.735596	43.2192
0.596566	40.9692	0.882742	43.605	1.170006	44.5986	1.45806	44.2742	1.746648	43.3458
0.607526	41.1494	0.893766	43.6872	1.181098	44.539	1.469202	44.0988	1.757828	43.0874
0.618492	41.32	0.904798	43.7512	1.19214	44.615	1.48024	44.2252	1.768876	43.2246

1.

Appendix 3 : Experimental data of SENT specimen

COD [mm]	Force [kN]								
0	0	0.262684	109.1806	0.597472	130.6268	0.920082	139.797	1.235874	145.6538
0.006731	5.33322	0.274792	110.6884	0.609166	131.0536	0.931456	140.0478	1.24706	145.8262
0.01345	10.66976	0.286924	112.0684	0.620848	131.4702	0.942822	140.295	1.25824	145.9964
0.020188	15.99726	0.299056	113.348	0.632514	131.8778	0.95418	140.5384	1.269414	146.1644
0.026999	21.2976	0.311192	114.5328	0.644162	132.2758	0.965532	140.7784	1.280582	146.3304
0.033896	26.5648	0.323328	115.6402	0.655794	132.6648	0.976876	141.0152	1.291744	146.4946
0.040911	31.7862	0.335452	116.6762	0.667412	133.0454	0.988216	141.2486	1.3029	146.6568
0.04808	36.947	0.347564	117.653	0.679018	133.4176	0.999548	141.4788	1.314052	146.8174
0.055439	42.0326	0.359658	118.5734	0.690608	133.7812	1.010872	141.7056	1.325196	146.976
0.063021	47.0274	0.371736	119.4412	0.702186	134.1374	1.022186	141.9294	1.336336	147.133
0.070833	51.9242	0.383796	120.2634	0.71375	134.486	1.033494	142.1498	1.34747	147.288
0.078968	56.677	0.395838	121.0442	0.725302	134.828	1.044792	142.367	1.358596	147.4412
0.087455	61.2672	0.407864	121.7878	0.736844	135.1638	1.056082	142.5808	1.369718	147.5928
0.09632	65.6736	0.41987	122.501	0.748374	135.4936	1.067366	142.792	1.380834	147.7428
0.105567	69.8822	0.431858	123.1844	0.759892	135.8172	1.078644	143.0004	1.391944	147.891
0.115161	73.9038	0.44382	123.8382	0.771402	136.1348	1.089916	143.206	1.40305	148.0372
0.125142	77.7074	0.45576	124.4674	0.782902	136.4472	1.101182	143.4088	1.41415	148.1818
0.135435	81.3282	0.46768	125.0728	0.79439	136.7536	1.11244	143.6088	1.425246	148.3248
0.146035	84.7612	0.47958	125.6566	0.805866	137.0544	1.123694	143.8066	1.436334	148.4662
0.156913	88.0162	0.491458	126.222	0.81733	137.3498	1.134944	144.002	1.447416	148.6062
0.168038	91.1	0.503316	126.7708	0.828786	137.64	1.146184	144.1948	1.458492	148.7446
0.179391	94.0186	0.515154	127.3032	0.84023	137.9252	1.157416	144.3852	1.469564	148.8816
0.190954	96.7664	0.52697	127.8202	0.851666	138.2058	1.168646	144.5732	1.48063	149.0168
0.20269	99.3196	0.538764	128.3214	0.863092	138.4818	1.179866	144.7588	1.49169	149.1506
0.214548	101.6804	0.55054	128.8082	0.874508	138.7536	1.19108	144.9424	1.502746	149.2828
0.2265	103.8248	0.5623	129.2822	0.885916	139.0208	1.202286	145.1234	1.513798	149.4134
0.238526	105.7656	0.57404	129.7424	0.89731	139.2836	1.213486	145.3022	1.524844	149.5424

| 0.250594 | 107.5388 | 0.585764 | 130.1898 | 0.908698 | 139.5422 | 1.224682 | 145.4792 | 1.535884 | 149.67 |

Appendix 4 : Experimental of the mockup FP1

COD	Force								
[mm]	[kN]								
0	0	0.839178	1860.764	1.837056	2301.228	2.3236	2402.812	2.84936	2482.424
0.039129	155.9668	0.860478	1877.22	1.846654	2303.708	2.33388	2404.688	2.86078	2483.88
0.078561	311.6304	0.882066	1893.388	1.856208	2306.184	2.34496	2406.436	2.87202	2485.36
0.118744	467.048	0.903956	1909.112	1.865918	2308.62	2.3553	2408.304	2.88342	2486.816
0.160501	622.864	0.926156	1924.604	1.87567	2311.04	2.36604	2410.108	2.89482	2488.26
0.204956	779.216	0.948664	1939.764	1.885794	2313.392	2.37666	2411.984	2.90626	2489.696
0.25366	936.468	0.97149	1954.592	1.895656	2315.776	2.38738	2413.756	2.91772	2491.12
0.261164	961.608	0.99465	1969.12	1.905766	2318.108	2.3983	2415.492	2.92958	2492.484
0.269414	986.684	1.01817	1983.34	1.915568	2320.476	2.40872	2417.292	2.94062	2493.964
0.277876	1011.66	1.042066	1997.188	1.92556	2322.804	2.41974	2419.004	2.95256	2495.312
0.286538	1036.46	1.066274	2010.88	1.935236	2325.164	2.43006	2420.828	2.96386	2496.744
0.295392	1061.32	1.090818	2024.264	1.945158	2327.524	2.44084	2422.632	2.9759	2498.068
0.304464	1086.068	1.115686	2037.432	1.954722	2329.872	2.45128	2424.416	2.98704	2499.508
0.313738	1110.804	1.140852	2050.352	1.964622	2332.156	2.46208	2426.12	2.99906	2500.832
0.323244	1135.424	1.166288	2063.02	1.974324	2334.46	2.47296	2427.812	3.0106	2502.208
0.332986	1159.988	1.191944	2075.432	1.98428	2336.712	2.4837	2429.592	3.02254	2503.532
0.34298	1184.484	1.21783	2087.588	1.994216	2338.976	2.49468	2431.26	3.03398	2504.916
0.353236	1208.932	1.243984	2099.456	2.00438	2341.196	2.50536	2432.968	3.04558	2506.28
0.363772	1233.232	1.270368	2111.096	2.01444	2343.42	2.51628	2434.7	3.05772	2507.568
0.374586	1257.484	1.296954	2122.492	2.02456	2345.624	2.52698	2436.38	3.069	2508.964
0.38578	1281.664	1.323674	2133.696	2.03458	2347.832	2.53772	2438.064	3.0812	2510.236
0.39725	1305.692	1.350574	2144.688	2.0446	2350.032	2.54854	2439.784	3.09224	2511.656
0.409038	1329.576	1.377684	2155.492	2.05442	2352.256	2.55934	2441.496	3.1051	2512.836
0.421176	1353.272	1.405008	2166.1	2.06478	2354.384	2.57056	2443.076	3.11624	2514.24
0.43366	1376.776	1.432496	2176.604	2.0746	2356.584	2.5816	2444.732	3.12854	2515.484
0.44649	1400.036	1.460198	2186.96	2.08492	2358.756	2.59252	2446.456	3.13972	2516.876
0.459674	1423.06	1.488158	2197.18	2.09472	2360.928	2.60372	2448.068	3.15196	2518.112
0.47322	1445.84	1.51639	2207.188	2.10488	2363.036	2.61456	2449.752	3.16348	2519.44

0.487128	1468.372	1.545046	2216.96	2.1147	2365.188	2.62582	2451.272	3.1756	2520.688
0.501402	1490.672	1.573536	2226.58	2.12488	2367.268	2.6367	2452.808	3.18738	2521.976
0.516068	1512.748	1.602298	2235.988	2.13472	2369.408	2.6478	2454.448	3.1992	2523.256
0.531108	1534.564	1.631596	2245.144	2.14502	2371.476	2.65844	2456.14	3.21114	2524.516
0.546504	1556.12	1.660366	2254.256	2.155	2373.58	2.67038	2457.652	3.22298	2525.784
0.562226	1577.4	1.689366	2263.172	2.1655	2375.6	2.68104	2459.328	3.2354	2526.968
0.578258	1598.392	1.700306	2265.64	2.1754	2377.692	2.69262	2460.876	3.24664	2528.312
0.594592	1619.088	1.712002	2267.956	2.18624	2379.632	2.70326	2462.536	3.25934	2529.46
0.611218	1639.464	1.721496	2270.616	2.1963	2381.66	2.71448	2464.116	3.2707	2530.772
0.628164	1659.54	1.732016	2273.096	2.20704	2383.62	2.7253	2465.744	3.2831	2531.948
0.645464	1679.348	1.741452	2275.736	2.21694	2385.628	2.73654	2467.308	3.29438	2533.264
0.663132	1698.908	1.751464	2278.272	2.22776	2387.504	2.74786	2468.84	3.30712	2534.388
0.681196	1718.14	1.760982	2280.872	2.23778	2389.468	2.75896	2470.396	3.31836	2535.724
0.699624	1737.052	1.770876	2283.448	2.24868	2391.308	2.7704	2471.9	3.33124	2536.808
0.718422	1755.672	1.780312	2286.024	2.25866	2393.28	2.78136	2473.464	3.34286	2538.052
0.737626	1773.964	1.789836	2288.572	2.26934	2395.14	2.79322	2474.9	3.35528	2539.212
0.75721	1791.932	1.799246	2291.124	2.28146	2395.288	2.80388	2476.492	3.36716	2540.432
0.77718	1809.576	1.808664	2293.664	2.2918	2397.2	2.81566	2477.924	3.37912	2541.644
0.797504	1826.912	1.818054	2296.204	2.30248	2399.12	2.82656	2479.476	3.39152	2542.792
0.818174	1844.008	1.827548	2298.724	2.31276	2401.02	2.83822	2480.916	3.40312	2544.036

3.4155	2545.18	4.00996	2594.432	4.63592	2631.504	5.29062	2660.732	5.98494	2683.216
3.42728	2546.396	4.02302	2595.256	4.64938	2632.172	5.30488	2661.24	6.00192	2683.428
3.43948	2547.552	4.03538	2596.164	4.6627	2632.848	5.3182	2661.848	6.0152	2684.068
3.45114	2548.776	4.04876	2596.952	4.67638	2633.516	5.33268	2662.332	6.03178	2684.296
3.46342	2549.912	4.06124	2597.844	4.68914	2634.24	5.34572	2662.964	6.0445	2684.98
3.47562	2551.06	4.074	2598.696	4.70318	2634.82	5.3613	2663.364	6.06092	2685.272
3.48764	2552.22	4.08654	2599.58	4.71612	2635.532	5.37404	2664.016	6.07404	2685.956
3.50048	2553.276	4.0991	2600.452	4.73046	2636.096	5.38924	2664.4	6.09144	2686.124
3.5121	2554.476	4.11194	2601.292	4.74284	2636.888	5.40204	2665.048	6.10484	2686.78

3.52468	2555.56	4.12544	2602.052	4.75724	2637.428	5.4176	2665.412	6.12114	2687.076
3.53668	2556.712	4.13828	2602.888	4.76976	2638.188	5.43078	2666.032	6.13394	2687.748
3.54954	2557.748	4.15146	2603.684	4.78394	2638.76	5.44684	2666.344	6.15098	2687.964
3.56146	2558.896	4.1642	2604.536	4.79676	2639.484	5.4594	2667.076	6.16464	2688.536
3.57412	2559.952	4.17698	2605.376	4.81128	2640.016	5.47548	2667.36	6.18014	2688.956
3.58592	2561.108	4.18916	2606.288	4.82396	2640.748	5.49136	2666.212	6.1938	2689.528
3.59876	2562.136	4.2028	2607.02	4.83844	2641.28	5.5065	2666.66	6.20972	2689.964
3.61034	2563.312	4.21512	2608.744	4.85112	2642.008	5.52018	2667.264	6.2237	2690.544
3.62336	2564.308	4.22924	2608.556	4.86522	2642.576	5.53524	2667.72	6.2391	2690.956
3.6351	2565.456	4.24136	2609.46	4.87766	2643.332	5.54856	2668.34	6.25346	2691.488
3.64808	2566.452	4.25574	2610.1	4.89172	2643.904	5.56394	2668.752	6.26982	2691.852
3.65994	2567.58	4.26762	2611.024	4.90462	2644.604	5.57724	2669.38	6.28388	2692.404
3.6724	2568.632	4.28192	2611.664	4.91884	2645.156	5.59274	2669.776	6.30088	2692.656
3.68426	2569.752	4.29418	2612.532	4.93204	2645.816	5.60596	2670.44	6.3147	2693.292
3.6969	2570.776	4.30838	2613.176	4.94598	2646.396	5.62166	2670.804	6.33122	2693.656
3.70936	2571.816	4.32042	2614.068	4.95892	2647.084	5.635	2671.412	6.34496	2694.324
3.7218	2572.86	4.33396	2614.78	4.97358	2647.576	5.65018	2671.832	6.3617	2694.68
3.73434	2573.88	4.34614	2615.652	4.98638	2648.284	5.66358	2672.452	6.37586	2695.312
3.74694	2574.848	4.35958	2616.368	5.00148	2648.728	5.67852	2672.912	6.39274	2695.64
3.75934	2575.848	4.37196	2617.204	5.0141	2649.444	5.69252	2673.468	6.40612	2696.356
3.77146	2576.888	4.38582	2617.868	5.0289	2649.956	5.7078	2673.888	6.42394	2696.588
3.78392	2577.86	4.39844	2618.676	5.04136	2650.676	5.72128	2674.496	6.4379	2697.288
3.79638	2578.844	4.41262	2619.292	5.05568	2651.192	5.73594	2674.98	6.45434	2697.604
3.80894	2579.788	4.42486	2620.136	5.0684	2651.88	5.74972	2675.556	6.46776	2698.304
3.82152	2580.74	4.43874	2620.788	5.08338	2652.336	5.7649	2676.028	6.48464	2698.644
3.83372	2581.724	4.45112	2621.608	5.09608	2652.896	5.77888	2676.568	6.4988	2699.28
3.84612	2582.68	4.4649	2622.268	5.11122	2653.352	5.79404	2676.992	6.51528	2699.64
3.85854	2583.632	4.47758	2623.048	5.1239	2654.052	5.80764	2677.576	6.52894	2700.308
3.87158	2584.512	4.4914	2623.692	5.1386	2654.532	5.823	2677.996	6.54672	2700.504
3.88386	2585.464	4.50412	2624.46	5.1509	2655.268	5.8366	2678.596	6.56042	2701.268
3.89676	2586.344	4.51748	2625.152	5.16646	2655.656	5.8524	2678.968	6.57728	2701.544
3.90894	2587.308	4.52988	2625.952	5.1794	2656.32	5.86568	2679.604	6.59124	2702.184

1.

3.92196	2588.168	4.5433	2626.668	5.19442	2656.756	5.88196	2679.928	6.6084	2702.476
3.93414	2589.128	4.55606	2627.408	5.2067	2657.488	5.89486	2680.648	6.62246	2703.132
3.9472	2589.964	4.56972	2628.048	5.2225	2657.836	5.91164	2680.892	6.6395	2703.408
3.95938	2590.908	4.5827	2628.76	5.235	2658.54	5.92478	2681.536	6.65358	2704.04
3.9726	2591.724	4.59644	2629.4	5.24994	2658.976	5.94266	2681.504	6.67044	2704.364
3.98456	2592.712	4.6094	2630.128	5.26326	2659.588	5.95584	2682.248	6.6845	2705
3.99764	2593.524	4.6233	2630.748	5.27744	2660.108	5.9724	2682.46	6.70188	2705.256

7.92376	2728.48	10.22458	2748.592	12.03078	2729.736	13.9527	2698.912
7.93768	2729.3	10.24128	2748.924	12.0476	2730.128	13.9804	2697.28
7.95744	2729.14	10.26344	2748.348	12.07132	2729.276	13.99676	2697.956
7.97162	2729.72	10.27988	2748.772	12.0881	2729.704	14.02628	2695.944
7.99254	2729.316	10.30228	2748.152	12.11458	2728.288	14.04316	2696.556
8.00666	2730.032	10.319	2748.524	12.13066	2728.924	14.06646	2695.852
8.02602	2729.952	10.34008	2748.156	12.15496	2727.96	14.08424	2696.184
8.04046	2730.6	10.35632	2748.604	12.17126	2728.472	14.10988	2694.996
8.06086	2730.204	10.37848	2748.024	12.195	2727.616	14.12746	2695.408
8.07552	2730.828	10.39444	2748.56	12.2115	2728.096	14.1558	2693.644
8.09508	2730.712	10.41858	2747.572	12.23724	2726.836	14.17366	2694.044
8.10974	2731.268	10.43424	2748.176	12.2533	2727.452	14.19716	2693.308
8.12858	2731.308	10.45812	2747.256	12.27914	2726.168	14.21516	2693.604
8.14356	2731.768	10.4738	2747.836	12.29564	2726.7	14.23964	2692.668
8.16418	2731.384	10.49706	2747.04	12.3197	2725.784	14.2584	2692.832
8.17892	2732.12	10.51294	2747.592	12.33616	2726.28	14.2827	2691.912
8.19964	2731.668	10.53786	2746.452	12.36124	2725.164	14.30122	2692.116
8.21386	2732.428	10.55364	2747.068	12.3775	2725.72	14.32774	2690.764
8.23662	2731.68	10.57642	2746.36	12.40488	2724.128	14.34598	2691.06
8.25088	2732.524	10.5923	2746.9	12.42064	2724.852	14.37122	2689.96
8.27064	2732.456	10.61796	2745.628	12.44652	2723.552	14.38936	2690.252
8.28522	2733.052	10.63318	2746.376	12.46244	2724.192	14.41652	2688.74
8.30608	2732.644	10.65966	2744.936	12.48728	2723.12	14.43432	2689.156

8.32086	2733.512	10.67486	2745.7	12.5034	2723.708	14.46184	2687.568
8.34206	2732.932	10.69778	2744.932	12.52748	2722.788	14.47974	2687.94
8.35654	2733.82	10.71332	2745.528	12.54398	2723.272	14.50318	2687.22
8.37772	2733.352	10.73832	2744.38	12.56838	2722.3	14.5217	2687.424
8.39282	2734.084	10.75374	2745.056	12.58488	2722.8	14.54574	2686.568
8.41232	2734.14	10.778	2744.06	12.6111	2721.452	14.56382	2686.928
8.42708	2734.84	10.79348	2744.684	12.62728	2722.08	14.59106	2685.316
8.44782	2734.596	10.81874	2743.476	12.65488	2720.436	14.60832	2685.864
8.46234	2735.408	10.83426	2744.136	12.67134	2721.024	14.63718	2683.96
8.4851	2734.8	10.8603	2742.776	12.6945	2720.316	14.65406	2684.62
8.49958	2735.672	10.87594	2743.428	12.71126	2720.756	14.68192	2682.988
8.52076	2735.36	10.90118	2742.224	12.7357	2719.788	14.69894	2683.572
8.53502	2736.24	10.91766	2742.72	12.7525	2720.248	14.72672	2681.96
8.55816	2735.572	10.94336	2741.376	12.77662	2719.332	14.74458	2682.364
8.57252	2736.48	10.95934	2742	12.79396	2719.684	14.76828	2681.624
8.59252	2736.428	10.98348	2741.028	12.81862	2718.66	14.78602	2681.992
8.60688	2737.232	10.9992	2741.624	12.83544	2719.124	14.81002	2681.168
8.62944	2736.676	11.02476	2740.36	12.86318	2717.46	14.82786	2681.516
8.64436	2737.464	11.04024	2741.056	12.87924	2718.196	14.85712	2679.58
8.66438	2737.428	11.06494	2739.96	12.90626	2716.644	14.87426	2680.212
8.67922	2738.124	11.0808	2740.532	12.92262	2717.248	14.90334	2678.312
8.7007	2737.752	11.1053	2739.488	12.94822	2716.056	14.92004	2679.004
8.71556	2738.536	11.12126	2740.056	12.96466	2716.636	14.9478	2677.388
8.7375	2738.076	11.14368	2739.412	12.99158	2715.156	14.96474	2678.016
8.75192	2738.944	11.16066	2739.756	13.00816	2715.744	14.99248	2676.408
8.7759	2738.104	11.18444	2738.872	13.03344	2714.616	15.00946	2677.012
8.79	2739.096	11.2006	2739.38	13.04978	2715.2	15.0363	2675.6
8.81188	2738.656	11.22438	2738.48	13.07748	2713.556	15.05352	2676.148

1.

Appendix 5 : Script of the Backpropagation algorithm used to predict the failure of the SENT specimen :

```matlab
% Solve an Input-Output Fitting problem with a Neural Network
% Script generated by Neural Fitting app
% Created 19-Apr-2020 19:47:15
%
% This script assumes these variables are defined:
%
%   input - input data.
%   target - target data.

x = input;
t = target;

% Choose a Training Function
% For a list of all training functions type: help nntrain
% 'trainlm' is usually fastest.
% 'trainbr' takes longer but may be better for challenging problems.
% 'trainscg' uses less memory. Suitable in low memory situations.
trainFcn = 'trainlm';  % Levenberg-Marquardt backpropagation.

% Create a Fitting Network
hiddenLayerSize = 35;
net = fitnet(hiddenLayerSize,trainFcn);

% Setup Division of Data for Training, Validation, Testing
net.divideParam.trainRatio = 70/100;
net.divideParam.valRatio = 15/100;
net.divideParam.testRatio = 15/100;

% Train the Network
[net,tr] = train(net,x,t);
```

```matlab
% Test the Network
y = net(x);
e = gsubtract(t,y);
performance = perform(net,t,y)


% View the Network
view(net)


% Plots
% Uncomment these lines to enable various plots.
%figure, plotperform(tr)
%figure, plottrainstate(tr)
%figure, ploterrhist(e)
%figure, plotregression(t,y)
%figure, plotfit(net,x,t)
```

1.

Appendix 6 : Script of the Backpropagation algorithm used to predict the failure of the PIPELINE :

```matlab
% Solve an Input-Output Fitting problem with a Neural Network
% Script generated by Neural Fitting app
% Created 25-oct-2020 08:50:23
%
% This script assumes these variables are defined:
%
%   input - input  data.
%   target - target data.

x = input;
t = target;

% Choose a Training Function
% For a list of all training functions type: help nntrain
% 'trainlm' is usually fastest.
% 'trainbr' takes longer but may be better for challenging problems.
% 'trainscg' uses less memory. Suitable in low memory situations.
trainFcn = 'trainlm';  % Levenberg-Marquardt backpropagation.

% Create a Fitting Network
hiddenLayerSize = 50;
netpipe = fitnet(hiddenLayerSize,trainFcn);

% Setup Division of Data for Training, Validation, Testing
netpipe.divideParam.trainRatio = 85/130;
netpipe.divideParam.valRatio = 20/130;
netpipe.divideParam.testRatio = 20/130;

% Train the Network
[netpipe,tr] = train(netpipe,x,t);
```

```matlab
% Test the Network
y = netpipe(x);
e = gsubtract(t,y);
performance = perform(netpipe,t,y)


% View the Network
view(netpipe)


% Plots
% Uncomment these lines to enable various plots.
%figure, plotperform(tr)
%figure, plottrainstate(tr)
%figure, ploterrhist(e)
%figure, plotregression(t,y)
%figure, plotfit(netpipe,x,t)
```

1.

Appendix 7 : Isotropic elasticity parameters of the large and mni CT speicmens

Logarithmic plastic strain	Equivalent stress
0	578
2.00E-02	630
4.00E-02	685
6.00E-02	728
8.00E-02	762
1.00E-01	781
1.20E-01	801
1.40E-01	816
1.60E-01	830
1.80E-01	844
2.00E-01	859
2.20E-01	8.73E+02
2.40E-01	8.85E+02
2.60E-01	8.97E+02
2.80E-01	9.08E+02
3.00E-01	9.19E+02
3.20E-01	9.29E+02
3.40E-01	938
3.60E-01	9.47E+02
3.80E-01	9.55E+02
4.00E-01	9.64E+02
4.20E-01	9.71E+02
4.40E-01	979
4.60E-01	9.86E+02
4.80E-01	9.93E+02
5.00E-01	1.00E+03
5.20E-01	1.01E+03

5.40E-01	1.01E+03
5.60E-01	1.02E+03
5.80E-01	1.02E+03
6.00E-01	1.03E+03
6.20E-01	1.04E+03
6.40E-01	1.04E+03
6.60E-01	1047
6.80E-01	1.05E+03
7.00E-01	1.06E+03